

2003

Molecular cytogenetic evaluation of uveal melanoma cell lines and archival tissue

Jason Scott White
West Virginia University

Follow this and additional works at: <https://researchrepository.wvu.edu/etd>

Recommended Citation

White, Jason Scott, "Molecular cytogenetic evaluation of uveal melanoma cell lines and archival tissue" (2003). *Graduate Theses, Dissertations, and Problem Reports*. 1951.
<https://researchrepository.wvu.edu/etd/1951>

This Dissertation is protected by copyright and/or related rights. It has been brought to you by the The Research Repository @ WVU with permission from the rights-holder(s). You are free to use this Dissertation in any way that is permitted by the copyright and related rights legislation that applies to your use. For other uses you must obtain permission from the rights-holder(s) directly, unless additional rights are indicated by a Creative Commons license in the record and/ or on the work itself. This Dissertation has been accepted for inclusion in WVU Graduate Theses, Dissertations, and Problem Reports collection by an authorized administrator of The Research Repository @ WVU. For more information, please contact researchrepository@mail.wvu.edu.

**Molecular Cytogenetic Evaluation of
Uveal Melanoma Cell Lines and Archival Tissue**

Jason Scott White

**Dissertation submitted to the
College of Agriculture, Forestry and Consumer Sciences
West Virginia University
in partial fulfillment of the requirements
for the degree of**

Doctor of Philosophy

In

Genetics & Developmental Biology

Joginder Nath, Ph.D., Chair, WVU

Alison E. Director -Myska, Ph.D., AFIP

Sharon L. Wenger, Ph.D., WVU

Robert L. Becker, Jr., M.D., Ph.D., Col, USAF, MC, AFIP

Walter J. Kaczmarczyk, Ph.D., WVU

Daniel Pannaccione, Ph.D., WVU

Morgantown, West Virginia

2003

**Keywords: Cytogenetics, Uveal Melanoma, CGH, SKY, FISH
Copyright 2003 Jason S. White**

ABSTRACT

Molecular Cytogenetic Evaluation of Cell Lines and Archival Tissue

Jason Scott White

Uveal melanoma is the most common intraocular tumor in adults and often results in unilateral blindness and/or death. Previous cytogenetic characterizations of this tumor have consistently revealed chromosomal abnormalities involving chromosomes 3, 6, and 8; reports of other abnormalities vary in frequency. We further defined cytogenetic abnormalities of this tumor using molecular cytogenetic techniques on 10 uveal malignant melanoma cell lines and 100 formalin-fixed paraffin-embedded (FFPE) tumors.

The synthesis of comparative genomic hybridization (CGH) and spectral karyotyping (SKY) results revealed that chromosomal rearrangement plays a significant role in the generation of DNA sequence copy number abnormalities throughout the genome, but none of the cell lines demonstrated monosomy 3. Centromeric fluorescence *in situ* hybridization (FISH) for chromosome 3 revealed approximately one signal per cell, but further evaluation with telomeric probes demonstrated multiple signals per cell, suggesting chromosomal rearrangement without the loss of an entire chromosome 3. Based on combined CGH, SKY and FISH data, we propose that chromosome 3 is more frequently involved in chromosomal rearrangements rather than whole-chromosome loss in uveal melanoma.

CGH was similarly employed to elucidate characteristic DNA-sequence copy number abnormalities of FFPE archival cases of uveal melanoma, and correlate genomic

imbalance abnormalities with a prognosis. We set out to study 100 archival uveal melanoma cases, each with comprehensive patient follow-up, by correlation of copy number imbalances with survival. Fifty-one patients survived more than 9 years without evident metastasis, and the remaining 49 patients died with metastatic disease. Viable probe was generated from 82 of the 100 cases, allowing correlation of CGH findings with patient histories for all but 18 of the cases. Significant copy number imbalances were tested for univariate prognostic significance. The most powerful predictor of prognosis was gain of 18q11.2, which was subsequently compared with other significant chromosomal regions, as well as histological and clinical factors in a multivariate analysis. Multivariate analyses revealed that the gain of 18q11.2 and concomitant loss of 1p33 was the strongest indicator of a poor prognosis.

Our large-scale molecular cytogenetic analysis of cell lines and archival material contributes significantly to the characterization of uveal melanoma. This research is intended to direct further gene-specific study of malignancy in uveal melanoma.

To my parents,

Joan and Hal White,

who have made innumerable sacrifices for my education,

so I could learn without limitations

TABLE OF CONTENTS

Dedications	iv
Table of Contents	v
List of Abbreviations	vi
List of Figures	x
List of Tables	xiii
Acknowledgements	xiv
Introduction	1
Literature Review	12
Materials and Methods	42
Results	71
Discussion	102
Summary	116
References	117
Appendix A	130
Appendix B	139
Vitae	145

LIST OF ABBREVIATIONS

AAF	aminoacetylfluorene
AFIP	Armed Forces Institute of Pathology
bp	base pair(s)
BSA	bovine serum albumin
CaCl₂	calcium chloride
CCD	charge-coupled device
CGH	comparative genomic hybridization
CISS	chromosomal <i>in situ</i> suppression
CO₂	carbon dioxide
cRNA	complementary ribonucleic acid
DAPI	4',6-diamidino-2-phenylindole
dATP	2'-deoxyadenosine 5'-triphosphate
dCTP	2'-deoxycytidine 5'-triphosphate
del	deletion
der	derivative chromosome
dGTP	2'-deoxyguanosine 5'-triphosphate
dH₂O	distilled water
dic	dicentric chromosome
DIG	digoxigenin-11-dUTP
DMEM	Dulbecco's Modified Eagle's Medium
DNA	deoxyribonucleic acid
DNA Pol I	DNA Polymerase I
DNP	dinitrophenyl
dNTP	2'-deoxynucleotide 5'-triphosphate
DOP-PCR	degenerate oligonucleotide primed-polymerase chain reaction
dTTP	2'-deoxythymidine 5'-triphosphate
dUTP	2'-deoxyuridine 5'-triphosphate
EDTA	ethylenediaminetetraacetic acid
FA	formamide
FAM-M	familial atypical mole and melanoma

FBS	fetal bovine serum
FFPE	formalin-fixed paraffin-embedded
FISH	fluorescence <i>in situ</i> hybridization
FITC	fluorescein isothiocyanate
g	gram
H & E	hematoxylin and eosin
H₂O	water
HCl	hydrochloric acid
HEPES	N-2-Hydroxyethylpiperazine-N'-2-ethanesulfonic acid
HPLC	high performance liquid chromatography
HPBL	human peripheral blood lymphocytes
i	isochromosome
ins	insertion
ISH	<i>in situ</i> hybridization
KCl	potassium chloride
len1	distance, in pixels, representing a unit change in copy number on x-axis of a CGH ratio profile
LOH	loss of heterozygosity
LTD	largest tumor dimension
M	molar concentration
Mb	megabase(s)
M-FISH	multiplex fluorescence <i>in situ</i> hybridization
mg	milligram(s)
MgCl₂	magnesium chloride
ml	milliliter(s)
MM	master mix
mm	millimeter(s)
mM	millimolar
mr	marker chromosome
NA	net area
NaCl	sodium chloride

Na₂CO₃	sodium carbonate
NaHCO₃	sodium bicarbonate
ND	no data
NEAA	non-essential amino acids
NFDM	non-fat dried milk
ng	nanogram(s)
NT	nick translation
PBS	Dulbecco's Phosphate-buffered saline
PCI	phenol/chloroform/isoamyl alcohol
PCR	polymerase chain reaction
PHA	phytohemagglutinin
pg	picogram(s)
PL	profile length
PN	total pixels designated for cytogenetically normal copies of a given chromosome in a SKY image
PT	total pixels designated for a given chromosome in a SKY image
QCD	quantitative comparison data
QPD	quantitative profile data
RB	relative balance
RCE	relative chromosome equivalent
rDNA	ribosomal deoxyribonucleic acid
RNA	ribonucleic acid
rpm	revolutions per minute
RPMI	Roswell Park Memorial Institute
rRNA	ribosomal ribonucleic acid
SAGE	serial analysis of gene expression
SDS	sodium dodecyl sulfate
SE	standard error
SKY	spectral karyotyping
SSC	saline-sodium citrate
t	translocation

TBE	Tris-Borate EDTA
TE	Tris-EDTA
TIL	tumor-infiltrating lymphocytes
TRITC	tetramethylrhodamine isothiocyanate
U	unit(s)
UTP	uridine 5'-triphosphate
UV	ultraviolet
v/v	volume per volume
w/o	without
WVU	West Virginia University
mg	microgram(s)
ml	microliter(s)
mm	micron(s), micrometer(s)
~	approximately
3cen	chromosome 3 centromere
³H	tritium
3p	chromosome 3 telomere, p-arm
3q	chromosome 3 telomere, q-arm

LIST OF FIGURES

1. Anatomy of a Nucleus	2
2. Basic FISH Protocol	4
3. Anatomy of the Ocular Globe	6
4. Examples of Uveal Melanoma Tumors	9
5. Anatomy of the Chromosomes	13
6. Denaturation/Renaturation of DNA	15
7. Comparison of Directly and Indirectly-Labeled Probes	17
8. DOP-PCR Amplification of Genomic DNA	26
9. Schematic for SKY Image Capture and Analysis	34
10. Probe Production via Nick Translation	48
11. Agarose Gel Electrophoresis Comparing DNA Extracts with Nick Translation Products	50
12. DNA Probe Production via PCR	53
13. A Flowchart for CGH	54
14. A Schematic for the Process of Hybridization for CGH	55
15. Step-wise Process of CGH Visualization	59
16. Image Capture for CGH Analysis	60
17. DNA Counterstain	61
18. A Schematic for the Process of CGH Analysis	62
19. Quantitative Comparison Data for Genomic Imbalances in Ten Cell Lines	72
20. Minimal Common Regions of Gain and Loss Distilled from	73

CGH Mean Profile Data of Ten Uveal Melanoma Cell Lines	
21. Complex Aberrations Detected by Spectral Karyotyping	83
22. Chromosomal Rearrangements Seen Across Ten Uveal Melanoma Cell Lines	84
23. Overall Comparison of Calculated CGH RB and SKY RB Values for the 22 Autosomes in Nine Cell Lines	88
24. Visual Comparison of CGH and SKY	89
25. Comparisons of FISH, SKY and CGH Results for Chromosomes 3, 6, and 8, the Three Chromosomes Most Frequently Implicated in Uveal Melanoma	90
26. Visual Comparison of FISH and SKY	92
27. Minimal Common Regions of Gain and Loss Distilled from CGH Mean Profile Data of 82 FFPE Uveal Melanoma Cases	94
28. Quantitative Comparison Data and Minimal Common Regions for the Sex Chromosomes of the Male Archival Cases	95
29. Quantitative Comparison Data and Minimal Common Regions for the Sex Chromosomes of the Female Archival Cases	96
30. Minimal Common Regions of Gain and Loss Distilled from CGH Mean Profile Data of 43 FFPE Uveal Melanoma Cases, Representing Those Patients that Survived Beyond 9 Years Post-Diagnosis	97
31. Minimal Common Regions of Gain and Loss Distilled from CGH Mean Profile Data of 39 FFPE Uveal Melanoma Cases,	98

Representing Those Patients that Succumbed to Hematogenous Metastasis	
32. Minimal Common Regions for the Sex Chromosomes	99
33. Univariate Kaplan-Meier Cause Specific Survival Correlation Curve	100
34. Multivariate Kaplan-Meier Cause Specific Survival Correlation Curve	101
35. Image Capture for CGH Analysis from an Archival Uveal Melanoma Case	140
36. An Example of CGH Profile Data	141
37. Interphase FISH Control Using Centromere Probe for Chromosome 3	142
38. Interphase FISH Control Using Telomere Probes for 3p and 3q	143
39. Telomere Probe Signals (3p and 3q) in Uveal Melanoma Cell Lines	144

LIST OF TABLES

1. Uveal Melanoma Cell Lines Used in This Study	8
2. A Comparison of Gains Seen in Ten Uveal Melanoma Cell Lines with Previously Reported Chromosomal Abnormalities in Uveal Melanoma	74
3. A Comparison of Losses Seen in Ten Uveal Melanoma Cell Lines with Previously Reported Chromosomal Abnormalities in Uveal Melanoma	76
4. A Correlation of Copy Number Abnormalities in Ten Uveal Melanoma Cell Lines and Genes Associated with Uveal Melanoma or its Predisposing Factors	78
5. Summary of Aberrations Identified by SKY in Ten Uveal Melanoma Cell Lines	82
6. Chromosome 3 FISH Signals for Ten Uveal Melanoma Cell Lines	86
7. Comparison of CGH, SKY and FISH in Relative Balance (RB) and Relative Chromosome Equivalent (RCE) for Chromosomes 3, 6 and 8	91

ACKNOWLEDGEMENTS

First and foremost, I would like to acknowledge Dr. Joginder Nath, Chair, Genetics and Developmental Biology Program, WVU, for always knowing best, and caring so deeply on a professional as well as personal level. Secondly, I would like to thank the faculty and staff of WVU, who have been so helpful throughout my academic tenure. I credit Dr. Sharon Wenger for opening my eyes to human genetics, and always making time for additional instruction and advice. I also thank Dr. Walt Kaczmarczyk for balancing challenging coursework with a note of levity, and Dr. Dan Panaccione for providing instruction and encouragement.

There are numerous individuals that have been of assistance throughout my time at the AFIP. I extend my deepest thanks to Dr. Alison Director-Myska, AFIP, for sticking with me through thick and thin, and for making the learning process a pleasure. I thank Dr. Ian McLean for making this project possible, and Dr. Timothy O'Leary for sharing his expertise and keeping his door open for me. Thanks to Dr. Robert Becker for offering candid evaluations of my work, and always having one more idea. I extend my gratitude to Karen Bijwaard taking time out of her busy schedule for training in molecular techniques, and Dr. Bill (William) Oliver for keen insight into statistical approaches. Special thanks to Annette Geissel, for putting everything in perspective, and Michelle Webb, for putting up with me and helping me through the rough spots. Finally, I thank Dr. Kimberlee Potter for her career advice and for providing a model of perseverance.

To my fellow students at WVU, whose paths I have crossed, I thank you for making me a better person. I thank Dr. Shawna Jackman, my best friend, without whom

I would not have excelled at WVU, and certainly would not have been able to accomplish this body of work. Thanks also to Dr. Mike Rossi, for setting the standard and never failing to raise the bar, and Jonnie Lane, for breaking the mold and never obeying the norm.

Finally, to Adrian Walleigh, a true friend from beyond the scientific community, who has provided invaluable advice on life and perspective on so many issues. To anyone I may have omitted, my heartfelt apology. Your contribution is not forgotten, but my memory misplaced.

INTRODUCTION

Our understanding of cancer continues to evolve as we develop new approaches in the pursuit of the elusive cure for this multifaceted disease. With each passing day, either a new technique or a new application of an existing technique propels cancer research. At times it seems that the more that is discovered about cancer, the more questions that are encountered. However, significant progress has been made, and will continue to be made, in this arena.

Pathology is concentrated on the morphology and characteristics of tissue at the cellular level. The advent of cytogenetic analyses provided insight beneath the level of the cell, allowing researchers access to information about the chromosome complement within individual cells (Fig. 1). Classical cytogenetics provides us with a karyotype, or a catalogue of chromosome homologues, and allows for banding as well as copy number analysis. Cytogenetics contributes immensely to cancer research, as chromosome abnormalities are often associated with the mechanisms underlying carcinogenesis as well as other disease pathways. Application of *in situ* hybridization (ISH) methods to tumor cells yields a variety of information including numerical data and regarding inter- and intra-chromosomal rearrangements (Cremer *et al.*, 1986; Lichter *et al.*, 1988a; Devilee *et al.*, 1988; Eastmond and Pinkel, 1989; Trask, 1991; Joos *et al.*, 1994). The combination of epifluorescence microscopy and *in situ* hybridization techniques resulted in fluorescence *in situ* hybridization (FISH), which is capable of providing chromosome enumeration, whole chromosome painting, marker identification and gene mapping (Chang and Mark, 1997). In brief, FISH is a fairly rapid technique that involves localization of a labeled deoxyribonucleic acid (DNA) sequence to cellular DNA in

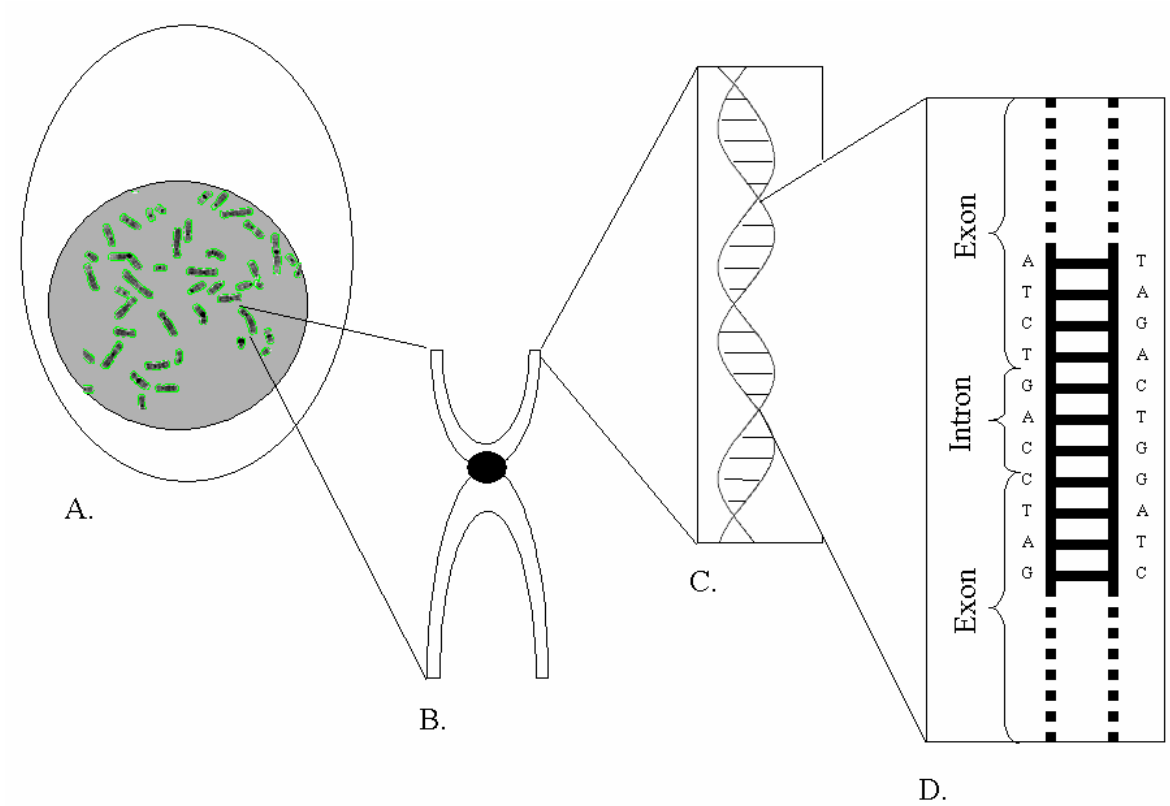


Figure 1. Anatomy of a Nucleus. (A) A stylized drawing of a cell showing a nucleus (gray) containing DNA in the form of chromosomes. (B) A single metaphase chromosome from within the nucleus. (C) Chromosomes are comprised of tightly packed DNA in a double helical conformation. (D) The DNA is made up of nucleotides, of which specific sequences form the exons and introns of genes.

whole tissue, interphase cells or metaphase chromosomes (Fig. 2) (Carpenter, 2001). FISH spawned comparative genomic hybridization (CGH) and spectral karyotyping (SKY), which represent more sophisticated applications of molecular cytogenetics (Kallioniemi *et al.*, 1992; Schröck *et al.*, 1996).

CGH is the comparison of two genomes by hybridization, and is intended to give researchers the ability to locate DNA copy number anomalies with greater frequency and increased sensitivity as compared to conventional cytogenetic methodologies. In CGH, researchers generate fluorescent probes from normal and tumor genomes, and simultaneously hybridize these probes to normal metaphase spreads (Thompson and Gray, 1993; Ried *et al.*, 1997). Comparison of the relative fluorescence along each chromosome results in a ratio profile that shows chromosomal regions of relative gain (e.g., amplification) and loss (e.g., deletion) in the tumor genome. This is predicated upon the normal genomic probe binding uniformly to the normal chromosomes, whereas the tumor genomic probe will show an excess or deficit of specific chromosomes or portions of chromosomes, thereby revealing gains and losses of chromosomal material for the tumor.

The development of CGH preceded SKY, which is in essence a genomic scan using 24-color FISH (Schröck *et al.*, 1996; Macville *et al.*, 1997; Schröck *et al.*, 1997). In SKY, each of the 22 autosomes and the 2 sex chromosomes are assigned a unique combination of fluorochromes, which allows for identification of all 24 of the chromosomes in a single hybridization. The development of ratio-labeling and combinatorial labeling schemes, in particular the inclusion of haptens, allowed for the number of differentially-labeled chromosome paints to exceed the number of

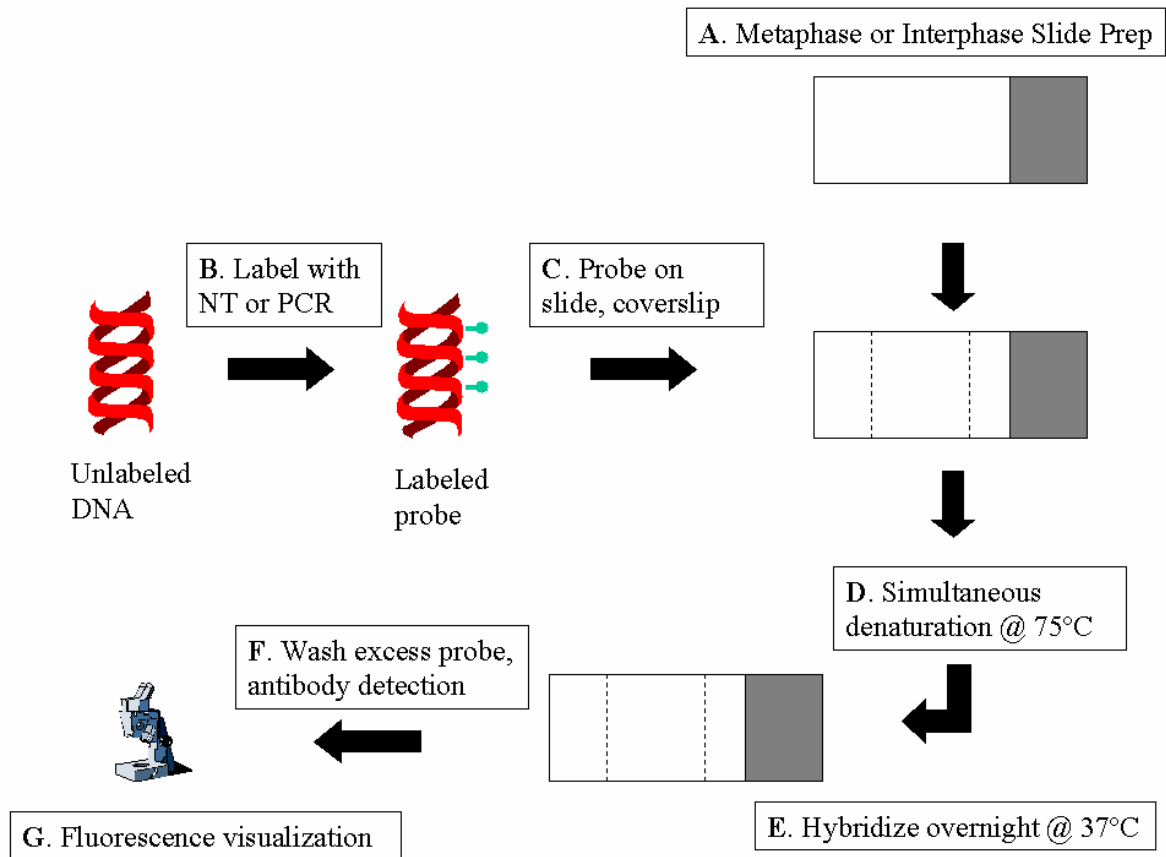


Figure 2. Basic FISH Protocol. This schematic outlines the critical steps in FISH. **(A)** The first step is to prepare metaphase spreads or interphase nuclei on microscope slides, and age these slides for at least a week. Pretreatment of the slide may or may not be necessary. **(B)** Probe is generated via nick translation or polymerase chain reaction. **(C)** This probe is placed on the slide and coverslipped. **(D)** The slide and probe are simultaneously denatured at or near 75°C in order for hybridized probe and target DNA to anneal. **(E)** The hybridized slide is incubated overnight at or near 37°C. **(F)** On the following day, a post-hybridization wash removes excess unbound probe from the slide, and the probe is detected using antibody layering schemes as needed. **(G)** A DNA counterstain is applied prior to mounting of the slide in antifade solution for visualization with fluorescence microscopy.

fluorochromes (Garini *et al.*, 1996; Schröck *et al.*, 1997; Tonon *et al.*, 2000; Schröck and Padilla-Nash, 2000). Although the human eye can not resolve the subtle color differences between some fluorochromes, a Fourier transformation of emitted fluorescence gives each chromosome a distinct spectrum. Construction of the spectral karyotype elucidates both numerical and structural anomalies. This allows determination of an accurate karyotype of many tumor metaphase spreads, which often contain both subtle and complex chromosome rearrangements. An additional feature of SKY is that chromosomal material that can not be karyotyped with confidence in a classical cytogenetic analysis (such as marker chromosomes) can be correctly identified.

Uveal melanoma is but one of a myriad of cancers afflicting humans today. This particular solid tumor is the primary intraocular tumor manifested in adults, and results in loss of vision and in many cases death. Uveal melanoma is any malignant melanocytic tumor originating in the pigmented vascular layer of the eye including the iris, ciliary body and choroid (Fig. 3). Epidemiologic studies show that those at greatest risk are individuals with lightly pigmented skin and/or lightly pigmented eyes (McLean and Gamel, 1996; Regan *et al.*, 1999). The most frequent chromosomal abnormalities are found on chromosomes 3, 6, and 8; other chromosomes have been implicated with varying consistency (Speicher *et al.*, 1994; Prescher *et al.*, 1996; White *et al.*, 1998a). The tumor is thought to share commonalities with other melanomas, yet maintain its own defined subset of causal aberrations (Griffin *et al.*, 1988).

In order to ascertain the chromosomal aberrations that contribute to uveal melanoma, we pursued 2 avenues of research. The first was to employ CGH, SKY and

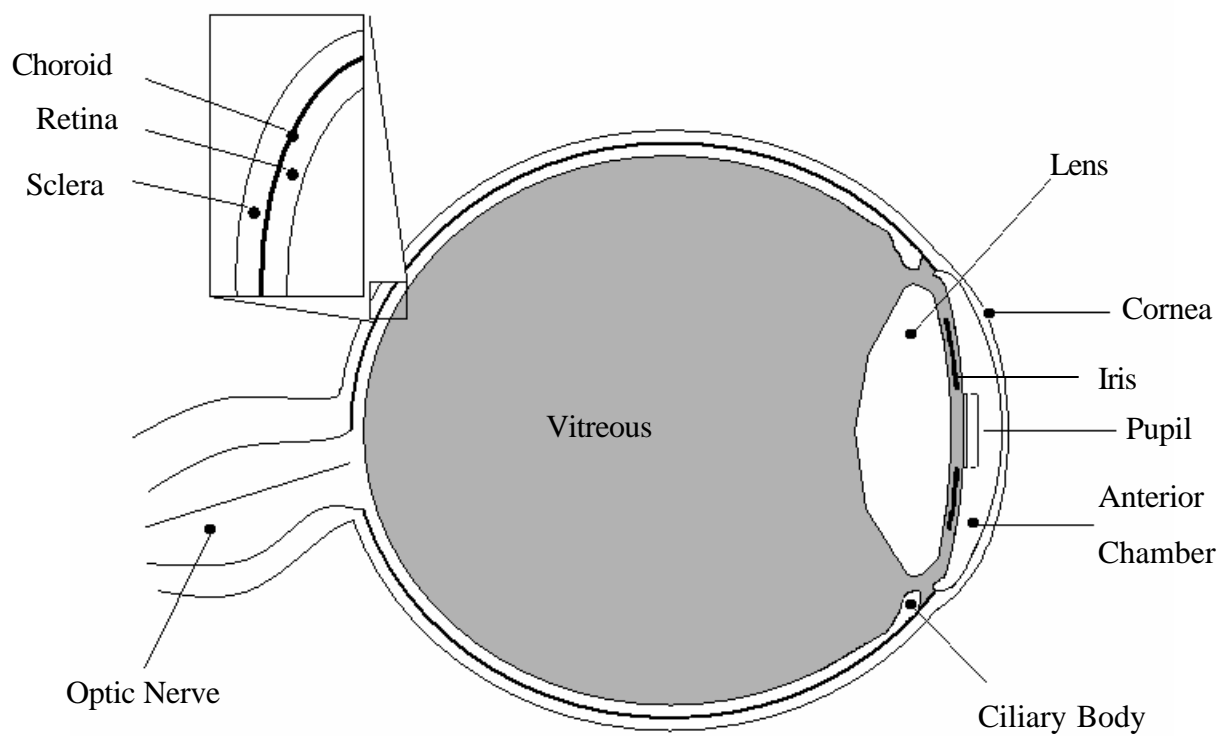


Figure 3. Anatomy of the Ocular Globe. This schematic identifies landmarks within the human eye, and orients the reader with regard to the regions of origin for uveal melanoma. These regions include the choroid, ciliary body and the iris.

FISH to provide a complete molecular cytogenetic evaluation of 10 uveal melanoma cell lines. The second was a comprehensive CGH analysis of 100 archival formalin-fixed paraffin-embedded (FFPE) uveal melanoma tissue samples.

In the first portion of our study, we characterized 10 uveal melanoma cell lines (Table 1) by CGH, SKY and FISH to identify chromosome abnormalities. Characterization of cell lines is often employed as an initial step in characterization and classification of a disease, as they model the alterations in actual tumors. Uveal melanoma cell lines are typically derived from enucleated tissue. Enucleation, or removal of the entire globe of the eye, is a common treatment strategy. Cells from enucleated tissue can be transformed, cultured in an appropriate medium, and maintained as immortal cell lines for subsequent characterizations (De Waard-Siebinga *et al.*, 1995; Luyten *et al.*, 1996). Previous characterizations of uveal melanoma cell lines included not only classical cytogenetic analysis, but also evaluations of specific genes and their expression (Blom *et al.*, 1997; Luyten *et al.*, 1998; Chana *et al.*, 1999). Uveal melanoma cell lines have also been used to model the effects of developing or established treatments (Logani *et al.*, 1995a and b). We expected that a combination of CGH, SKY and FISH would increase sensitivity for detection of abnormalities, and reveal chromosomal regions applicable to uveal melanoma diagnosis, prognosis and treatment. We also expected that the combination of these 3 techniques would ascertain the prevalence of monosomy 3, as it is a hallmark of uveal melanoma (Speicher *et al.*, 1994; Prescher *et al.*, 1996; White *et al.*, 1998a).

For the second portion of our study, we analyzed 100 archival FFPE uveal melanoma cases by CGH. These cases were obtained from the Armed Forces Institute of

Table 1. Uveal Melanoma Cell Lines Used in this Study

Code	Cell Line	Tumor	Origin ^a	Sex ^a	Media	Reference ^b
1	92-1	primary	choroid	F	RPMI 1640	De Waard-Siebinga <i>et al.</i> , 1995
2	MEL270	primary	ciliary body	M	"	Chen <i>et al.</i> , 1997
3	MEL285	primary		F	"	
4	MEL290	primary		F	"	
5	OCM-1	primary	choroid	F	Ham's F-12	Kan-Mitchell <i>et al.</i> , 1989
6	OCM-3	primary			"	
7	OCM-8	primary			"	
8	OM431	primary	choroid		"	Albert <i>et al.</i> , 1984
9	OMM-1	metastatic	subcutaneous metastatic lesion post-enucleation	M	DMEM	Luyten <i>et al.</i> , 1996
10	OMM-2.3	metastatic	liver metastasis of ciliary body tumor (MEL270)	M	RPMI 1640	

^aBlank entries reflect data unavailable at the time of the study.

^bAll cell lines provided courtesy of Dr. Jerry Y. Niedercorn and Ms. Elizabeth Mayhew, both at the Department of Ophthalmology at the University of Texas Southwestern Medical Center at Dallas, in Dallas, TX. Those that have establishment papers in the published literature have been cited.

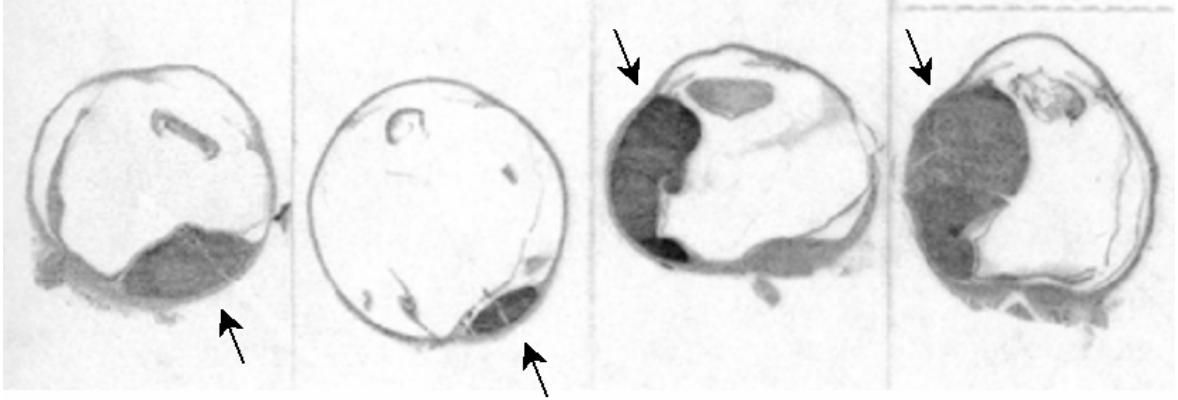


Figure 4. Examples of Uveal Melanoma Tumors. Four hematoxylin and eosin (H&E) stained archival FFPE tissue sections from different uveal melanoma tumor cases. The darkest mass in each ocular globe (indicated by arrows) is the uveal melanoma tumor.

Pathology (AFIP) tissue archives, and comprised of 2 slide-mounted 6 μ m sections of archival FFPE tumor tissue from enucleated human eyes (Fig. 4). Utilization of archival tissue allows for analysis of a larger number of cases, particularly when studying a tumor of low incidence that yields only a few fresh tissue samples each year. Also, archival FFPE tissue allows for correlation of experimental findings with comprehensive patient follow-up, such as visible manifestations of the disease, tumor characterization and grading, patient progress after tumor excision, and survival. Of the 100 cases, 51 survived greater than 9 years without detectable metastasis, and the remaining 49 cases succumbed to metastatic disease within 9 years of diagnosis. It was expected that the regions of amplification and deletion seen in the samples from each patient would be homologous to those seen in the cell line study, and would correlate with survival to allow determination of prognostic factors associated with uveal melanoma. Tumor progression is thought of as a stepwise accumulation of abnormalities in critical genes, and it was our expectation that some chromosomal regions of gain and loss would correlate with malignancy and progression of uveal melanoma (Forozan *et al.*, 1997). Anomalies were tested for univariate prognostic significance, and the most powerful predictors were compared with other histological or clinical predictors in a multivariate analysis.

The amalgamation of results from the cell line and archival tumor portions of our study yielded extensive insight into the chromosome dosage abnormalities characteristic of uveal malignant melanoma. Further, the synthesis of our results allowed us to identify not only predictive loci for this tumor, but also to make some speculation about the genes

involved in development and/or progression of this tumor. Our ultimate goal was to direct further gene-specific study of malignancy in uveal melanoma.

LITERATURE REVIEW

CYTOGENETICS.

The foremost discovery in genetics was the elucidation of the double-helical structure of DNA by Watson, Crick, Wilkins and Franklin by X-ray diffraction (Watson and Crick, 1953). At around the same time, T. C. Hsu first described the use of a hypotonic gradient to swell a cell, allowing for a closer glimpse of the components within the cell membrane (Fig. 1) (Hsu, 1952). In his initial work, Hsu found 23 pairs of autosomes and a pair of sex chromosomes (Fig. 5) (Hsu, 1952). By adapting Hsu's technique, Tjio and Levan revised Hsu's findings of 48 chromosomes, and instead found that humans have a 46 chromosome complement (Tjio and Levan, 1956). A few years later, Hungerford and colleagues produced the first karyotype from peripheral blood culture (Hungerford *et al.*, 1959).

Chromosome banding was developed by Caspersen and colleagues in 1968, providing a useful technique that allowed the entire genome to be analyzed at once (Caspersen *et al.*, 1968; Pinkel *et al.*, 1986a and b; du Manoir *et al.*, 1993). Chromosome banding analyses are of particular import in cancer research, as chromosomal abnormalities can be linked with a cancer phenotype, and identification of consistent or recurrent chromosomal aberrations in tumors is a useful step toward identifying genes involved in the development or progression of the disease (Macville *et al.*, 1997). However, analyses of solid tumors are complicated by low mitotic indices and low quality chromosomal banding, making identification of complex chromosomal aberrations immensely difficult by banding alone (Macville *et al.*, 1997; Veldman *et al.*, 1997; Ried *et al.*, 1997; Rothmann *et al.*, 1998). Hence, there is a critical need

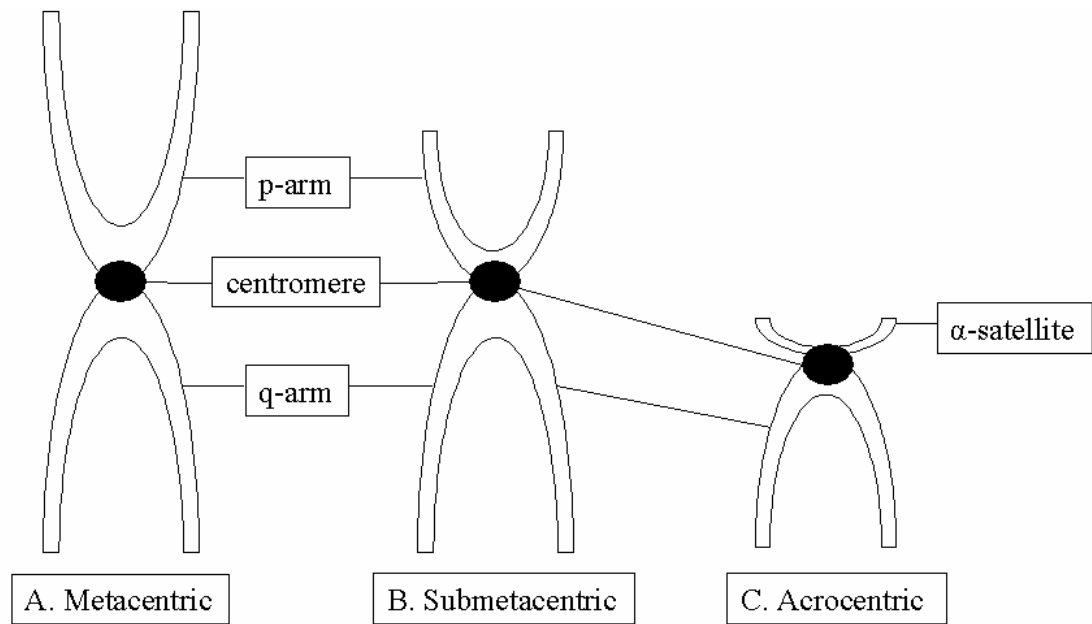


Figure 5. Anatomy of the Chromosomes. Chromosomes are comprised of 2 arms, the p- and the q-arm, and the arms are connected by a centromere. The exceptions are the acrocentric chromosomes, where the p-arm is actually alpha-satellite repeats. Chromosomes can be broken into 3 groups based on centromere location, and irrespective of size or relative DNA content. **(A)** The metacentric chromosomes are defined by their centrally-located centromere, and include 1, 2, 3, 16, 19 and 20. **(B)** The submetacentric chromosomes have an offset centromere that makes the p-arm shorter than the q-arm. This group includes 4, 5, 6, 7, 8, 9, 10, 11, 12, 17, 18 and X. **(C)** The acrocentric chromosomes are predominantly comprised of q-arm material, but have small satellites above the centromere, and include 13, 14, 15, 21, 22 and Y.

to develop more accurate and reliable methods for determination of chromosome abnormalities.

FLUORESCENCE *IN SITU* HYBRIDIZATION.

In situ hybridization (ISH) was developed as a means of detecting nucleic acid sequences in morphologically intact samples (Gall and Pardue, 1969; John *et al.*, 1969). It is based on the principle that DNA is able to denature and renature in a complementary fashion (Fig. 6). In principle, two nucleic acid sequences are found to be complementary; (1) the probe, which is the isolated and tagged sequence that the researcher is interested in localizing, and (2) the target sequence, which is a length of nucleotides within the DNA of the sample that matches the probe sequence. When both the sample and probe are denatured together, and allowed to reanneal, the probe binds to its complementary sequence in the target DNA. After the DNA has reannealed, the probe can be visualized and its location pinpointed within the sample.

The first applications of ISH were in 1969, when Gall and Pardue hybridized radioisotope-labeled ribosomal ribonucleic acid (rRNA) to tissue squashes, revealing the complementary ribosomal deoxyribonucleic acid (rDNA) *in situ* (Gall and Pardue, 1969). Also in 1969, John and colleagues experimented with RNA-DNA hybrids visualized by autoradiography (John *et al.*, 1969). In the earliest applications of ISH, the nucleic acid probe (either DNA or RNA) was labeled with a radioisotope, hybridized to its complementary DNA sequence in a cell or tissue sample, and visualized using autoradiography (Gall and Pardue, 1969; John *et al.*, 1969). The first non-isotopic ISH application involved immunofluorescence detection of the RNA-DNA hybrids by a

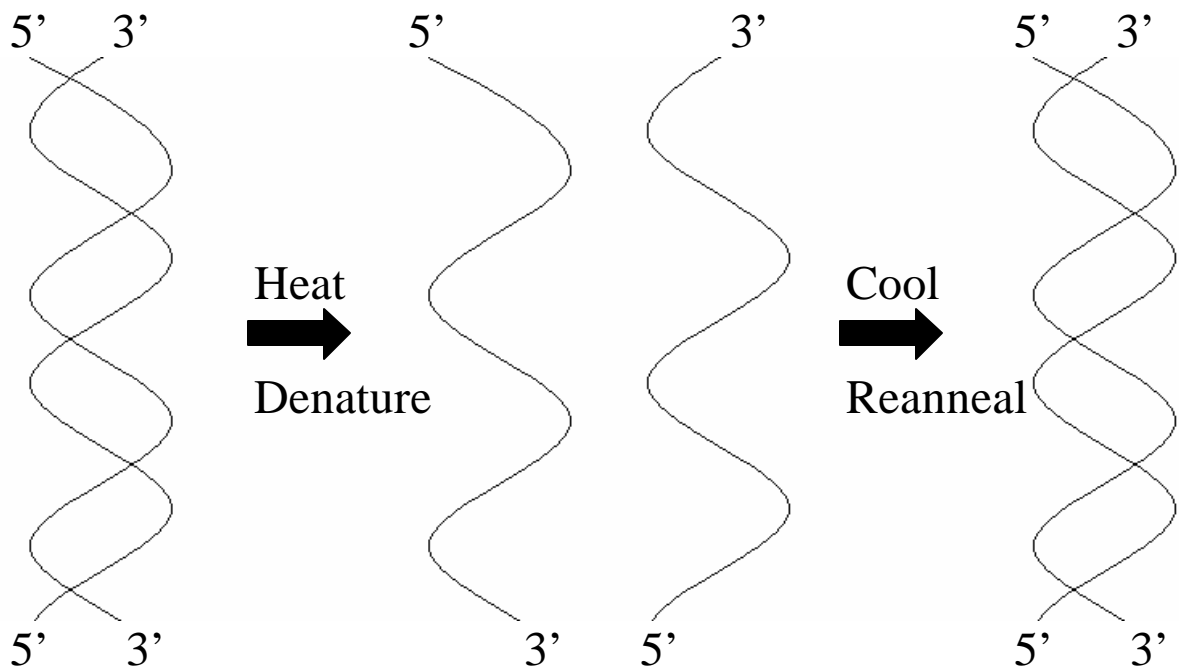


Figure 6. Denaturation/Renaturation of DNA. DNA will denature when the ambient temperature is sufficiently high, and will reanneal when the temperature falls below the melting point. It is this property of DNA that makes hybridization feasible. In a basic hybridization, the probe will find its complementary sequence of nucleotides in the target DNA and bind to them, which functionally incorporates the probe into the target DNA once all of the DNA has had an opportunity to reanneal. Then, the probe can be visualized and localized within the target DNA. This simple property of DNA forms the basis for such techniques as ISH, FISH, CGH and SKY.

This figure was adapted from University of Michigan Health System, <http://seqcore.brcf.med.umich.edu/doc/educ/dnapr/pg2.html>.

fluorescent antibody bound to the hybrids (Rudkin and Stollar, 1977). Use of radioisotope labeling was superseded by applications of non-isotopic conjugated probes in 1980s (Bauman *et al.*, 1980; Langer *et al.*, 1981; Pinkel *et al.*, 1986b). Bauman and colleagues described the covalent linkage of tetramethyl rhodamine isothiocyanate (TRITC) to RNA, which when used simultaneously with a ^3H -labeled complementary RNA (cRNA) allowed both fluorescence and scintillation quantitation (Bauman *et al.*, 1980). Technically, this was the first application of a directly-labeled fluorescent probe.

FISH completed its evolution from ISH, by replacing all radioisotopes with fluorescence labeling (Fig. 2). The first alternatives to labeling with radioisotopes were biotin-labeled UTP and dUTP, described by Langer and colleagues in 1981 (Langer *et al.*, 1981). The use of non-isotopic probes has led to improved resolution, decreased preparation time and increased probe stability (Trask, 1991).

In 1986, Pinkel and colleagues described the first fluorescent hybridizations employing biotinylated probes and fluorescently-labeled avidin (Pinkel *et al.*, 1986a and b). Indirectly-labeled probes are conjugated with a reporter-binding molecule (or hapten), whereas directly-labeled probes are conjugated with a fluorochrome (Joos *et al.*, 1994) (Fig. 7). Haptens include biotin, digoxigenin, dinitrophenyl (DNP), aminoacetylfluorene (AAF), mercury and sulfonate (Trask, 1991; Luke and Shepelsky, 1998). Biotin is detected with either a fluorochrome-conjugated avidin or an anti-biotin antibody, while mercury is detectable with a ligand bearing a sulfhydryl group (Trask, 1991). Digoxigenin and the remaining haptens are detected with fluorescently-labeled antibodies (Trask, 1991). The use of directly-labeled probes is a more time-efficient method, and generally results in less background than indirectly-labeled probe

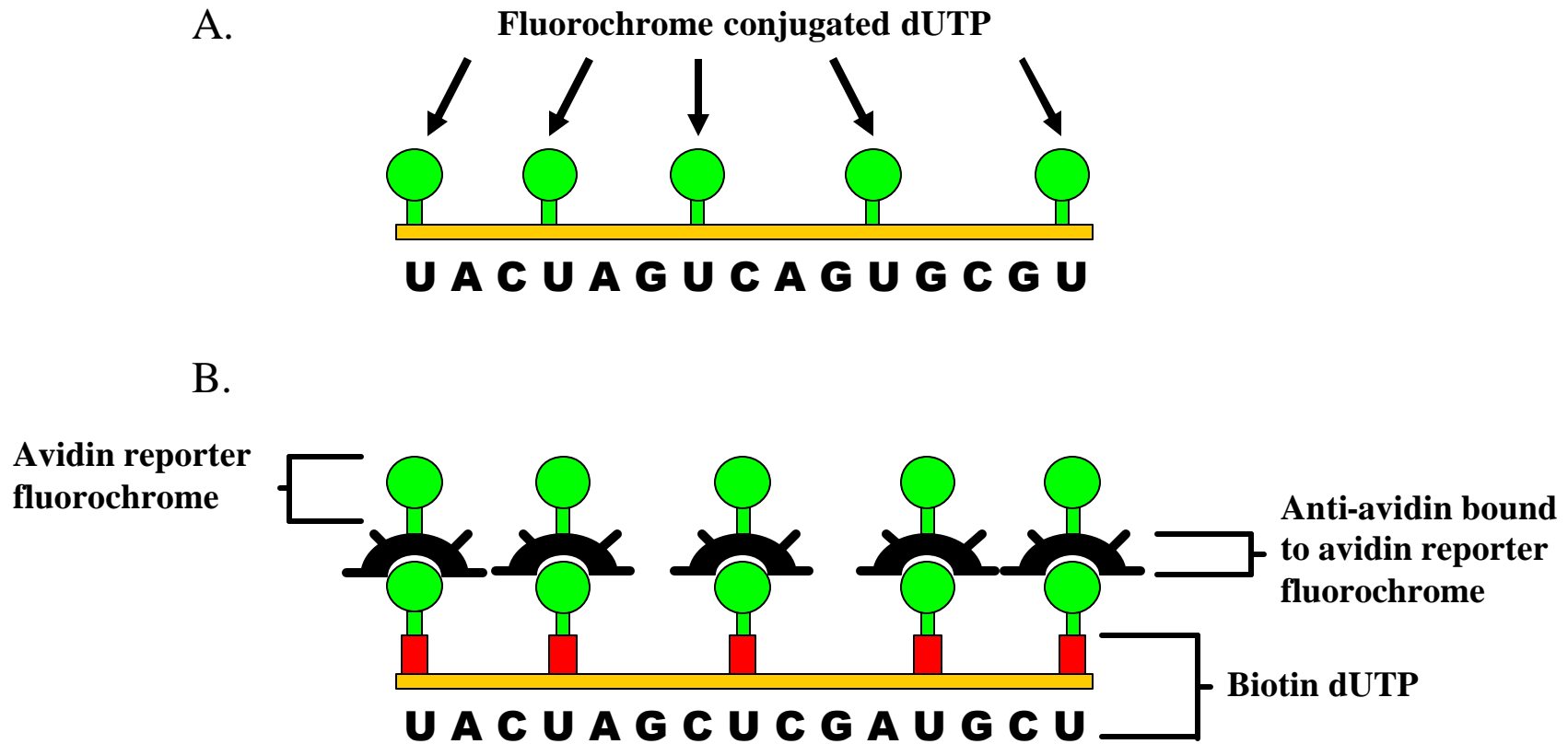


Figure 7. Comparison of Directly- and Indirectly-labeled Probes. **(A)** Directly-labeled probe. The reporter fluorochrome is directly conjugated to the dUTP, and visualization of the probe is possible immediately following hybridization. **(B)** The indirectly-labeled probe has a hapten-labeled dUTP incorporated into its sequence, in this case biotin-dUTP, and detection using antibody layering is required following hybridization. An avidin reporter fluorochrome binds to each biotin-dUTP, and a biotinylated anti-avidin binds to each avidin. A second avidin reporter fluorochrome then binds to the biotinylated anti-avidin. The antibody layering process is repeated as needed to amplify the probe signal by successive addition of avidin reporter fluorochrome layers.

This figure courtesy of Dr. Alison E. Director-Myska, AFIP.

applications upon visualization. The advantage of direct incorporation of the fluorochrome into the probe, is that the fluorochrome is confined to the binding site. In indirect applications, the dyes precipitate around the binding site and are therefore less specific and result in increased background noise (Demetrick, 1999). However, increased sensitivity is achieved through the use of an indirectly-labeled probe, which allows for multiple layers of antibodies, thus increasing the signal intensity.

The advent of FISH narrowed the gap between cytogenetics and molecular genetics, and gave rise to the field of molecular cytogenetics (Macville *et al.*, 1997). FISH, as used in molecular cytogenetics, is equally applicable to metaphase spreads, interphase nuclei preparations, and tissue sections (Cremer *et al.*, 1986; Lichter *et al.*, 1988a; Devilee *et al.*, 1988; Eastmond and Pinkel, 1989; Trask, 1991; Joos *et al.*, 1994). “Interphase cytogenetics” was a term coined by Cremer and colleagues in 1986 for the detection of chromosome aberrations in interphase cells (Cremer *et al.*, 1986). They later expanded this definition to include detection in non-mitotic cells at any stage of cell division, due to modifications made by Lichter *et al.*, (Cremer *et al.*, 1988; Lichter *et al.*, 1988a).

Lichter and colleagues refined suppression of non-informative regions of repeat, found in regions such as centromeres, telomeres, heterochromatin, and other families of repeat sequences in the genome, thus enhancing detection of chromosome-specific regions of repeat (Lichter *et al.*, 1988a). “Chromosomal *in situ* suppression” (CISS), a term first coined in 1988, described the use of unlabeled competitor DNA to suppress of regions of repeat (Lichter *et al.*, 1988a). These regions of repeat are common on many chromosomes in the genome, and also are very quick to reassociate after denaturation

(Lichter *et al.*, 1988a and b). Both of these factors interfere with accurate hybridization between the probe and target DNA. Incorporation of human Cot-1 DNA inhibits the binding of repetitive sequences such as the *Alu I* and *Kpn I* repeat families (Lichter *et al.*, 1988a and b). Incorporation of salmon testes DNA binds repeat sequences other than the two previously mentioned families of repeats, and prevents non-specific binding of the probe to the slide or coverslip (Lichter *et al.*, 1988a). Each of these are included in the probe cocktail for suppressive hybridization schemes.

The most important reason for development of interphase FISH techniques, is that it alleviates the need for metaphase preparations, which are often limited or otherwise unavailable in tumor preparations (Bayani and Squire, 2002). The use of interphase nuclei provides higher resolution due to the decreased condensation of nuclear DNA (Lawrence *et al.*, 1988; Devilee *et al.*, 1988; Joos *et al.*, 1994).

Once the ability to detect a single probe in interphase applications had been refined, the detection of multiple targets was the next logical step. A double-labeled single-target FISH experiment by Cremer and colleagues marked the first multicolor fluorescence FISH experiment, and a double-labeled double-target FISH hybridization was carried out in solid tumors shortly thereafter (Cremer *et al.*, 1988; Hopman *et al.*, 1988). These experiments further demonstrated the increased resolution in interphase cells as compared to metaphase preparations (Hopman *et al.*, 1988). In 1989, Nederlof and colleagues were able to detect 3 hybridization targets using a third fluorochrome spectrally distinct from fluorescein isothiocyanate (FITC) and TRITC (Nederlof *et al.*, 1989). In 1990, the same group expanded the number of hybridization sites to 4 using the first combinatorial labeling schemes (involving 2 fluorochromes) (Nederlof *et al.*, 1990).

At that time, it was postulated that the number of spectrally-distinct fluorescent hybridization sites could be expanded to 7 using a combination of fluorochromes and conjugated haptens. The complex hybridization of 7 probes to 7 loci was not realized until 2 years later (Ried *et al.*, 1992a).

Ried and colleagues were also able to utilize 5 distinct whole chromosome paints in a single hybridization to assay ploidy of 5 chromosomes critical in prenatal diagnosis (Ried *et al.*, 1992b). Also in 1992, Dauwerse *et al.* demonstrated that combining 2 fluorochromes in varying ratios (ratio-labeling) allowed for the distinction of up to 7 whole chromosome paints in a single exposure, significant because the maximum possible number of distinct loci was also 7 at that time (Dauwerse *et al.*, 1992). They also suggested that inclusion of a third fluorochrome in their ratio-labeling scheme would allow distinction of half of the chromosome complement (Dauwerse *et al.*, 1992). FISH was only limited by the ability to distinguish the spectra of multiple probes in a single preparation. In other words, the number of hybridization sites was only limited by the ability of the analysis software and the user to distinguish between different fluorochromes or combinations of fluorochromes (Joos *et al.*, 1994; Garini *et al.*, 1996). The evolution of multicolor FISH analyses would eventually lead to development of genome-labeling techniques, such as multiplex-FISH (M-FISH) and SKY, which allow distinction of all 22 autosomes and the sex chromosomes in a single hybridization.

Since its inception, FISH has evolved into a technique applicable to dividing or non-dividing cells in either fresh or archival tissue (Trask, 1991). FISH can be used as an exploratory or a confirmatory technique. Given an appropriate hybridization scheme, FISH can be employed to detect inversions, translocations, deletions, dicentrics and ring

chromosomes (Trask, 1991). The technique itself is generally not very time consuming, as detection and/or visualization can often be performed a day or two after hybridization. Specificity of a probe depends on base-pair composition (G-C bonds are stronger than A-T), temperature of denaturation and hybridization, as well as the salt and formamide concentrations in the hybridization mixture (McNicol and Farquharson, 1997).

There are essentially three types of probes currently widespread in use, each with a slightly different intended application. The first are locus-specific probes, which, hybridize to a specific chromosomal locus (Tonon *et al.*, 2000). These probes are generated from plasmids, phages, cosmids, or YAC-clones (Cremer *et al.*, 1986; Joos *et al.*, 1994). The efficiency of the hybridization is proportional to the size of the probe, because the ability to detect a hybridization decreases as the probe size decreases (Trask, 1991). A gene-specific probe, one kind of locus-specific probe, is generated from an entire gene or a portion of a gene and hybridized to determine where it will localize (e.g. the location of the gene on a chromosome).

The second type of probe is a chromosome-specific repetitive sequence probe, and this type of probe can be targeted to centromeres (heterochromatin containing alphoid repeats or alpha-satellite DNA) or telomeres (highly repetitive sequences at the ends of each chromosome). These probes are typically used in chromosome enumeration studies, which are focused on determination of the number of copies of a given chromosome in a preparation (Pinkel *et al.*, 1986b; Eastmond and Pinkel, 1989; Joos *et al.*, 1994; McNicol and Farquharson, 1997; Demetrick, 1999). Hybridization of these probes is typically very intense, as the areas hybridized in conserved portions of heterochromatin are often very compact (Trask, 1991).

The third type are whole chromosome probes, also known as whole chromosome paints, which are in actuality a group of probes all generated from a single chromosome that fluoresce along the length of the entire chromosome when hybridized (Pinkel *et al.*, 1988). This type of FISH probe is used to identify chromosome-specific material and determine rearrangements associated with the probed chromosome in the genome (Tucker *et al.*, 1994; Carter, 1994; Demetrick, 1999). These genomic rearrangements can be symmetrical (e.g. reciprocal translocations) or asymmetrical (e.g. insertions and non-reciprocal translocations) exchanges (Tucker *et al.*, 1994). Initially, flow-sorted chromosomes were used to generate DNA libraries, which were later used to make whole chromosome paints (Carter, 1994; Joos *et al.*, 1994; Luke and Shepelsky, 1998). Flow-sorting remains a viable technique for isolating normal chromosomes for painting, and can also be used to isolate populations of aberrant chromosomes for production of painting probes provided the aberrant chromosomes are distinguishable from normal chromosomes using this technique. Alternatively, microdissection of specific chromosomes is possible and allows for aberrant chromosomes to be individually selected and then used to generate probes (Ried *et al.*, 1997; Bayani and Squire, 2001). Combination of 24 chromosome-specific paints into a single hybridization cocktail is the essence of spectral karyotyping, while generation of single-fluorochrome whole genome probes for CGH applications is an expansion upon the use of whole chromosome paints. Even though combinatorial and ratio-labeling schemes increased the scope and application of FISH, it is cumbersome to screen tumor genomes for gains, losses, and rearrangements with individual FISH probes (Raap, 1995; Raap, 1998).

COMPARATIVE GENOMIC HYBRIDIZATION.

In 1992, Kallioniemi *et al.* developed a molecular cytogenetic technique capable of detecting and mapping relative DNA sequence copy number differences between 2 genomes competitively hybridized to normal chromosomes (Kallioniemi *et al.*, 1992). In this technique, a copy number karyotype is generated for a tumor by comparing the DNA from malignant and normal cells, thereby identifying regions of gain or loss in the DNA along the length of each chromosome. In actuality, the gains and losses are representative of global genetic variation in the test sample, and the data output is really a measure of genomic balance (Kallioniemi *et al.*, 1992; Thompson and Gray, 1993; Houldsworth and Chaganti, 1994; Ried *et al.*, 1997). The inception of CGH was directly linked to the need for a rapid and comprehensive assessment of genetic balance where DNA, not cells for culture and chromosome preparation, was the only available material (du Manoir *et al.*, 1993; du Manoir *et al.*, 1995b; Raap, 1995).

CGH is a quantitative two-color fluorescence *in situ* suppression hybridization technique useful in detecting copy number changes throughout an entire genome (Thompson and Gray, 1993; Ried *et al.*, 1997). In other words, it is essentially double-labeled double-target FISH, wherein total genomic tumor DNA and total genomic DNA from normal diploid tissue are differentially labeled and then simultaneously hybridized to normal metaphase chromosomes. The resulting copy number ratio reveals any genomic imbalance between the two. CGH is an improvement on single-color hybridizations, because the normal DNA is an “internal hybridization intensity control” for each location in the genome (Kallioniemi *et al.*, 1994).

CGH has numerous advantages, most notably it elucidates gains (e.g. amplifications) and losses (e.g. deletions) of DNA, often undetectable via classical cytogenetic techniques. Classical cytogenetic analyses are hindered by the inability to produce large numbers of high quality tumor metaphases due to low mitotic indices, poor growth in culture, and the increased likelihood of bacterial and/or necrotic tissue contamination (Joos *et al.*, 1994; Houldsworth and Chaganti, 1994; Isola *et al.*, 1994). In CGH, extracted genomic DNA is the only material required from the test sample, increasing its application to include both fresh and archival tissue (Houldsworth and Chaganti, 1994; Ghazvini *et al.*, 1996). Karyotypic analysis of solid tumors is difficult due to the instability of tumor cells in culture, but CGH alleviates the need for *in vitro* tumor cell culture, because, in contrast to traditional karyotyping, it only requires DNA and therefore reduces subpopulation selection (Joos *et al.*, 1994). Imbalances in a subset of the cells in a given sample do not interfere with the global analysis of the tumor as long as tumor cells account for most of the DNA (du Manoir *et al.*, 1993; Lundsteen *et al.*, 1995). However, the effect of intratumor genetic heterogeneity on sensitivity of CGH is variable, as heterogeneous aberrations in a given sample are averaged while homogeneous aberrations are emphasized (Kallioniemi *et al.*, 1992; Kallioniemi *et al.*, 1993). Similarly, if normal tissue accounts for more than 50% of the total DNA from the test sample, ratio changes may not be reliably detected (Kallioniemi *et al.*, 1994).

As mentioned earlier, one advantage of CGH is the construction of DNA probes from archival FFPE tissue; this is unique in that the vast majority of cytogenetic techniques require viable tissue (Isola *et al.*, 1994; du Manoir *et al.*, 1995b). Utilization of FFPE tissue allows for analysis of a larger number of cases and for correlation of

experimental findings with comprehensive patient follow-up and survival data. FFPE tumor analysis allows for investigation of very old samples, however, fixation methods may negatively affect DNA quality and yield (Isola *et al.*, 1994). In analysis of FFPE tumors, microdissection of tissue sections, using hematoxylin and eosin (H & E) stained slides for confirmation, has both advantages and disadvantages. An obvious advantage is the selection of only tumor material, because, as mentioned earlier, normal cells “dilute” the CGH results (du Manoir *et al.*, 1993; Houldsworth and Chaganti, 1994; Joos *et al.*, 1994). The disadvantages of tumor microdissection lie in the small yield of DNA, particularly from tissue of reduced cellular density such as the eye. This particular disadvantage can be overcome by polymerase chain reaction (PCR) amplification of relatively pure DNA. The use of degenerate oligonucleotide primed-PCR (DOP-PCR) for small quantities of DNA (as little as 100pg), as first described by Telenius and colleagues, ensures reliable amplification of the template DNA (Fig. 8) (Telenius *et al.*, 1992a and b; Speicher *et al.*, 1993; Kallioniemi *et al.*, 1994; Joos *et al.*, 1994). The DOP primer is actually a family of primers that have a degenerate middle sequence that allows the primers to bind to more sites within the template DNA, and thereby results in a probe that more accurately represents the original genomic DNA from the microdissected tumor.

The primary shortcoming of CGH, is that it does not detect balanced rearrangements, such as translocations, because there are no copy number gains or losses associated with such events. For this same reason, point mutations and small intragenic rearrangements go undetected as well (Kallioniemi *et al.*, 1994; Raap, 1995; Ried *et al.*, 1997). CGH provides no insight regarding the arrangement of chromosome segments

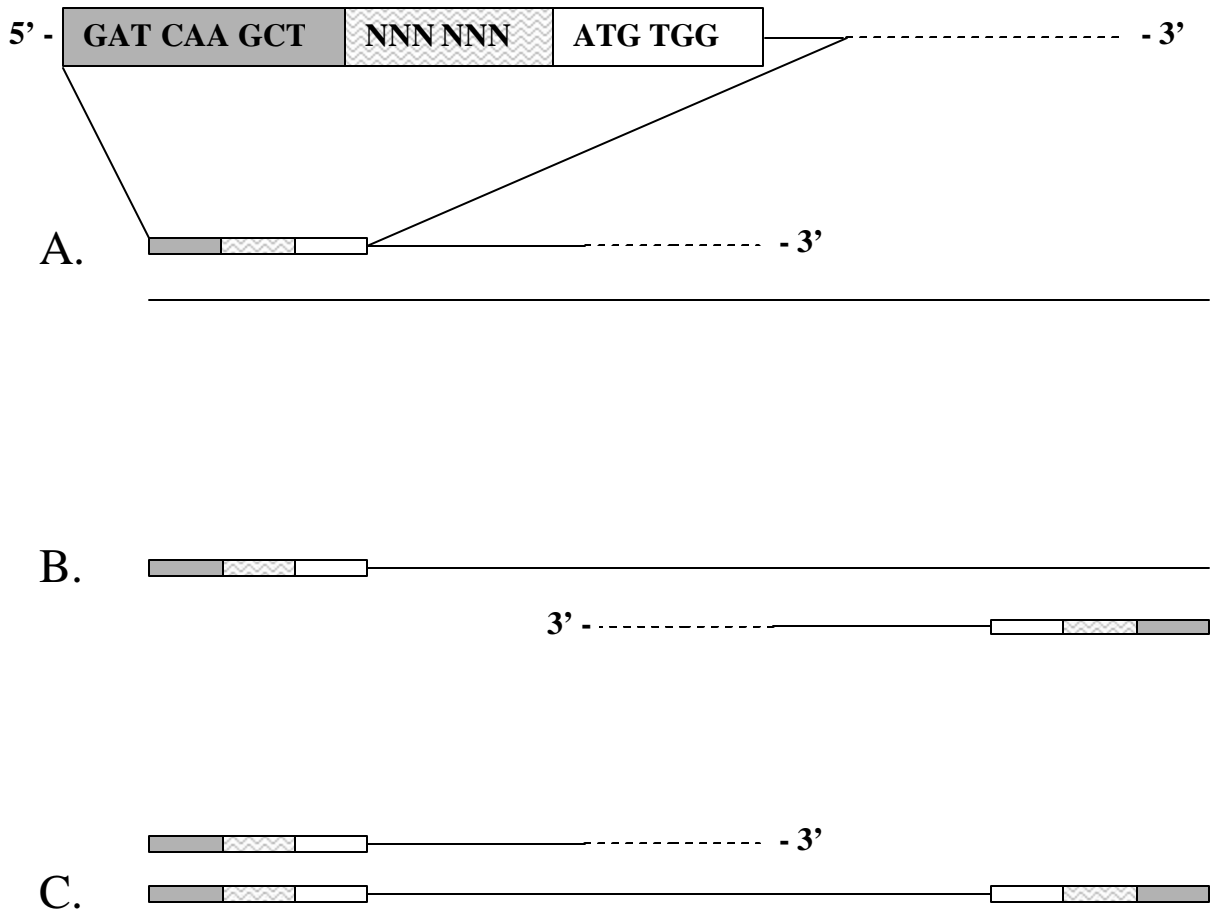


Figure 8. DOP-PCR Amplification of Genomic DNA. The 5' end sequence (gray) is more conserved than the 3' end of the primer (white). In between, is a variable six nucleotide sequence that introduces reduced stringency in to the PCR reaction. **(A)** In the first PCR cycle, the DOP primer binds to genomic DNA, and the inherent degeneracy of the primer combined with the reduced stringency of a relatively low annealing temperature allows it to bind with diminished specificity as compared to conventional PCR primers. The polymerase extends the sequence in the 3' direction from the sequence of primer attachment. **(B)** In the cycles that follow, the annealing temperature is still sufficiently low to allow relatively uniform amplification of all genomic sequences. **(C)** In the subsequent cycles, the annealing temperature is increased with each cycle, eventually requiring that the entire length of the primer binds to the template strand.

This figure was adapted from Telenius *et al.*, 1992a.

involved in reported gains and losses, nor does it help explain the origin of marker chromosomes. Further, the technique has no application for instances of clonal heterogeneity, since it only detects aberrations present in a majority of cells in a given sample (du Manoir *et al.*, 1993; Raap, 1995; Ried *et al.*, 1997; Chang and Mark, 1997). In such instances, abnormalities may cancel one another or be too infrequent to detect (Kallioniemi *et al.*, 1994). Since CGH only detects copy number changes relative to the average copy number it can not distinguish genomic changes in ploidy, as there is no difference in the test:reference ratio between or within specific chromosomes in these cases (Kallioniemi *et al.*, 1994). Sensitivity of detection for deletions is related to ploidy level as well; it is easier to detect a single copy loss in a diploid test sample than in a triploid or tetraploid test sample (Kallioniemi *et al.*, 1994). Copy number changes are also difficult to quantify, even if they are not the result of aneuploidy, as the fluorescent signal tends to spread over a region greater than the length of the amplicon. This presumably results from the complex organization of the target DNA (Kallioniemi *et al.*, 1992). An additional limitation is that some chromosomal aberrations will not be detected because they occur in regions smaller than can be resolved by CGH, which has a resolution of approximately 10-20Mb (Kallioniemi *et al.*, 1992; Kallioniemi *et al.*, 1993, Thompson and Gray, 1993). Therefore, such regions are only detected when the level of amplification is high (5-10 fold for 1Mb region) (Thompson and Gray, 1993; Houldsworth and Chaganti, 1994; Raap, 1995; du Manoir 1995b; Forozan *et al.*, 1997). CGH is predicated upon appropriate chromosome classification of the normal target metaphase, whether by the software, the user, or an interaction between the two. Chromosome classification is an inherent source of error, as misclassification seriously

affects the results, and it is also the greatest limiting factor in the processing of CGH data (Raap, 1995, Lundsteen *et al.*, 1995).

Image preparation is of paramount importance in CGH. Homogeneity in an image is usually recognizable given a uniform reference paint. Homogeneity is highest when hybridizing a directly-labeled probe, reduced with indirectly-labeled probe, and reduced again with multiple layers associated with signal amplification of an indirectly-labeled probe (Lundsteen, 1995). Reduced homogeneity is akin to increased granularity or improperly sized probe, and indicative of a poor hybridization. The spread of the metaphase chromosomes, image realignment due to pixel shift between filter changes, and proper plane of focus all merit consideration in the processing of CGH images (du Manoir *et al.*, 1995a). Selected metaphases should be of a similar degree of condensation, but some CGH analysis packages compensate for variations in condensation by normalization through linear stretching to fit the profile (Lundsteen, 1995; du Manoir *et al.*, 1995b). Criteria for a good metaphase for analysis are as follows: (a) hybridization is smooth and high in intensity; (b) test (green) and reference (red) distributions are similar among sister chromatids; (c) background is low and uniform; (d) binding at centromeres and other regions of repeat is minimal; and (e) chromosomes are of acceptable morphology providing for adequate 4',6-diamidino-2-phenylindole (DAPI) banding and there are few or no overlaps (Kallioniemi *et al.*, 1994). A minimum of 5 to 10 examples of each chromosome should be measured. In our lab, the preference was for 10 metaphases, which should yield 20 measurable examples of each chromosome. It should be noted that analysis of many chromosomes is not a substitute for quality hybridizations (du Manoir *et al.*, 1995a and b).

Fundamentally, CGH results are a comparison of green to red fluorescence intensities. These intensities are integrated along the length of each chromosome for both chromatids, and the result is the green:red ratio profile. Copy number gains and losses are determined by assigning absolute thresholds to the ratio profiles. Thresholds are determined by desired sensitivity, and may be adjusted to compensate for ploidy if a determination using independent methods is possible (du Manoir *et al.*, 1993; du Manoir, 1995b). All of the green:red ratio profiles collected across all chromosomes represent the copy number karyotype (ratio comparisons) for test (green) and reference (red) samples. The copy number karyotypes from multiple metaphases are combined to reduce noise from spread variation and enhance “visibility” of true copy number aberrations in a given test sample (Kallioniemi *et al.*, 1994; Piper *et al.*, 1995).

Regions of repeat must be suppressed to accurately measure ratios in adjacent chromosomal regions. Typically, these centromeric, heterochromatic and telomeric regions are partly suppressed with human Cot-1 DNA and salmon testes DNA, but still vary widely in copy number (either extremely high or low) (Kallioniemi *et al.*, 1994; du Manoir *et al.*, 1995b; Ried *et al.*, 1997). This variation in heterochromatin is elevated if the test and reference are of different donors (du Manoir *et al.*, 1993; Kallioniemi *et al.*, 1994). Similar difficulties are encountered with telomeric DNA.

Thompson and Gray suggested that CGH be enhanced by follow-up with FISH to detect or confirm changes in chromosome number, translocations, inversions, or derivative chromosomes (Thompson and Gray, 1993). While this remains true, a more sensitive and revealing analysis on a per-cell basis was made available with the introduction of SKY. In consideration of all of the benefits of CGH, the most notable

downside to the technique is the inability to detect the chromosomal structure underlying the gains and losses (Houldsworth and Chaganti, 1994). The development of SKY fostered the detection of most structural rearrangements, and allowed for a more complete molecular cytogenetic analysis of tumors when used in conjunction with CGH.

SPECTRAL KARYOTYPING.

FISH has become an integral technique in cancer research and other cytogenetic diagnoses, but the field of molecular cytogenetics benefits greatly from FISH-based techniques that screen the entire genome (Schröck *et al.*, 1996; Macville *et al.*, 1997; Schröck *et al.*, 1997). SKY is one such technique wherein the structural and numerical analysis of all chromosomes is made possible by a combinatorial labeling scheme and advances in image acquisition and analysis (Schröck *et al.*, 1997; Schröck and Padilla-Nash, 2000). Unlike CGH, SKY is only applicable to fresh material capable of cell division (Schröck *et al.*, 1996; Ried *et al.*, 1997). One of the most attractive features of this technique, is the ability to identify chromosomal aberrations rapidly and without any previous indication of the abnormalities, as the technique explores the entire genome in a single hybridization (Cohen *et al.*, 1997; Rothmann *et al.*, 1998). In addition, the chromosomal composition of previously unclassified marker chromosomes is revealed (Rothmann *et al.*, 1998; Bayani and Squire, 2001). In essence, SKY is the ideal hybrid of the functionality of CGH and FISH; it provides a screen of an entire genome, like CGH, with the sensitivity of FISH for detection of structural and numerical chromosomal aberrations (Chang and Mark, 1997; Schröck *et al.*, 1997).

In particular, this technique facilitates a differential display of all human chromosomes in a color karyotype using 24 distinct colors, with a resolution of 1-2Mb

(Macville *et al.*, 1997; Rothmann *et al.*, 1998; Tonon *et al.*, 2000; Bayani and Squire, 2001). Whole chromosome probes are generated via DOP-PCR and differentially labeled with various combinations of 5 fluorochromes, thus producing 24 distinctly colored paints (Garini *et al.*, 1996; Schröck *et al.*, 1997; Tonon *et al.*, 2000; Schröck and Padilla-Nash, 2000). Typically, 3 of the fluorochromes are directly incorporated into the probes via fluorochrome-labeled dNTPs (rhodamine, Texas-Red or Spectrum Orange, FITC or Spectrum Green, and Cy3). The other 2 are incorporated via hapten-cojugated dNTPs, typically detected with avidin Cy5 and mouse anti-dig Cy5.5, and sometimes amplified further by antibody layering (Garini *et al.*, 1996; Macville *et al.*, 1997; Tonon *et al.*, 2000). Inclusion of unlabeled competitor DNA (i.e. Cot-1 and salmon testes DNA), as previously described for CGH and FISH, allows for suppression hybridization and contributes to accurate chromosome painting and resolution of chromosome abnormalities (Macville *et al.*, 1997).

As stated earlier, a specific color is assigned to each chromosome using a combination of these direct and indirect labels. SKY is similar to M-FISH, in that each technique uses combinatorial labeling to identify chromosomes. The use of combinatorial labeling allows for the number of targets to exceed the number of fluorochromes, particularly given the breadth of hapten-labeling and detection schemes (Garini *et al.*, 1996; Macville *et al.*, 1997; Ried *et al.*, 1997; Garini *et al.*, 1999). Basic FISH applications are hampered by the fact that the spectra of the available fluorochromes overlap, and therefore it is not possible to define 24 separate probes (Ried *et al.*, 1997). However, M-FISH overcomes this by detecting each fluorochrome separately using a set of applicable filters, and requires separate image captures and

subsequent overlay prior to image analysis (Speicher *et al.*, 1996). On the other hand, SKY simultaneously excites all fluorochromes and determines the emission spectra, or peak intensity and wavelength, at each pixel in a single image for the entire metaphase spread (Schröck *et al.*, 1996; Ried *et al.*, 1997; Rothmann *et al.*, 1998; Lee *et al.*, 2001).

Spectral imaging, the foundation for SKY, is based upon a combination of spectroscopy and imaging (Garini *et al.*, 1996; Macville *et al.*, 1997; Ried *et al.*, 1997; Rothmann *et al.*, 1998). Spectroscopic analysis is centered around a stained histological specimen that when illuminated, either absorbs or reflects the light, and emits photons revealing the properties of the dye (Rothmann *et al.*, 1998). The hybridization itself is fairly similar to other FISH-based protocols, and only a single CCD image capture is required for SKY analysis. After exposure through a triple bandpass filter, which excites all dyes simultaneously and blocks excitation light from the emission path, a Sagnac interferometer creates an optical path difference in the light emitted from the painted chromosomes (Fig. 9). An interferogram is generated for every pixel during the CCD image capture; this is a measure of emitted spectra in terms of intensity at a given wavelength (Schröck *et al.*, 1996; Garini *et al.*, 1996; Macville *et al.*, 1997; Ried *et al.*, 1997; Raap, 1998; Rothmann *et al.*, 1998; Garini *et al.*, 1999). The differences in the captured spectra may be visualized in the display colors of the CCD image. A Fourier transformation ensures that subtle changes in intensity and wavelength between similar spectra are assigned drastically different classification colors, or pseudo-colors, to allow appropriate discrimination (Schröck *et al.*, 1996; Garini *et al.*, 1996; Macville *et al.*, 1997; Ried *et al.*, 1997; Raap, 1998; Garini *et al.*, 1999; Bayani and Squire, 2001).

Multiple FISH probes can be used to query several genes at once, but the ability to simultaneously paint all 24 human chromosomes is a powerful tool for performing a global analysis of the chromosome complement of a given cell. Independently, FISH can not accommodate enough spectrally distinct fluorochromes for a global analysis, and SKY will not distinguish submicroscopic deletions, para- or peri-centric inversions, or small duplications or deletions that do not alter the size or composition of the chromosome (Garini *et al.*, 1996; Veldman *et al.*, 1997; Chang and Mark, 1997). Therefore, the combination of SKY and FISH in a single preparation is a very useful tool for looking at the involvement of a specific gene in a rearrangement event, and is a unique refinement on employing each technique individually and attempting to synthesize the results (Tonon *et al.*, 2000). Combination of these 2 techniques allows the researcher to assay the involvement of a specific gene and of specific chromosomes in a given rearrangement using a single preparation. SKY may also be employed as a screening technique for gene or chromosome involvement, perhaps best applied following an expression study such as serial analysis of gene expression (SAGE) or microarray analysis (Ried *et al.*, 1997; Tonon *et al.*, 2000).

Tumors, in particular solid tumors, often have complex karyotypes with multiple rearrangements in the genome (Ried *et al.*, 1997; Tonon *et al.*, 2000). While SKY remains very useful for such applications, it has the potential for misclassification, commonly due to fluorescence signal flaring that obscures a breakpoint or otherwise interferes with interpretation by the SKY software (Lee *et al.*, 2001). Although the resolution of SKY is estimated at 1-2Mb, actual resolution hinges upon the degree of chromatin condensation (Macville *et al.*, 1997; Schröck *et al.*, 1997; Bayani and Squire,

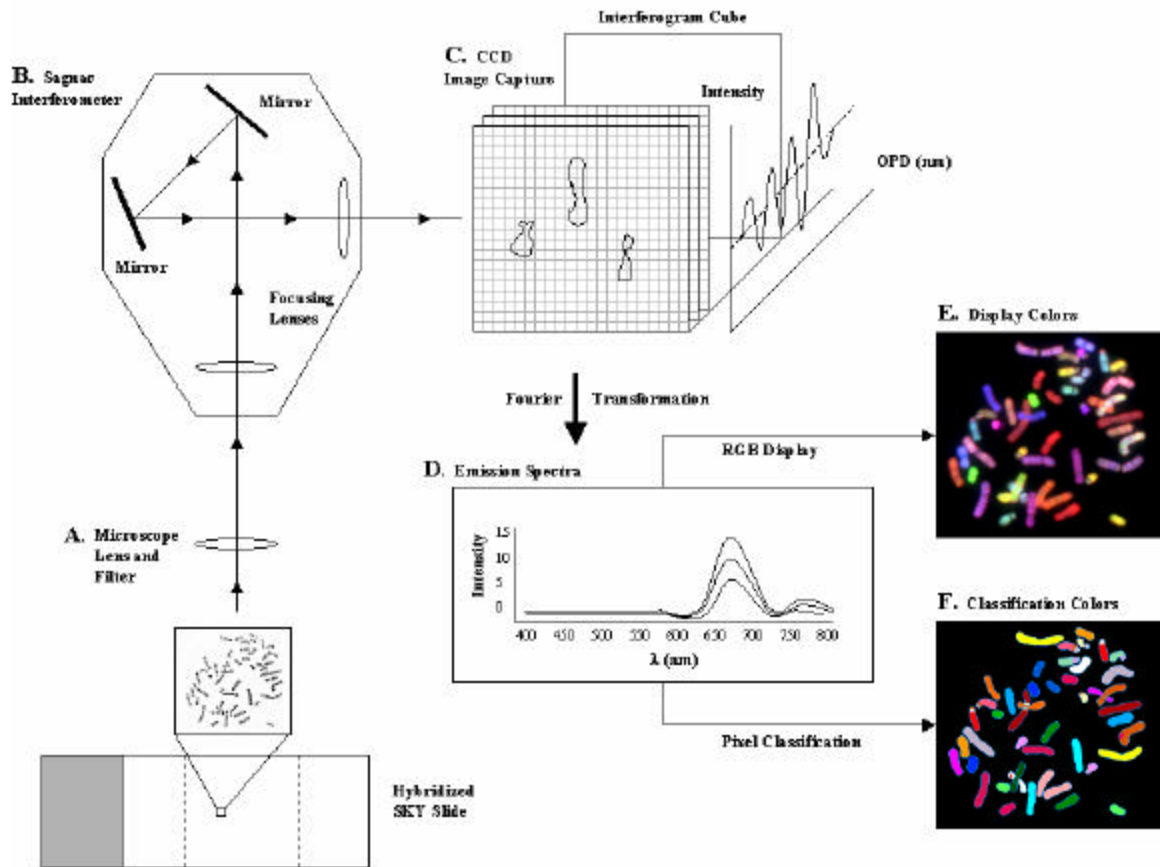


Figure 9. Schematic for SKY Image Capture and Analysis. The principle of spectral karyotyping is spectral imaging, which allows distinction of spectrally-overlapping fluorochromes in a SKY hybridization. Emitted light is visualized through a triple bandpass filter (A), the light is then passes through a Sagnac interferometer (B), and the image is captured in a single exposure using a CCD camera (C). The interferogram seen in (C) is the pixel-by-pixel detail of wavelength and intensity across the entire captured image. (D) The interferogram is analyzed using Fourier transformation to determine the spectrum of the light at each pixel. The spectra for the entire image can be visualized directly as an RGB image (E) similar to the image seen through the microscope. Alternatively, each pixel is classified and the image is pseudocolored (F) to distinguish overlapping fluorochromes.

This image was adapted from Schrock *et al.*, 1996.

2001). An additional drawback is the cost associated with SKY hybridization, making it potentially most effective as an initial screen of a number of cells prior to a thorough analysis with a specific target for FISH or a comprehensive CGH analysis (Lee *et al.*, 2001; Bayani and Squire, 2001). The combination of SKY with CGH allows for an amazingly powerful analysis to resolve structural and numerical chromosome aberrations, at which point the inclusion of FISH becomes useful as a confirmatory assay (Macville *et al.*, 1999).

UVEAL MELANOMA.

Uveal melanoma is the primary intraocular tumor observed in adults, and often results in blindness and/or death. Epidemiological studies show an incidence of approximately 6 per million per year in the Caucasian population; within this population it is more common in lightly pigmented individuals (McLean and Gamel, 1996). Lightly pigmented eyes are also demonstrated to be more susceptible to the melanoma (Regan *et al.*, 1999). The clinical course of the cancer is related to the size of the tumor, the cell type, and the variability of the nucleolar size (Gordon *et al.*, 1994; Prescher *et al.*, 1996). Additional considerations include gender, wherein males are slightly more susceptible than females, and predisposing factors (McLean and Gamel, 1996).

Previous studies have shown that ocular (dermal) melanocytosis, neurofibromatosis type 1, Li-Fraumeni syndrome, and familial atypical mole and melanoma (FAM-M) syndrome are predisposing factors (Singh *et al.*, 1996a; Kincaid, 1998). Due to the strong link between sunlight and cutaneous melanoma, researchers have also considered sunlight as a potential cause for uveal melanoma; the results have been ambiguous (Tucker *et al.*, 1985; Egan *et al.*, 1988; Holly *et al.*, 1990; Dolin *et al.*, 1994). There have

been rare cases of familial uveal melanoma, thought to be inherited in an autosomal dominant fashion and as yet unlinked to any genetic locus or cytogenetic anomaly (Lynch *et al.*, 1968; Singh *et al.*, 1996a; Singh *et al.*, 1996b).

In relation of gross pathology to prognosis, the most significant feature of this solid tumor is the largest tumor dimension (LTD) (Hungerford, 1993; McLean and Gamel 1996). Lesions are considered small if the LTD is at or below 10mm, medium if the LTD is 11-15mm, and large if the LTD exceeds 15mm (McLean and Gamel, 1996). The prognosis worsens as the tumor increases in size. Other features, including vascular supply, are far less significant (Kincaid, 1998).

Uveal melanomas may arise in the choroid, ciliary body, or the iris (Fig. 3). The origin of the tumor has prognostic significance, with melanomas originating in the iris having the most favorable prognosis (Hungerford, 1993; Kincaid, 1998). Iris melanomas are the least common, while choroidal melanomas are the most common (Hungerford, 1993; McLean and Gamel, 1996; Kincaid, 1998; Singh *et al.*, 2001). Choroidal melanomas often rupture the Bruch's membrane and invade the subretinal space, giving them a characteristic mushroom shape (McLean and Gamel, 1996; Kincaid, 1998). Ciliary body tumors can later invade the iris. Clinical diagnosis may occur following routine examination of a asymptomatic eye, blurring or loss of vision, pain from inflammation, or retinal detachment and intraocular hemorrhage (McLean and Gamel, 1996).

Uveal melanoma tumors are generally classified based on cell type, using a modified version of the Callender classification system (Callender, 1931; McLean *et al.*, 1983; McLean and Gamel, 1996). In this system, uveal melanomas containing

epithelioid cells are designated “mixed-cell type,” melanomas without epithelioid cells are termed “spindle-cell type,” and tumors with too much necrosis to be classified by cytology are designated “necrotic type.”

Approximately 50% of patients die from hematogenous metastasis (McLean and Gamel, 1996). Metastasis occurs hematogenously, due to the lack of a lymph system in the eye, and almost exclusively localizes to the liver. The preferential metastasis to the liver is not well understood, but can not be explained through lymphatic drainage pathways (McLean, 1995).

The process of hematogenous metastasis is sequential, where each step is fully completed before the following step can take place. Interruption of the metastatic process translates into a cure for the patient. The stepwise process of hematogenous metastasis is as follows: growth and local invasion of primary site, neovascularization, vascular invasion, embolization, transport to the metastatic site, arrest at the metastatic site, extravascularization at the metastatic site, growth and neovascularization, growth of tumor cells in newly established metastasis, and finally re-metastasis (Fidler, 1990; McLean, 1993). Survival time is primarily a function of the growth rate of tumor cells, because this determines the pace of the metastatic process. The significance of lead time and tumor burden (also known as LTD) are thereby decreased in uveal melanoma. Lead time is the length of time between metastasis and treatment, and its significance is decreased because metastases are often not discovered prior to removal of the eye. The relevance of tumor burden on survival time is decreased, because the exponential growth of a tumor has a larger effect on tumor size than prognosis since the critical number of doubling times before metastasis can not be estimated (McLean, 1993). In addition,

patient to patient variation in tumor size decreases the strength of this prognostic indicator. The mean of the diameters of the 10 largest nucleoli, measured from at least 50 fields of the tumor, has been found to be a good predictor of survival; “the larger the nucleoli the lower the cure-rate and the shorter the median survival time” (McLean, 1993; McLean, 1995; Periera *et al.*, 2001). This measurement is similar, but slightly different, in cutaneous melanoma, where the mean of the 10 largest nuclei, rather than nucleoli, is of prognostic significance (Periera *et al.*, 2001). Survival time following metastasis is also dependent on the immunologic defense system of the host, which is primarily tumor-infiltrating lymphocytes (TIL). In most solid tumors, presence of TIL are associated with a better prognosis; for indeterminate reasons, the opposite is true when infiltration occurs in uveal melanoma (McLean, 1993; McLean, 1995; McLean and Gamel, 1996).

The primary treatment for uveal melanoma is enucleation, or removal of the eye. Conservative therapies include radiation and eye-wall resection, with the intent of preserving the eye and maintaining vision (McLean and Gamel, 1996; Kincaid, 1998). Radiation therapy is done using a precisely focused particle beam or a radioactive plaque sutured to the sclera beneath the tumor. Eye-wall resection can be used on medium or small tumors (≤ 15 mm), but is not feasible on large tumors (>15 mm) (McLean and Gamel, 1996). Survival studies are in progress to compare prognosis and survival following enucleation or more conservative therapies, such as radiation and resection (Hungerford, 1993; McLean and Gamel, 1996). The conservative treatments are currently favored in smaller tumors, which researchers hope will one day result in tumor control and preservation of vision (Kincaid, 1998).

Investigations at the sub-cellular level have begun to unveil the genetics underlying tumor development, progression, and metastasis. Cytogenetic evidence indicates that copy number abnormalities prevail within uveal melanoma (Gordon *et al.*, 1994; Speicher *et al.*, 1994; Ghazvini *et al.*, 1996). Results from cytogenetic analyses suggest that the most frequent abnormalities occur in chromosomes 3, 6, and 8; monosomy 3 is associated with a poor prognosis (Speicher *et al.*, 1994; Prescher *et al.*, 1996; White *et al.*, 1998a). Monosomy 3 is seen in uveal melanoma of the ciliary body, whereas disomy or polysomy of chromosome 3 are reported in choroidal melanoma (Sisley *et al.*, 1993; McNamara *et al.*, 1997). Abnormalities of chromosome 6 are also seen in cutaneous melanoma, which suggests the cancers may share some common genetic alterations (Griffin *et al.*, 1988). Other recurrent abnormalities have been noted with varying consistency, including those on 7q, 9p, and 13q (Gordon *et al.*, 1994).

Evidence suggests a bifurcated pathway for tumor progression, wherein an aberration of either chromosome 3 or 6 occurs, eventually followed by alteration of chromosome 8 and metastasis. Chromosome 8 abnormalities are not seen unless accompanied by an aberration of chromosome 3 or 6 (Parella *et al.*, 1999).

Due to its strong link with prognosis, chromosome 3 copy number is frequently assayed in the uveal melanoma research community. Monosomy 3 was first identified using classical cytogenetic techniques, and was generally reported in 50% of the tumors studied (Horsman *et al.*, 1990; Sisley *et al.*, 1990; Prescher *et al.*, 1990; Horsthemke *et al.*, 1992; Sisley *et al.*, 1992; Horsman and White, 1993; Wiltsire *et al.*, 1993; Singh *et al.*, 1994; Prescher *et al.*, 1994; Prescher *et al.*, 1995; Prescher *et al.*, 1996; White *et al.*, 1998b; Parada *et al.*, 1999; Sisley *et al.*, 2000; Tschentscher *et al.*, 2001). Similar results

were found by hybridization-based techniques, including analyses of chromosome 3 loss using FISH (Wiltshire *et al.*, 1993; Sisley *et al.*, 1997; Naus *et al.*, 2002). CGH studies report monosomy with similar frequency as well (Speicher *et al.*, 1994; Gordon *et al.*, 1994; Prescher *et al.*, 1996; Ghazvini *et al.*, 1996; Tschentscher *et al.*, 2001; Naus *et al.*, 2001). Studies employing a combination of these methods offer an internal validation of their findings (Wiltshire *et al.*, 1993; Prescher *et al.*, 1996; Tschentscher *et al.*, 2001). However, the comprehensive cytogenetic characterization of uveal melanoma remains incomplete, largely because most studies involve small sample sizes almost exclusively comprised of fresh material.

The absence of chromosome 3, 6, and 8 abnormalities in some cases, suggests that there are additional pathways of malignant transformation (Singh *et al.*, 1996a). Several papers seem to refute or question the bifurcated model of development (White *et al.*, 1998b; Sisley *et al.*, 2000; Naus *et al.*, 2001). This indicates that while there may be exclusivity with regard to the sequence in which chromosome abnormalities appear in some tumors, it does not hold true in every case. Alternatives to monosomy 3 have also been reported recently, and are starting to receive some attention. Decreases in copy number of chromosome 3 have sometimes been reported in lieu of monosomy, where CGH showed a tendency toward loss of a portion of the chromosome rather than complete loss (Gordon *et al.*, 1994; Ghazvini *et al.*, 1996). LOH studies have demonstrated losses on either arm of the chromosome rather than along the length of the entire chromosome (Sisley *et al.*, 1993; White *et al.*, 1998a; Parella *et al.*, 1999; Myatt *et al.*, 2000; Tschentscher *et al.*, 2001). Furthermore, isodisomy of chromosome 3, trisomy

3, and tetrasomy 3 have been reported in the literature (McNamara *et al.*, 1997; White *et al.*, 1998a).

MATERIALS and METHODS

HUMAN PERIPHERAL BLOOD LYMPHOCYTE (HPBL) CULTURE.

Venipuncture was performed on healthy and karyotypically normal male and female donors with informed consent, and 0.8ml blood was added to 10ml RPMI 1640 media (Invitrogen Life Technologies, Carlsbad, CA) supplemented with 20% FBS (Sigma Co., St. Louis, MO), 100µl penicillin/streptomycin (100U/ml and 100µg/ml, respectively) and 1% sodium heparin (Invitrogen Life Technologies, Carlsbad, CA). Then, 216µl phytohemagglutinin (PHA) (Invitrogen Life Technologies, Carlsbad, CA) was added to each T-25 culture. The cultures were incubated at 37°C in 5% CO₂ for 72 hours.

UVEAL MELANOMA CELL LINES.

Ten uveal melanoma cell lines were obtained from the Department of Ophthalmology, University of Texas Southwestern Medical Center at Dallas (Dallas, TX), and maintained in culture using standard techniques (Table 1). The cell lines were derived from 8 primary uveal melanomas and 2 metastases.

METAPHASE CHROMOSOME PREPARATIONS.

We prepared metaphase chromosome spreads from normal, cultured human peripheral blood lymphocytes (HPBL) and cultured cell lines via conventional techniques (Tucker *et al.*, 1994). After 72 hours of culture, 0.1µg/ml, or 100µl, of colcemid (Karyomax Colcemid Solution, Invitrogen Life Technologies, Carlsbad, CA) was added to each culture flask. Cultures with colcemid were incubated an additional 15 minutes, after which the T-25 cultures were gently agitated and transferred to 15ml conical centrifuge tubes, and centrifuged at 1200rpm for 8 minutes. The supernatant was

aspirated, the cell pellet resuspended in 5ml of a 75mM KCl (see appendix) hypotonic solution pre-warmed to 37°C, and incubated for 20 minutes at 37°C. The hypotonic solution was used to swell the cells, eventually causing the cells to burst and release their chromosomes when dropped onto slides, forming metaphase spreads. Following incubation, the addition of 2ml fresh Carnoy's fixative (see appendix), and subsequent centrifugation for 8 minutes at 1200rpm, stopped the swelling of the cells. The supernatant was again aspirated, and the cells resuspended in 5-10ml fresh fixative. The cells were centrifuged, the supernatant aspirated, and the pellet resuspended. This process was repeated until the cell pellet appeared to be clean and completely white upon visual inspection.

At this point the cells were dropped onto slides; alternatively, the cells were resuspended in fixative, stored upright at 4°C and dropped onto slides within the next few days. The best results were observed when slides were dropped on the same day as the harvest. In order to make metaphase slide preparations, the supernatant was aspirated and the cells resuspended in approximately 0.5-1ml glacial acetic acid with a 200µl pipette after the final centrifugation. A clean slide, swabbed with ethanol until free of debris, was placed over an 80°C water bath and misted with dH₂O. The pipette tip was loaded, and 2 adjacent drops of the cell suspension were placed onto the slide from a height ranging from 6 inches to 3 feet above the slide. The slide was dried over the water bath, checked for quality, stored in a slide box to age for approximately 1 week. For long-term storage, aged slides were kept in a slide box with desiccant, flushed with gaseous nitrogen, sealed in a plastic bag and kept at -20°C until needed.

NUCLEI PREPARATIONS.

For FISH analysis, nuclei from the uveal melanoma cell lines and a normal male donor were harvested from 25ml culture flasks using the procedure for metaphase spread preparation, but in the absence of colcemid (Tucker *et al.*, 1994). Nuclei preparations were aged and stored in the same manner as the metaphase preparations.

UVEAL MELANOMA TUMOR CASES.

One hundred FFPE uveal melanoma tumors were selected at random from the AFIP tissue archives. Two 6 μ m tissue sections per case were available for microdissection, and were accompanied by photocopies of corresponding H & E stained slides for tumor identification (Fig. 4). Of these cases, 51 patients (23 male, 28 female) survived more than 9 years without evident metastasis, and the remaining 49 patients (29 male, 20 female) succumbed to metastatic disease. Determination of gender was required for appropriate hybridization, but no other patient characteristics were revealed until completion of the analysis.

MICRODISSECTION.

Initial approaches involved using a sterile razor blade to scrape the entire paraffin tissue section from the slide for DNA isolation. It was found that the quality of the DNA was improved if the tumor was exclusively excised from the slide. Microdissection is a useful technique for ensuring the highest possible proportion of tumor cells, with as few contaminating normal cells in the sample as possible (du Manoir *et al.*, 1993; Kallioniemi *et al.*, 1994). Microdissection was performed on two 6 μ m tissue sections for each of 100 uveal melanoma cases. The accompanying H & E slides were used to locate and isolate the uveal melanoma tumor in the FFPE tissue section. A sterile 20-gauge needle, a sterile

razor blade, or a fresh microtome blade was used in manual microdissection of the tumor tissue from the slide. The tumor tissue from both tissue sections was combined in a single 1.7ml microcentrifuge tube for each case to ensure the availability of sufficient tumor DNA for DOP-PCR; this was a concern due to the variability in tumor size from case to case.

DNA ISOLATION.

Normal (reference) DNA.

Reference samples for the entire study were collected via venipuncture from a single normal male and a single normal female donor with informed consent, and the majority of blood was aliquoted into T-25 flasks for culture of HPBL as previously described. A small volume of blood was set aside for isolation of whole genomic DNA; the addition of 200 μ l whole blood to a microcentrifuge tube yielded approximately 35 μ l purified DNA upon completion of the isolation protocol.

The isolation protocol began with the addition of 20 μ l RNase A (see appendix) (Roche Molecular Biochemicals, Indianapolis, IN) to 200 μ l whole blood, mixed by vortexing. Then, 25 μ l 20mg/ml Proteinase K (Roche Molecular Biochemicals, Indianapolis, IN) and 200 μ l cell lysis buffer (see appendix) were added to the tube, vortexed thoroughly, and incubated for 10 minutes at 70°C. Proteinase K digestion increased the yield of high molecular weight DNA (Isola *et al.*, 1994). Then, 500ml phenol/chloroform/isoamyl alcohol solution (PCI) (25:24:1, v/v) (Invitrogen Life Technologies, Carlsbad, CA) was added to the tube(s) after removal from the oven, and then the tube was vortexed again. This was followed by a full speed (14,000rpm) centrifugation for 5 minutes in a microcentrifuge. The upper aqueous layer was removed

and put into a clean microcentrifuge tube, and another 500 μ l PCI was added, again followed by vigorous vortexing. The tube(s) was spun at full speed for another 5 minutes. The upper layer was again removed and placed into a clean tube.

The following reagents were then added to this solution: 25 μ l 3M sodium acetate (Quality Biological, Inc., Gaithersburg, MD), 1.5 μ l 20mg/ml glycogen (Roche Molecular Biochemicals, Indianapolis, IN), and 100% ethanol at volume equal to 3x the volume of the tube. The tube was again vortexed to ensure an evenly distributed solution, and incubated at -20°C for up to 2 hours. The DNA was precipitated via full speed centrifugation for 5 minutes. The supernatant was aspirated, 0.5ml 85% ethanol added to the pellet, and vortexed thoroughly. Following a second 5 minute centrifugation at full speed, the ethanol was decanted, and the 85% ethanol wash repeated. The resulting supernatant was aspirated, and the pellet of DNA in the bottom of the tube was dried in a lyophilizer set on high for 5 minutes. The pellet was finally resuspended in 35 μ l TE buffer (pH 7) (see appendix) for long-term storage at -20°C. DNA quantification was performed using a GeneQuant II (Pharmacia Biotech, Cambridge, England); the 260/280 ratios and DNA concentration recorded.

Cell Line DNA.

DNA was extracted from uveal melanoma cell lines maintained in culture. The media was removed from the T-25 flask and set aside. Two milliliters of 1xTrypsin-EDTA (Mediatech, Inc., Herndon, VA) were added to the flask, and when the cells were fully suspended in the Trypsin-EDTA solution, the media was replaced into the flask. The contents of the flask were pipetted into a 15ml conical centrifuge tube, and centrifuged at 1500rpm for 6 minutes. The supernatant was aspirated, and the cell pellet

was washed twice in 10ml 1xPBS (w/o $MgCl_2$ or $CaCl_2$); each time the supernatant was aspirated. The cell pellet was resuspended in approximately 1ml of 1xPBS (w/o $MgCl_2$ or $CaCl_2$) following the second wash. The sample was pipetted from the 15ml conical tube into microcentrifuge tubes in 200 μ l aliquots. From this point on, the DNA isolation procedure was identical to that described for normal HPBL DNA.

Tumor (test) DNA.

Following microdissection, as previously described, tumor DNA was extracted via a protocol similar to that described earlier for normal DNA. First, 800 μ l Hemo-De (Fisher Scientific, Inc., Pittsburgh, PA) was added to each tube containing microdissected tumor tissue. Following addition of Hemo-De, the tubes were vortexed, and 400 μ l ethanol were added. The tube was vortexed again, and centrifuged at full speed for 5 minutes. The supernatant was decanted, and 800 μ l ethanol was added. Once again, the tube was vortexed and centrifuged at full speed for 5 minutes. The supernatant was decanted, and the pellet dried in a 55°C oven for 5 minutes. Then, 250 μ l cell lysis buffer and 25 μ l 20mg/ml Proteinase K were added to the tube, and vortexed thoroughly. The tube(s) was incubated overnight at 55°C in an Eppendorf Thermo Mixer (Brinkmann Instruments, Inc., Westbury, NY). The remainder of the DNA isolation protocol, from PCI extraction through DNA quantification, was identical to that described for normal DNA.

NICK TRANSLATION.

For the cell line CGH experiments, all whole genomic probes were generated via nick translation of extracted DNA (Fig. 10). Each 50 μ l nick translation reaction contained the following reagents: 1 μ g DNA (volume variable), 5 μ l 10xNT buffer (see

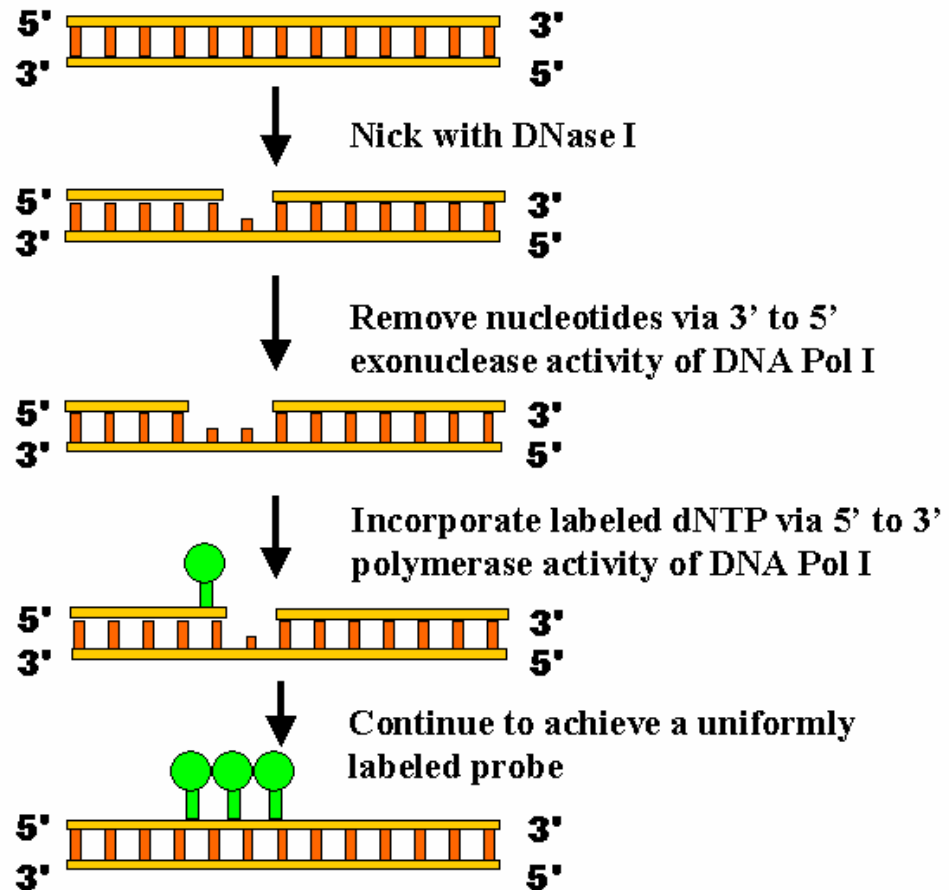


Figure 10. Probe Production via Nick Translation. Genomic DNA is randomly nicked with Dnase I, after which DNA Polymerase I excises nucleotides in the 3' to 5' direction. Then, the same polymerase will replace the patch of excised nucleotides using the available pool of dNTPs. Due to the decreased ratio of dTTP in the dNTP mixture, hapten- or fluorochroms -labeled dUTP will be preferentially incorporated. The dUTP is labeled, but the preferential incorporation is not skewed enough to cause steric hindrance of the resulting labeled probe DNA.

This figure courtesy of Dr. Alison E. Director-Myska, AFIP.

appendix), 5µl dNTP mixture (see appendix), 5µl 0.1M β-Mercaptoethanol (see appendix), 2µl of either biotin-16-dUTP or digoxigenin-11-dUTP (Roche Molecular Biochemicals, Indianapolis, IN), with the remainder being sterile H₂O. The solution was vortexed, 5µl 1:1000 DNase I (see appendix) (Roche Molecular Biochemicals, Indianapolis, IN) and 1µl Kornberg polymerase (Roche Molecular Biochemicals, Indianapolis, IN) were added. The reaction tubes were incubated for 2 hours at 15°C. Following the incubation, 5µl samples of each reaction were run on a 1.7% agarose gel (see appendix) to size the fragments. After the labeled DNA fragments were sized by agarose gel electrophoresis and ethidium bromide visualization by UV (ultraviolet) excitation, optimal probe size was seen as a smear of DNA between 200- and 1000-bp in length (Fig. 11) (Kallioniemi *et al.*, 1994; Houldsworth and Chaganti, 1994). To load the gel, 5µl nick translation product were added to 0.5µl loading buffer (see appendix), and at least 1 well was loaded with a 100bp ladder (Roche Molecular Biochemicals, Indianapolis, IN). If the probe length exceeded 1000bp in length, additional DNase I was added, and the reaction continued at 15°C with size checks every 30 to 60 minutes. If the probe was smaller than 200bp, it was discarded and a new reaction was set-up. Once the probe was in the appropriate size range, 1µl 0.5M EDTA (Digene, Gaithersburg, MD) was added and tubes were incubated at 65°C for 10 minutes to halt the reaction; the probes were available for immediate use, or could be stored at -20°C until needed.

POLYMERASE CHAIN REACTION (PCR).

Whole genomic probes, for the tumor study, were generated through DOP-PCR, as first described by Telenius and colleagues (Fig. 8) (Telenius *et al.*, 1992a and b). DOP-PCR, accepted as an accurate method of probe creation for CGH, results in larger

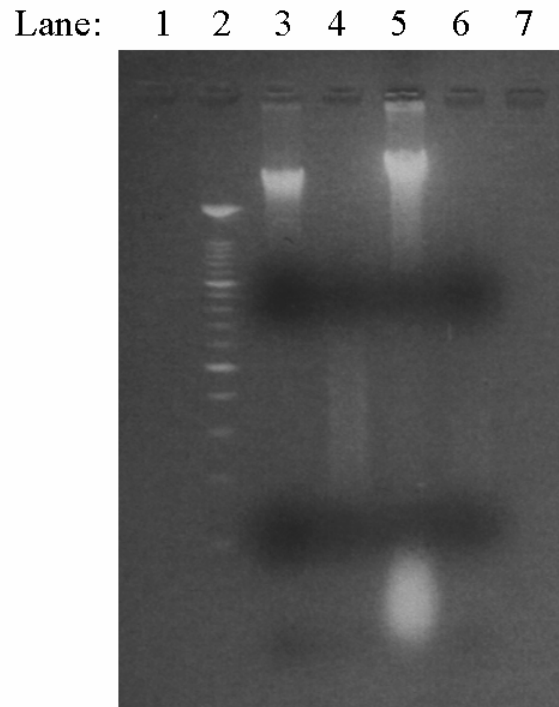


Figure 11. Agarose Gel Electrophoresis Comparing DNA Extracts with Nick Translation Products. Phenol/chloroform/isoamyl alcohol (PCI) extraction procedures were used to isolate normal DNA from normal male and female donors, as well as each of ten uveal melanoma cell lines. Whole genomic probes were generated through nick translation of extracted DNA, and normal DNA and tumor DNA genomic extracts were labeled with digoxigenin-11-dUTP and biotin-16 dUTP, respectively (Roche Molecular Biochemicals, Indianapolis, IN). The resultant labeled DNA fragments were measured via agarose gel electrophoresis, visualized with ethidium bromide staining coupled with visualization through UV excitation, and determined to be between 200 and 1000 base pairs in length. Lane 2 is the DNA molecular weight marker XIV 100 base pair ladder (Roche Molecular Biochemicals, Indianapolis, IN). Lanes 3 and 4 are normal male DNA extract and nick-translated male DNA, respectively. Lanes 5 and 6 are cell line extract from an uveal melanoma cell line and the nick-translated probe product, respectively.

labeled fragments than nick translation (Kallioniemi *et al.*, 1994). This technique, frequently applied when there was a small volume of the template DNA available, reliably amplifies quantities of DNA as small as 100pg (Speicher *et al.*, 1993). Hapten-labeled dUTP was included in the DOP-PCR reaction mix to allow probes to be visualized indirectly (Fig. 12). Reference and tumor DNA were labeled with digoxigenin-11-dUTP and biotin-16-dUTP, respectively.

DOP-PCR primers were obtained with the sequence 5'- GAT CAA GCT NNN NNN ATG TGG - 3' (Integrated DNA Technologies, Inc., Coralville, IA). Amplification was performed using a GeneAmp® PCR System 9700 thermocycler (PE Applied Biosystems, Foster City, CA). Each 100µl DOP-PCR reaction mixture contained the following reagents: 10µl of a 1:25 dilution of test or reference DNA in TE Buffer, 10µl 10x PCR Buffer II (w/o MgCl₂) (Roche Applied Biosystems, Foster City, CA), 10µl 20mM DOP Primer (see appendix), 24 µl 25mM MgCl₂ (Roche Applied Biosystems, Foster City, CA), 5µl biotin- or dig-dNTP mixture (see appendix), 39µl sterile H₂O, and 2µl AmpliTaq Gold (see appendix) (Roche Applied Biosystems, Foster City, CA). All reagents, except the DNA, can be combined into a DOP-PCR master mix (PCR MM) (see appendix) to simplify PCR set-up. Conditions were as follows: 95°C for 10 minutes initial soak, 15 cycles of 94°C for 1 minute, 30°C for 1 minute, 72°C for 1 minute, and then 60 cycles of 94°C for 30 seconds, 52°C for 30 seconds, 72°C for 1 minute with a 1 second per cycle addition to each step in the 60 cycles, and completed with a final extension of 72°C for 10 minutes before a hold at 4°C. Labeled DNA fragments were sized by agarose gel electrophoresis and ethidium bromide visualization by UV

excitation. Optimal probe size was seen as a smear of DNA between 200- and 1000-bp in length (Kallioniemi *et al.*, 1994; Houldsworth and Chaganti, 1994).

COMPARATIVE GENOMIC HYBRIDIZATION.

In brief, slides were first pretreated in order to remove unwanted cytoplasm and protein from the metaphase preps. Indirectly-labeled reference and tumor probes were simultaneously hybridized to the normal metaphase chromosomes. Following a 2-night hybridization, the indirectly-labeled probes were detected using antibody layering detection procedures, and as a final step, the slides were counterstained and coverslipped prior to visualization via fluorescence microscopy (Fig. 13).

Slide pretreatment for hybridization involved several steps. Initially, slides were equilibrated in 2xSSC (see appendix) at room temperature. Following a short equilibration period, 200µl of a 1:200 dilution of 20mg/ml RNase A stock (see appendix) in 2xSSC was applied to each slide, and the slides were incubated in a hybridization chamber at 37°C for 1 hour. Three washes in 2xSSC for 5 minutes each, complete the digestion of RNA from the slide. Then, slides were treated with a solution prepared from 15µl 100mg/ml pepsin stock solution (see appendix) added to 50ml of pre-warmed 37°C 0.01M HCl, and the slides incubated in a 37°C oven for 6 minutes. After the pepsin/HCl treatment (see appendix), the slides were washed twice in 1xPBS (w/o MgCl₂ or CaCl₂) (see appendix) for 5 minutes, followed by a third 5-minute wash in 1xPBS/MgCl₂ (see appendix). Postfixation was performed in a 50ml solution of 1% formaldehyde in 1xPBS/MgCl₂ (see appendix) for 10 minutes, followed by a single 5-minute wash in 1xPBS (w/o MgCl₂ or CaCl₂) prior to slide dehydration in a series of 3 ethanol dilutions (70%, 85%, and 100%) for 3 minutes apiece, which completes the slides.

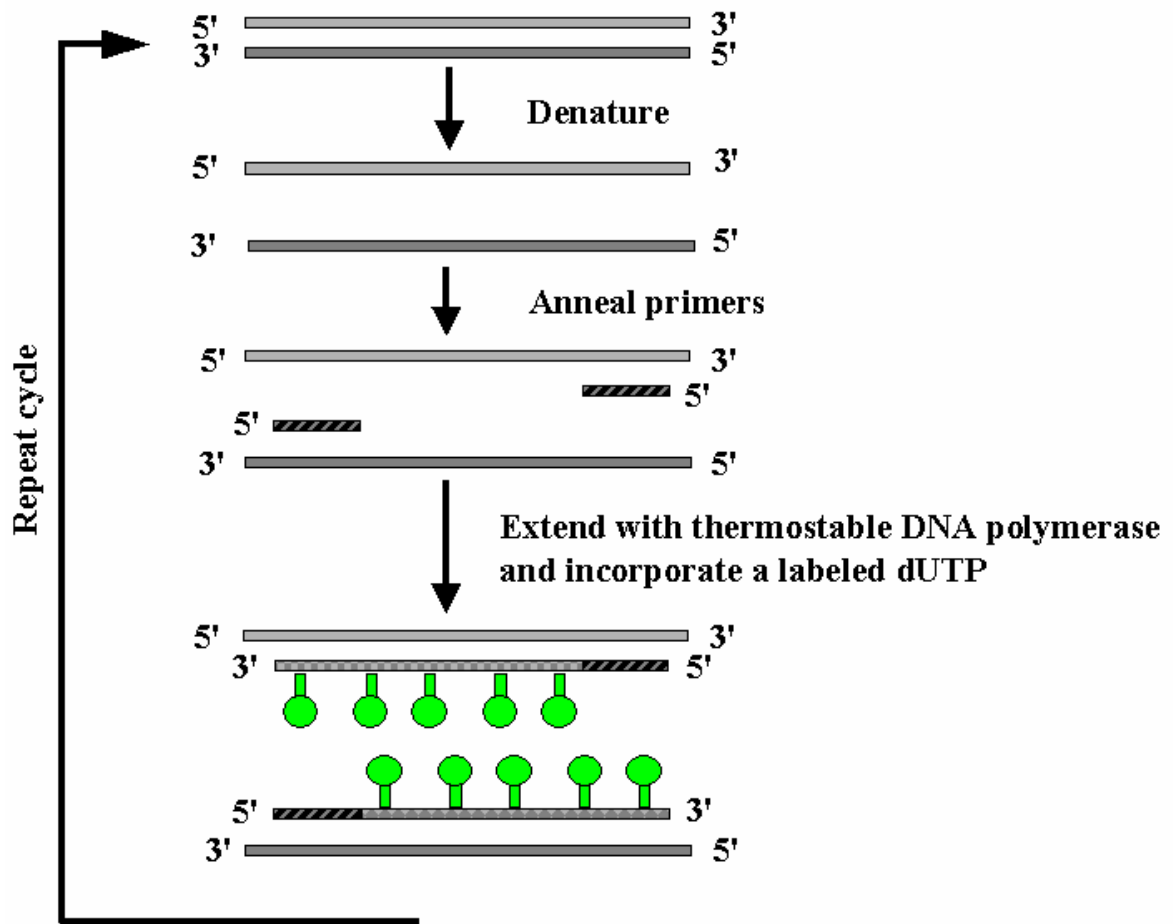


Figure 12. DNA Probe Production via PCR. The process of PCR, simplified, is a series of DNA denaturation, annealing of primers, and extension of the DNA. The primers are specific for sequences within the target DNA to be amplified. When two primers bind within an allowable proximity, the polymerase will create complementary lengths of DNA in the 5' to 3' direction. If a labeled dUTP is incorporated in the dNTP mixture, and the ratio of dTTP is reduced, the dUTP will be incorporated with increased frequency without resulting in steric hindrance. Repetition of the cycle many times amplifies the pool of labeled target DNA probe sequence.

This figure courtesy of Dr. Alison E. Director-Myska, AFIP.

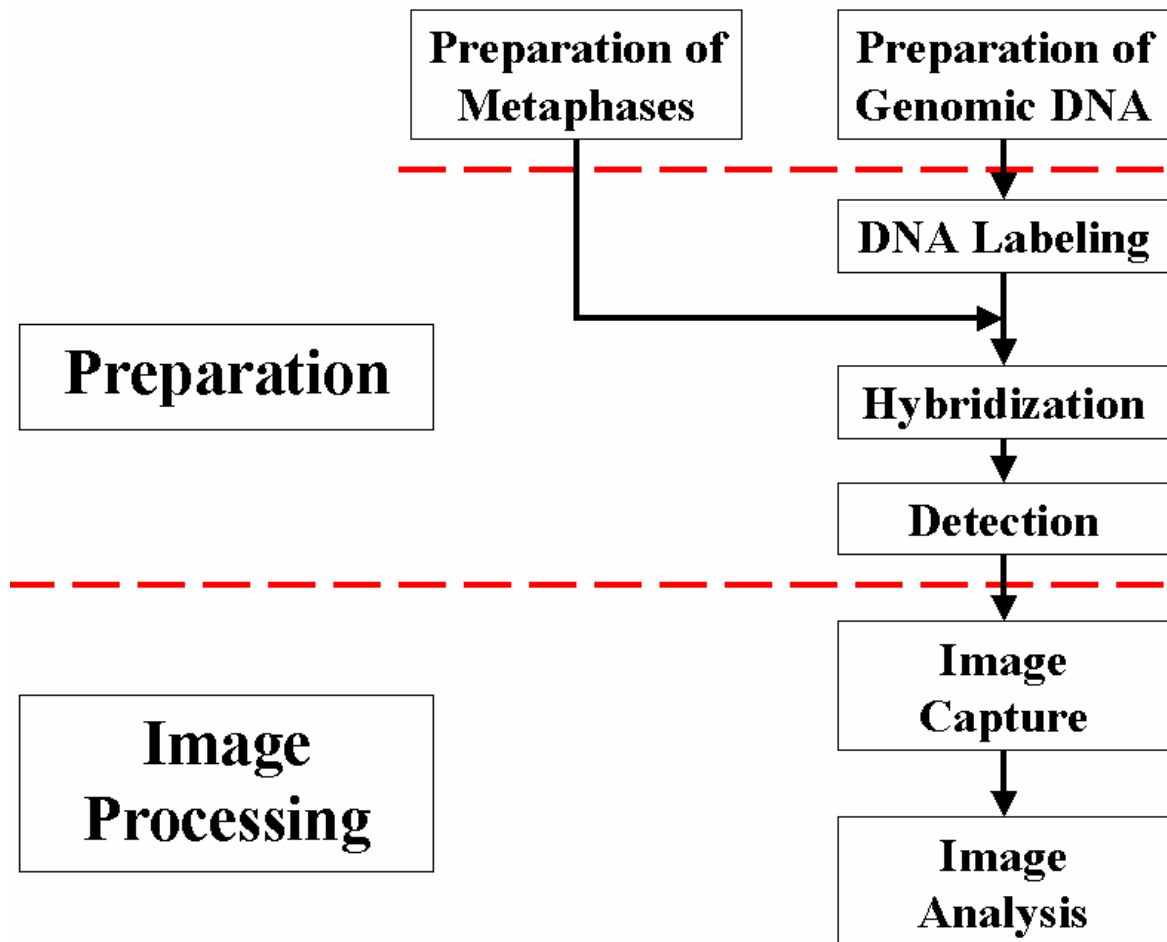


Figure 13. A Flowchart for CGH. This is intended as a general description of the steps for CGH, and is elaborated upon in Figures 14, 15, and 18. The preparation of normal target metaphases occurs in parallel with the preparation and labeling of normal and tumor genomic DNA. Both DNA probes are simultaneously hybridized to the pre-treated target slide, and following a 2-night hybridization, the indirectly-labeled probes are detected. For image processing, the target metaphase is captured using DAPI, FITC, and TRITC filters. The combination of images captured using each filter creates a CGH overlay image suitable for analysis.

This figure was adapted from Institut für Pathologie, University Hospital Charité,
<http://amba.charite.de/cgh/protocol/02/prot02.html>.

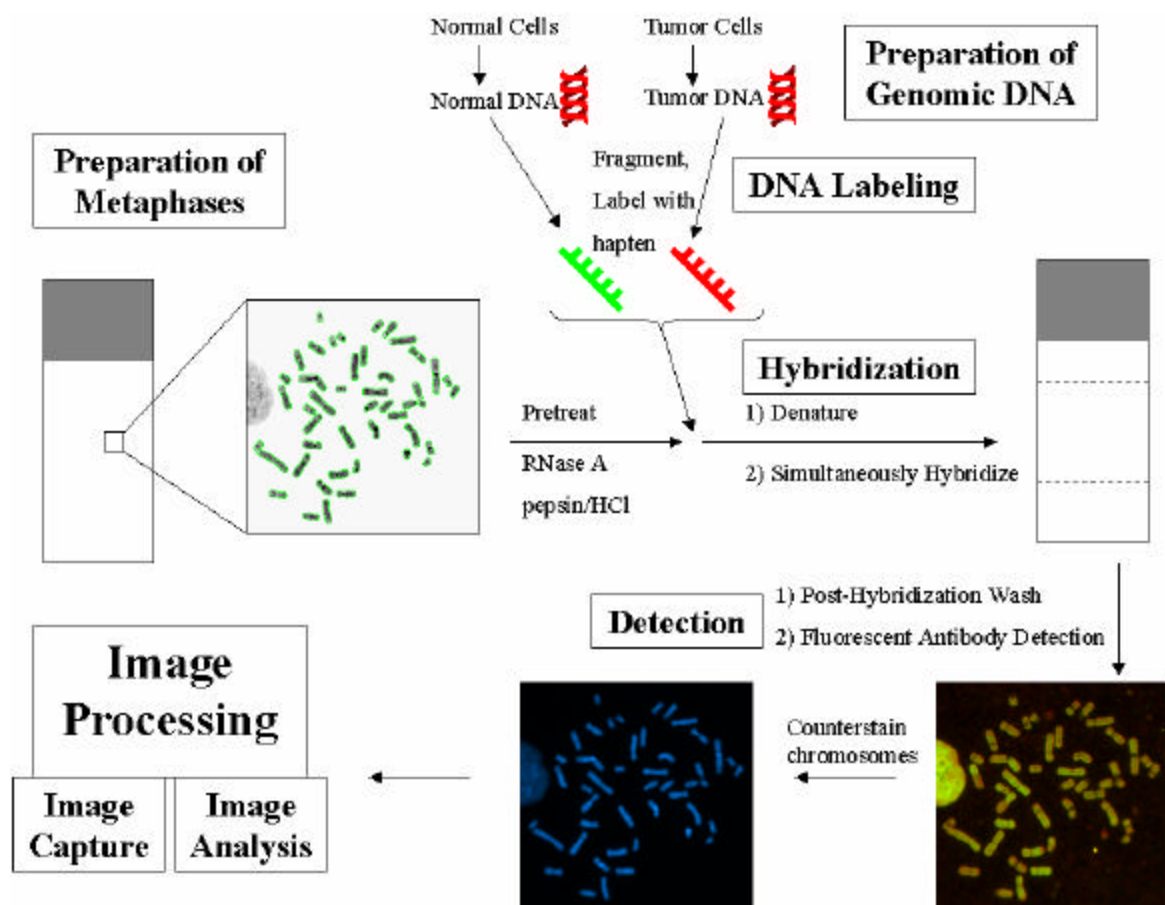


Figure 14. A Schematic of the Process of Hybridization for CGH. The process begins with the preparation of genomic DNA, wherein DNA is extracted from tumor and normal cells. Extracted DNA is digested (NT) or amplified (PCR) into shorter fragments, or lengths of nucleotides, and during that process the DNA is also labeled with a hapten. Equimolar ratios of the labeled tumor (test) and normal (reference) DNA are simultaneously hybridized to a pre-treated slide of normal male metaphase spreads. The hybridized area is sealed beneath a coverslip (dashed outline), and incubated for 2 nights. On the third day, the slide undergoes post-hybridization washes to remove excess probe, and fluorescence antibody detection for the hapten-labeled genomic probes. To complete the slide, the normal target metaphase chromosomes are counterstained with DAPI, and mounted in an antifade solution for image processing, which includes image capture and analysis.

CGH was performed as described by Kallioniemi and colleagues (Fig. 14) (Kallioniemi *et al.*, 1992). The normal and tumor probes, created via DOP-PCR, were combined into a single probe cocktail. To make and precipitate the probe cocktail, 30 μ l each (tumor and reference) DOP-PCR product, 60 μ l human Cot-1 DNA (Invitrogen Life Technologies, Carlsbad, CA), 1 μ l salmon testes DNA (Sigma Co., St. Louis, MO), 12.1 μ l 3M sodium acetate, and 400 μ l ice cold absolute ethanol were combined in a microcentrifuge tube for each case to be hybridized. The DNA was precipitated by incubation at -20°C for 2 hours. Precipitate was collected by a 30-minute centrifugation at 14,000rpm. The supernatant was decanted, and the probe pellet was lyophilized for 5 minutes. Then, 5 μ l molecular grade formamide (Fisher Scientific, Inc., Pittsburgh, PA) was added to each pellet, vortexed, and incubated at 37°C for 30 minutes. Afterwards, 10 μ l hybridization master mix (see appendix) was added, the mixture was vortexed and denatured at 80°C for 5 minutes, followed by a 2-hour pre-anneal at 37°C. One hour and forty minutes into the preanneal, 100 μ l of 70% formamide/2xSSC (FA/SSC) (see appendix) was added to each pretreated slide along with a 24x60mm glass coverslip. The slides were immediately incubated in an 80°C oven for 1.5 minutes, and then dehydrated in a series of ethanol dilutions (70%, 85%, and 100%) for 3 minutes each. The slides were dried, and the pre-annealed probe applied to the denatured slides. The hybridized slides were then covered with a 22mm² coverslip and sealed with Elmer's rubber cement (Elmer's Products, Inc., Columbus, OH), and incubated at 37°C for 2 nights prior to detection.

On the third day, the solutions for detection were pre-warmed for 1 hour before the procedure was started. Then, the rubber cement and coverslips were removed. The

slides were then washed at 45°C in 50% FA/SSC (see appendix) 3 times for 5 minutes per wash. This was followed by another three 5-minute washes in 0.1xSSC at 60°C, and then the slides were dipped in 4xSSC/0.1% Tween 20 (see appendix) pre-warmed to 37°C. A blocking solution of 3% bovine serum albumin (BSA) (Sigma Co., St. Louis, MO), pre-warmed to 37°C, was applied, and the slides were placed in a hybridization chamber at 37°C for 1 hour. The slides were again dipped in 4xSSC/0.1% Tween 20 pre-warmed to 45°C, before the first layer of antibodies was applied. For antibody layering, 100-200µl of a given antibody layer solution was applied to each slide, plastic coverslips were placed over the solution, and the slides were again placed in a hybridization chamber for 1 hour at 37°C, followed by three 5-minute washes in 4xSSC/0.1% Tween 20 pre-warmed to 45°C. This process of washing, layering, incubating was repeated for 4 layers. The layers were as follows: layer 1 = 1:200 avidin-conjugated FITC (Vector Labs, Burlingame, CA) and 1:100 mouse-anti-DIG (Sigma Co., St. Louis, MO), diluted in 1% BSA (see appendix); layer 2 = 1:200 biotinylated anti-avidin (Vector Labs, Burlingame, CA) and 1:200 rabbit anti-mouse TRITC (Sigma Co., St. Louis, MO), diluted in 1% BSA; layer 3 = 1:200 avidin-conjugated FITC in 1% BSA; and layer 4 = 1:200 goat anti-rabbit TRITC (Sigma Co., St. Louis, MO). Antibody layering was necessary to amplify the fluorescence signal prior to image capture and analysis. Following antibody detection procedures, slides were counterstained with DAPI (Sigma Co., St. Louis, MO) (see appendix). Finally, a coverslip was mounted over an antifade solution (see appendix) to complete each of the slides.

While some copy number alterations were obvious given the variation in green and red colorization in the hybridization, quantitative fluorescence analysis of digital

images was required for accurate CGH analysis (Raap, 1998). Image acquisition and analysis were performed on a Leica Q550CW cytogenetics workstation, which included a LEICA DM-RXA fluorescent microscope (Fig. 15) (Leica Inc., Exton, PA), and a SenSys cooled CCD camera (Photometrics Ltd., Tuscon, AZ). A CCD camera was mounted on the microscope for image capture and import into the software. DAPI, FITC, and TRITC images were acquired separately and combined to create a CGH image of each metaphase spread suitable for analysis in the Leica QCGH software (Fig. 16). Each image was visualized using an appropriate single bandpass filter, thus there was limited overlap in excitation and emission spectra (Joos *et al.*, 1994; du Manoir *et al.*, 1995a). Inverting the DAPI image approximated G-banding for accurate karyotyping of each metaphase spread (Fig. 17) (Trask, 1991). Compilation of CGH ratio profiles from a minimum of 10 metaphase spreads per cell line, allowed the generation of mean ratio profiles in the form of green:red (test:reference DNA) fluorescence ratios (Fig. 18). Ninety-five percent confidence intervals were applied to each of the collective means. The copy number thresholds for gain and loss were 0.2 units above or below the midline (1.2 and 0.8). While significant gains and losses were observed on the sex chromosomes, information on the sex of the parent tumor was not available for all cell lines (Table 1). Therefore, our cell line analysis considered only the autosomes.

SPECTRAL KARYOTYPING.

SKY was performed using the SkyPaint™ hybridization kit (Applied Spectral Imaging, Inc., Carlsbad, CA) and results were visualized using the SkyVision™ spectral imaging system (Fig. 9) (Applied Spectral Imaging, Inc., Carlsbad, CA). Metaphase spreads were prepared from each of the uveal melanoma cell lines via conventional

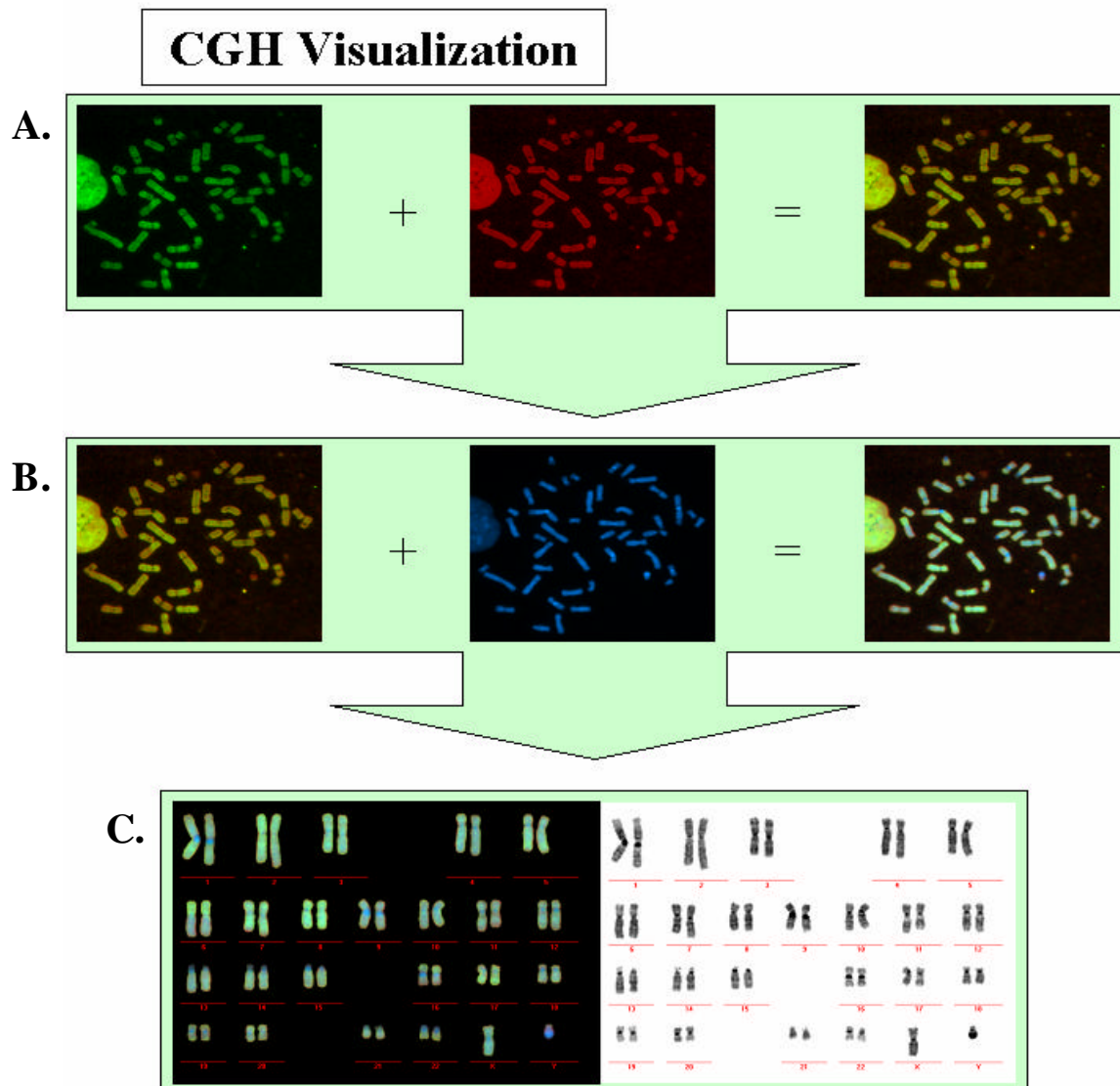


Figure 15. Step-wise Process of CGH Visualization. **(A)** The captured FITC and TRITC images are combined to form a single overlay image. **(B)** This image is combined with the DAPI counterstain to yield a completed CGH image. **(C)** The resultant image from **(B)** is karyotyped. In the completed color karyotype, similar variations in the amount of bound test probe are seen in homologous chromosome pairings. See Figure 16 for additional detail regarding image capture.

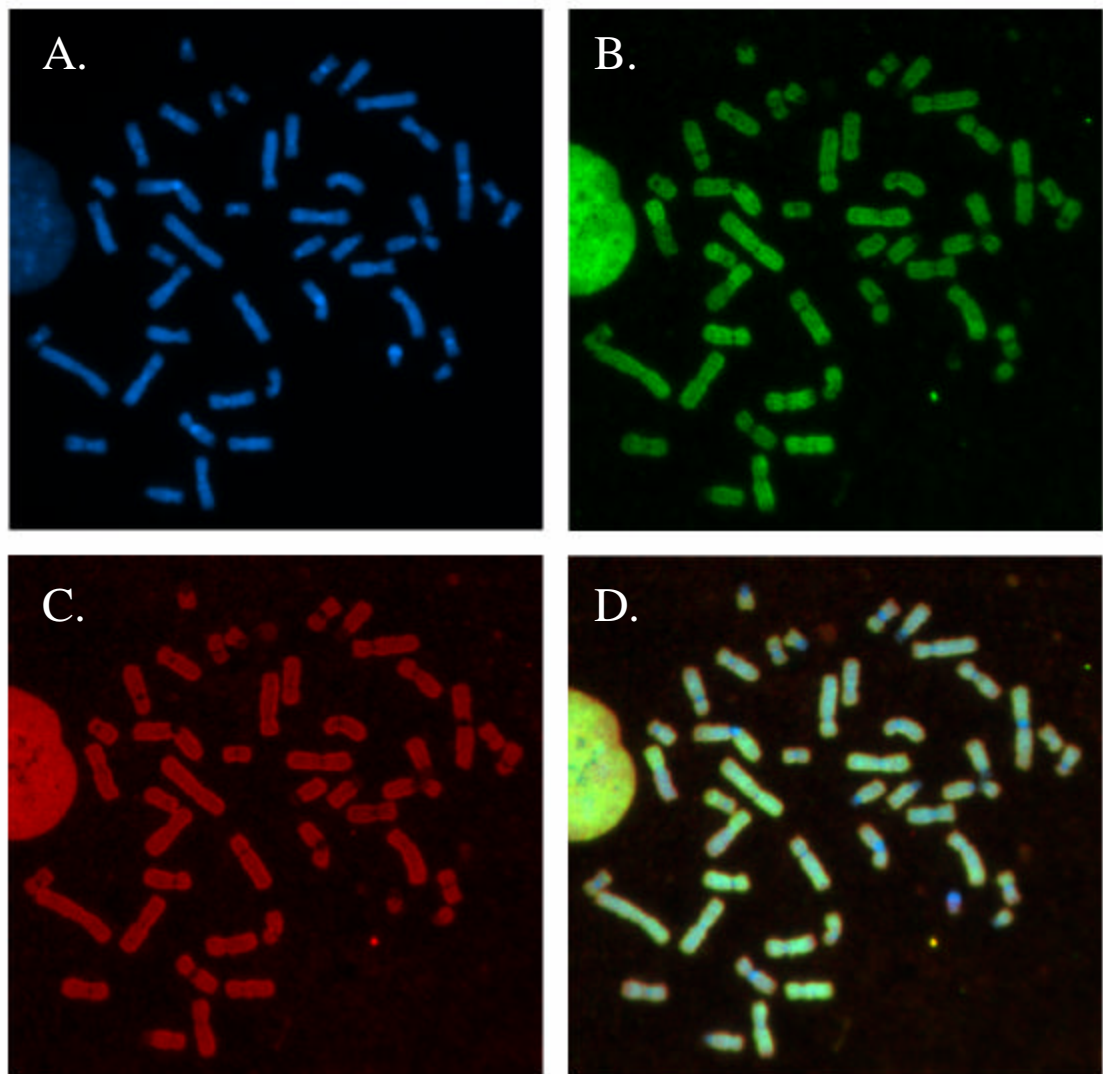


Figure 16. Image Capture for CGH Analysis. Each of these images is the identical normal male metaphase spread detected with three different fluorescent filters. **(A)** The metaphase chromosomes counterstained with 4',6-diamidino-2-phenylindole (DAPI) (Sigma Co., St. Louis, MO). Biotinylated tumor DNA signals were detected with avidin-conjugated fluorescein isothiocyanate (FITC) (Vector Labs, Burlingame, CA), and digoxigenin-11-dUTP-labelled normal DNA was visualized using tetramethylrhodamine isothiocyanate (TRITC) conjugated antibodies (Sigma Co., St. Louis, MO). **(B)** The FITC image, and **(C)** the TRITC image. These three fluorescent images **(A, B and C)** combine to form **(D)** the completed CGH image. This newly combined image is suitable for CGH analysis; the image is classified and karyotyped, followed by the generation of CGH profiles to illustrate the amplifications and deletions present within the tumor genome. All image acquisition was performed using a Leica Q550CW cytogenetics workstation which includes a Leica DM-RXA fluorescent microscope (Leica Inc., Exton, PA) and a SenSys cooled CCD camera (Photometrics Ltd., Tuscon, AZ).

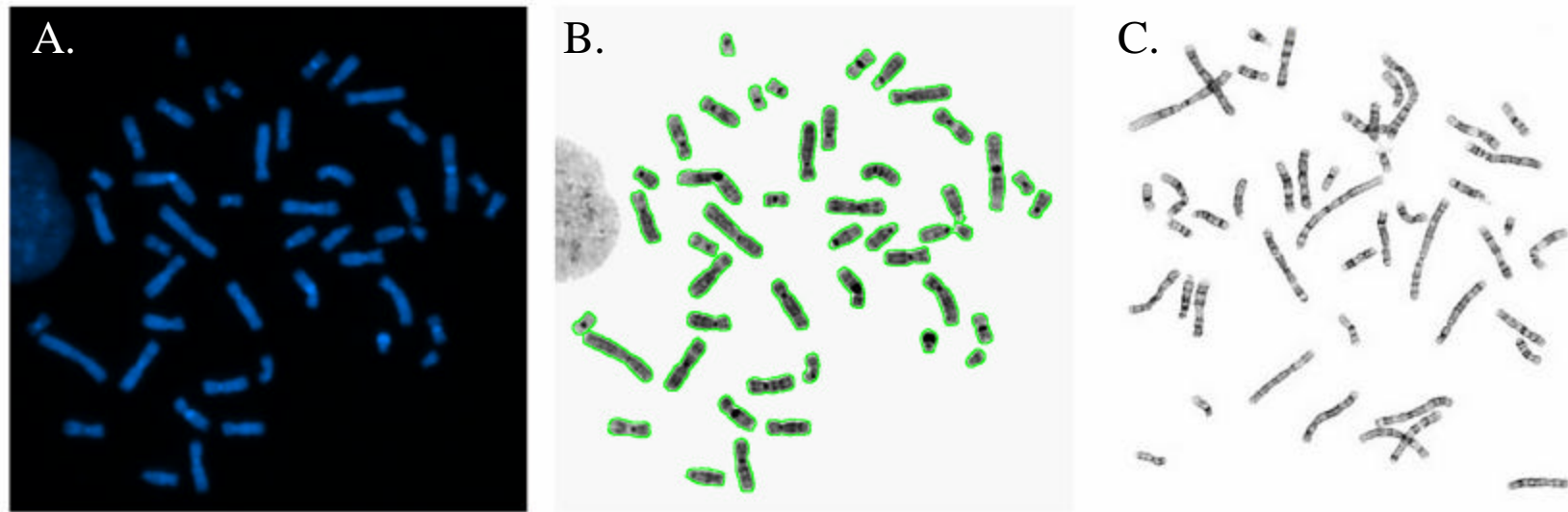


Figure 17. DNA Counterstain. (A) The counterstained metaphase spread stained with DAPI. (B) The inversion of the DAPI counterstain yields banding patterns comparable to G-banding, and allows for accurate karyotyping of the metaphase spread chromosomes. (C) For comparison purposes, a G-banded image from a different metaphase spread.

Image (C) was adapted from Genetics of Cancer Resource Center, <http://www.intouchlive.com/cancergenetics/chrm-anl.html>.

Image Processing

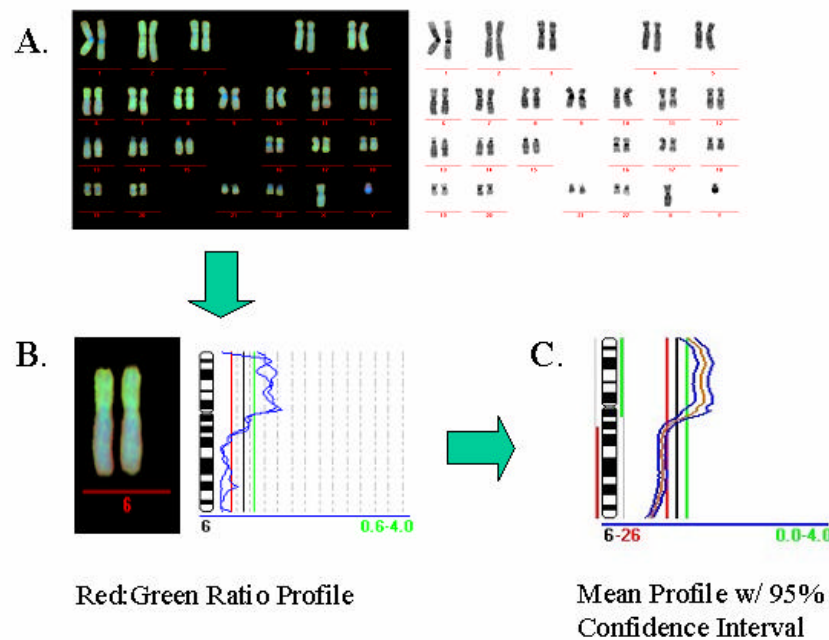


Image Analysis

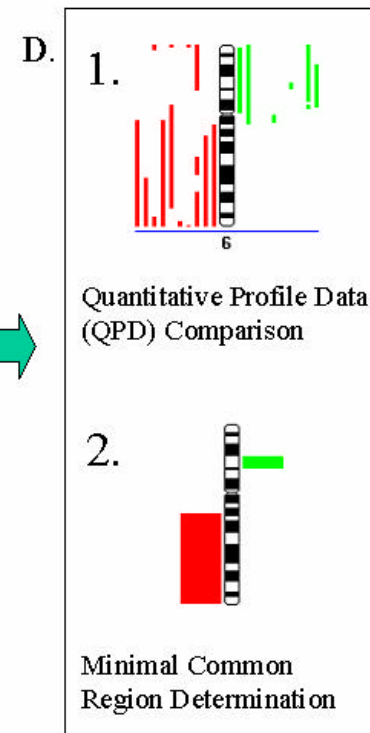


Figure 18. A Schematic for the Process of CGH Analysis. In (A), the completed karyotype from Figure 12 results in a (B) fluorescence ratio profile (red:green for reference:test), where each homologue has its own profile tracing as seen in blue. In (C), compilation of a minimum of 10 ratio profiles comprises the mean ratio profile, in which 95% confidence intervals are assigned to the data. Also shown are the gain (green) and loss (red) bars along the length of the ideogram, which correspond to the mean gains and losses in the test sample. In (D), the side-by-side comparison of all sample mean profiles results in a QPD comparison (1) and the derivation of minimal common regions (2) from the comparison of means.

cytogenetic techniques as described previously. Fresh slides were aged at room temperature for a week and then hybridized with SkyPaint™ probes as per the manufacturer's instructions. Selected metaphase slides were treated with 6µl pepsin stock solution in 50ml of 0.01M HCl for 5 minutes, washed twice in 1xPBS (w/o MgCl₂ or CaCl₂) for 5 minutes, once in 1xPBS/MgCl₂, and then dehydrated in a series of ethanol dilutions (70%, 85%, and 100%) for 2 minutes each. The SkyPaint™ probe mixture was denatured by incubation at 80°C for 7 minutes followed by a pre-anneal incubation at 37°C for 1 hour. Pretreated slides were denatured by incubation with 100µl 70% FA/SSC for at 80°C for 1.5 minutes. Ten microliters of denatured, pre-annealed probe was applied to the denatured, pretreated slides, a coverslip was placed atop the probe and sealed with rubber cement (Elmer's Products, Inc., Columbus, OH) prior to incubation at 37°C for 2 nights. On the third day the rubber cement seals and coverslips were removed. The slides were washed once in 50% FA/SSC at 45°C for 5 minutes, twice in 1xSSC (see appendix) at 45°C for 5 minutes each, and finally in 4xSSC/0.1% Tween 20 at 45°C for 2 minutes. Eighty microliters of the manufacturer-supplied blocking reagent was applied, the slides were coverslipped, and incubated at 37°C for 30 minutes. Following the blocking step, the coverslips were removed and 80µl antibodies, supplied as *buffer 1* (Applied Spectral Imaging, Inc., Carlsbad, CA), were applied. Slides were incubated at 37°C for 45 minutes followed by 3 washes in 4xSSC/0.1% Tween 20 at 45°C for 3 minutes each. Eighty microliters of a second set of antibodies, supplied as *buffer 2* (Applied Spectral Imaging, Inc., Carlsbad, CA), were applied and the slides were incubated at 37°C for 45 minutes. Following this incubation, the slides were washed 3 times in 4xSSC/0.1% Tween 20 at 45°C for 3 minutes each and once in dH₂O for 2

minutes. The slides were allowed to dry, 20µl of manufacturer-supplied DAPI/antifade solution was applied, and a coverslip was mounted over each slide. A minimum of 3 metaphase spreads per cell line were captured and analyzed using the SpectraCube® and a SkyVision™ workstation. While CGH data is stored in the form of CCD images captured through various filters, data from a spectral image is captured in a single exposure and stored in three dimensions, the x and y planes and the integration of light intensity on a wavelength scale, hence the use of the term “cube” in SpectraCube® (Rothmann *et al.*, 1998).

INTERPHASE FLUORESCENCE *IN SITU* HYBRIDIZATION (FISH).

Interphase FISH was performed on uveal melanoma cell lines, created via metaphase chromosome preparation techniques, using human chromosome 3-specific centromere (3cen) probe (Cambio Ltd., Cambridge, UK). Application of the slide pretreatment protocol for CGH prior to hybridization removed any RNA, cytoplasm, or proteins complexed with the DNA (Kallioniemi *et al.*, 1992). The protocol consisted of treating the normal male and cell line slide preparations with RNase A, pepsin/HCl, and 1% formaldehyde in 1xPBS/MgCl₂, and lastly dehydration in a series of ethanols (70%, 85%, and 100%), prior to denaturation and hybridization. The hybridization protocol for the 3cen probes was a slight modification of the manufacturer’s instructions for optimization. Pretreated slides were denatured in 70% FA/SSC at 70°C for 5 minutes, dehydrated in a series of ethanols and allowed to air dry on a 37°C slide warmer. Denaturation of 20µl of indirectly-labeled (biotinylated) 3cen probe at 75°C for 5 minutes occurred in parallel with slide denaturation and dehydration. The probe was

applied to the slide, sealed under a 22mm² glass coverslip with Elmer's rubber cement, and allowed to hybridize for 16 hours at 37°C.

Following hybridization, the coverslips were removed, and the slides washed twice in 45°C 50% FA/SSC for 5 minutes, and then twice in 45°C 0.4xSSC for 5 minutes. The slides were dipped in 45°C 4xSSC/0.05% Tween 20 (see appendix), incubated for 1 hour at 37°C with 150µl 3% non-fat dried milk (NFDM) blocking solution (see appendix), and then dipped in 4xSSC/0.05% Tween 20 a second time. Each slide had 100-200µl of a given antibody solution layered onto it, and slides were incubated for 1 hour with each of 3 separate antibody layers. The first layer of antibodies consisted of avidin-FITC and avidin-Rhodamine in 3% NFDM, the second layer was biotinylated anti-avidin, and the third layer was identical to the first. Following each antibody layer, slides were washed 3 times for 5 minutes each in 45°C 4xSSC/0.05% Tween 20. After the final wash, slides were counterstained with DAPI, rinsed with dH₂O for 5 minutes, and dehydrated in a series of ethanols (70%, 85%, and 100%) for 3 minutes each. Finally, a glass coverslip was mounted over an antifade solution to complete each of the slides. Visualization of the dual-colored probe was with the Leica Q550CW cytogenetics workstation, as described for CGH. FITC, TRITC, and DAPI images were acquired separately and combined to view signal localization and score signal counts within the nuclei. Two hundred nuclei per cell line were scored for 3cen signals. We closely adhered to the rules for analysis of signal distribution as set out by Herrington and colleagues, and the criteria for interphase FISH as described by Hopman *et al.* (Hopman *et al.*, 1988; Herrington *et al.*, 1995).

Interphase FISH was performed on uveal melanoma cell lines using directly-labeled telomere probes for 3p (FITC) and 3q (Texas Red) (Cytocell Ltd., Banbury, Oxfordshire, UK). Slide pretreatment was identical to that described for 3cen FISH. Tandem hybridization of the telomere-3 probes followed the manufacturer's instructions, except for the substitution of a 22mm² glass coverslip. Codenaturation of the probe and slide on a Vysis Hybrite block (Vysis Inc., Downer's Grove, IL), sealed together under a 22mm² glass coverslip, preceded overnight hybridization in a humidified chamber at 37°C. Slides were treated using the manufacturer's post-hybridization protocol, stained with DAPI and mounted with antifade as described above. Again, 200 nuclei per cell line were scored for 3p and 3q signals, and published criteria for interphase FISH and guidelines for analysis of signal distribution were adopted (Hopman *et al.*, 1988; Herrington *et al.*, 1995). Image capture was identical to that described for the 3cen hybridization.

Hardware requirements for FISH analysis are similar to those described for other molecular cytogenetic techniques. For our purposes, the hardware requirements described for CGH digital imaging microscopy were sufficient. Hybridized slides were scored using a Leica Q550CW cytogenetics workstation, which includes a LEICA DM-RXA fluorescent microscope (Leica Inc., Exton, PA), and a SenSys cooled CCD camera (Photometrics Ltd., Tuscon, AZ). Use of a CCD camera is the most sensitive method for obtaining high quality digital fluorescence images (Joos *et al.*, 1994).

STATISTICAL ANALYSES.

Extensive quantitative manipulations of the data from the cell line study were necessary in order to compare the results from CGH, SKY and FISH analyses. In the

tumor study, statistical analyses were used in order to isolate regions of prognostic significance.

Cell Line CGH Analysis.

To effectively manipulate the CGH data from the cell line study, a pixel quantification of net area under each ratio profile curve was applied using a Visual Basic v. 6.0 (Microsoft Corp., Redmond, WA) program created for Image Pro Plus v. 4.5 (Media Cybernetics, Silver Spring, MD) for each of the chromosomes in a given cell line. The intent was to extrapolate the extent of genomic imbalance represented by each of the profiles contributing to the mean. In other words, analyses were made to determine the quantity of shift from the midline of the profile represented in the CGH data given the addition or subtraction of the amount of chromosomal material shown to be gained or lost for a given chromosome. Analysis of individual profiles rather than the mean profiles was determined to be the most accurate approach, similar to an approach previously applied to pseudodiploid and pseudotriploid test samples (Rosenberg *et al.*, 1997). The following formula was applied to calculate relative balance (RB) represented in each individual chromosome profile in all metaphase spreads analyzed for each cell line:

$$\text{CGH RB} = (\text{NA/PL} \times 1/\text{len1}) + 1$$

For a given chromosome, **NA** was the number of pixels under ratio profile to the right of the midline minus the number of pixels under the ratio profile to the left of the midline, **PL** was the vertical profile pixel length, in pixels, and **len1** was the distance, in pixels, representing a unit change in copy number on the x-axis of the ratio profile. **CGH RB**, the extrapolated ratio value used as a measure of balance, was determined for a specific

chromosome in any given cell for each of the cell lines. This allowed a quantification of the expected amount of genomic imbalance relative to the copy number ratio.

Cell Line SKY Analysis.

A pixel quantification of each of the 24 chromosome classification colors in SKY was applied using a Visual Basic v. 6.0 (Microsoft Corp., Redmond, WA) program written for Image Pro Plus v. 4.5 (Media Cybernetics, Silver Spring, MD). This quantification was performed for each of the available spreads from the 10 cell lines, and normalized against representative whole chromosomes from within the same spread. The relative chromosome equivalent (RCE) feature was calculated for each of the 22 autosomes from the SKY classification images according to the formula:

$$\text{SKY RCE} = \text{PT/PN}$$

For a metaphase spread, **PT** was the number of pixels designated for a given chromosome throughout the SKY classification image, and **PN** was the number of pixels assigned to all cytogenetically normal chromosomes of the same classification divided by the number of normal chromosomes counted. This internal normalization resulted in determination of relative chromosome equivalents for each cell line. Using this method, the relative amount of genomic imbalance could be compared between chromosomes from a given cell line, but SKY RCE remained an absolute measure of chromosomal material and therefore was directly comparable with the FISH results.

A relative genomic balance for the SKY data (SKY RB) was calculated for each of the 22 autosomes by dividing the individual chromosome SKY RCE values by the mean SKY RCE (comparable to CGH midline) for all chromosome types. The SKY data, an absolute measure in its original form, becomes transformed into a ratio and was

thereby compensated for ploidy but not aneusomy. SKY RCE and SKY RB results for OCM-3 were not reported due to hardware failure while archiving SKY data.

Cell Line FISH Analysis.

A FISH relative chromosome equivalent (FISH RCE) feature was calculated for chromosome 3 in each cell line, as the sum of all 3cen, 3p and 3q hybridization signals (200 nuclei scored for each) divided by the total number of signals (divided by 600). This was essentially a combined average for the individual signal means. FISH RCE remained an absolute measure of chromosome 3 copy number, and was most readily compared with the SKY RCE. Since there was no available compensation for genomic ploidy, because FISH revealed only chromosome 3 copy number, determination of FISH RB was not reasonable.

Tumor CGH Analysis.

Minimal common regions were generated from mean ratio profiles of 82 archival FFPE tumor specimens analyzed by CGH, for those chromosomal regions evidencing gains or losses in greater than 30% and less than 70% of the cases. Minimal common regions were further subdivided by gender, for accurate analysis of copy number imbalances on the sex chromosomes, and survival, to determine which chromosomal regions were potentially of value in prognosis.

CGH data for individual cases was recorded as normal (1), gain (2), loss (0), or both (0 and 2) at each minor band for all 24 chromosomes in the mean ratio profiles. Minor band data was collated for each major band, and major bands were initially scanned for significant gains or losses with a two-tailed t-test. Only those chromosomal regions shown to be significant in the analysis of major bands were then analyzed at the

level of the minor band, also with a two-tailed t -test. Individual minor bands with univariate significance following that analysis were compared with cell type, tumor size, mean of the ten largest nucleoli, and survival in a Cox Regression analysis, to determine which chromosomal regions correlate most strongly with prognosis. Univariate Kaplan-Meier cause specific survival curves were generated for those regions determined to have prognostic significance in the Cox Regression analysis. Multivariate predictors of prognosis were also explored, as first described by McLean and colleagues, and multivariate Kaplan-Meier cause specific survival curves were also generated (McLean *et al.*, 1977).

RESULTS

UVEAL MELANOMA CELL LINES.

Comparative Genomic Hybridization.

Mean profiles for all 10 cell lines were compared (Fig. 19). Copy number abnormalities identified in greater than 50% of the mean ratio profiles comprise the minimal common regions, which were pinpointed based upon the most recent chromosome ideogram and genome mapping data available (Fig. 20).

Many of these abnormalities aligned with previously published findings, including CGH and classical cytogenetic data (Tables 2 and 3). Minimal common regions were used to identify genes likely to be involved in uveal melanoma (Table 4). Many of these genes have either been previously linked to uveal melanoma or its predisposing factors and/or are involved in cell-cycle control.

Gains and losses often consisted of large portions of chromosomes, and in some cases involved whole chromosomes. Whole chromosome gains were observed in individual cell lines: chromosome 7 (OMM-1), chromosome 8 (MEL270) and chromosome 17 (OCM-3). Whole chromosome gains were observed in 3 cell lines for chromosomes 20 (OCM-3, OCM-8, and OMM-1) and 22 (OCM-3, OCM-8, and OMM-2.3). The greatest gains of chromosome 3 were evidenced in OCM-1, OM431, and OMM-2.3. Only OCM-1 and OM431 had gains that included the centromere. Other significant p- and q-arm gains were seen in OCM-3 and OCM-8. A whole chromosome loss was observed in one instance on chromosome 4 (OCM-3).

The frequent involvement of chromosomes 3, 6 and 8 in copy number imbalances was apparent (Figs. 19 and 20). There were multiple consistent gains along chromosome

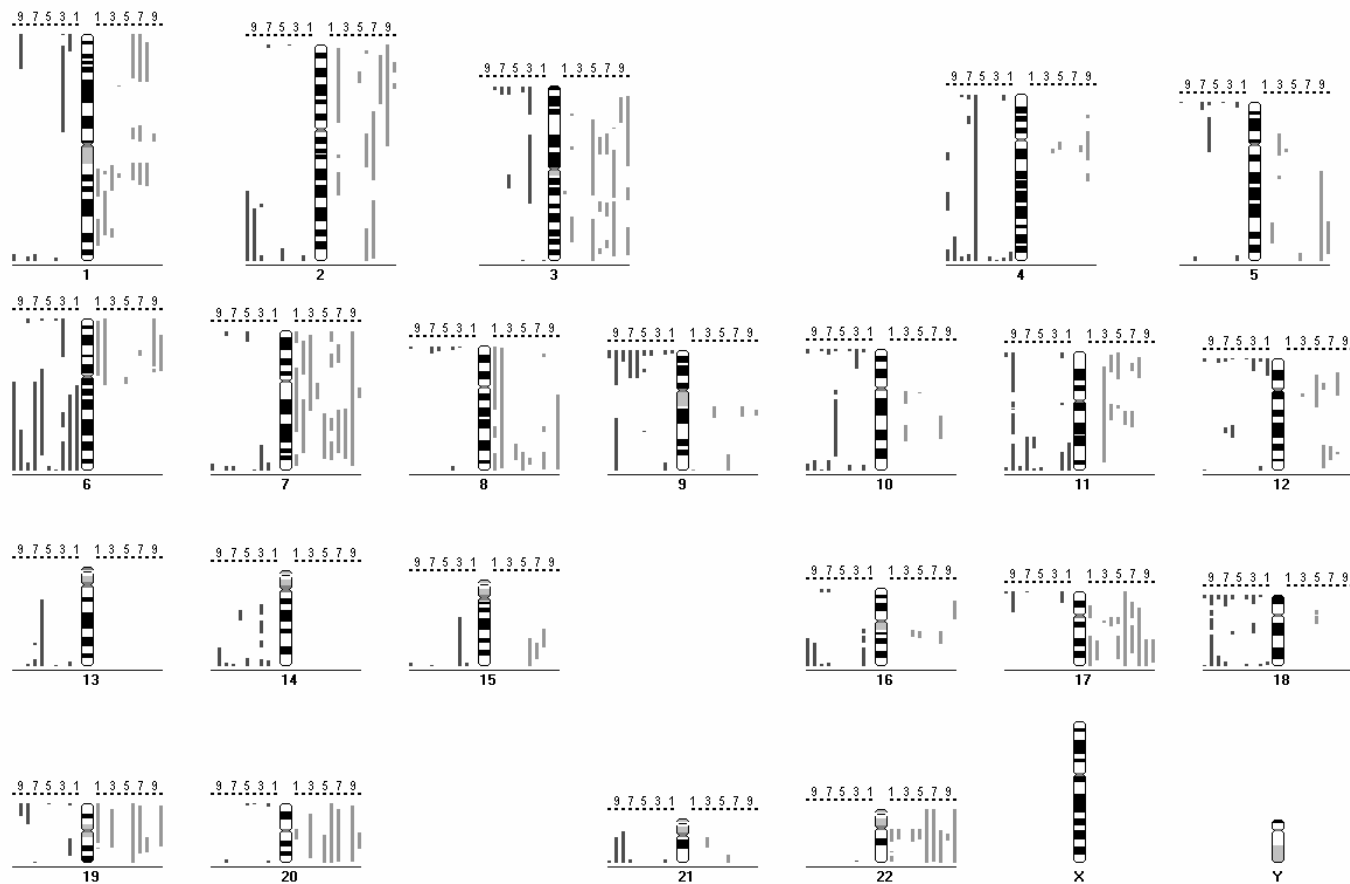


Figure 19. Quantitative Comparison Data for Genomic Imbalances in Ten Cell Lines. The gain threshold was set at a 1.2 copy number ratio, and the loss threshold was set at a 0.8 copy number ratio. Light gray bars to the right of the ideogram represent gains in a specific chromosomal region for each cell line, and dark gray bars to the left of each ideogram represent regions of loss in the cell line genome. The gain and loss bars are paired by cell line, starting with the pair closest to the ideogram, and then flanking outward. A scale with the numeric code for each cell line, as designated in Table 1, is provided above each ideogram: 1 = 92-1, 2 = MEL270, 3 = MEL285, 4 = MEL290, 5 = OCM-1, 6 = OCM-3, 7 = OCM-8, 8 = OM431, 9 = OMM1, and 10 = OMM2.3. Only autosomes are considered in our analysis.

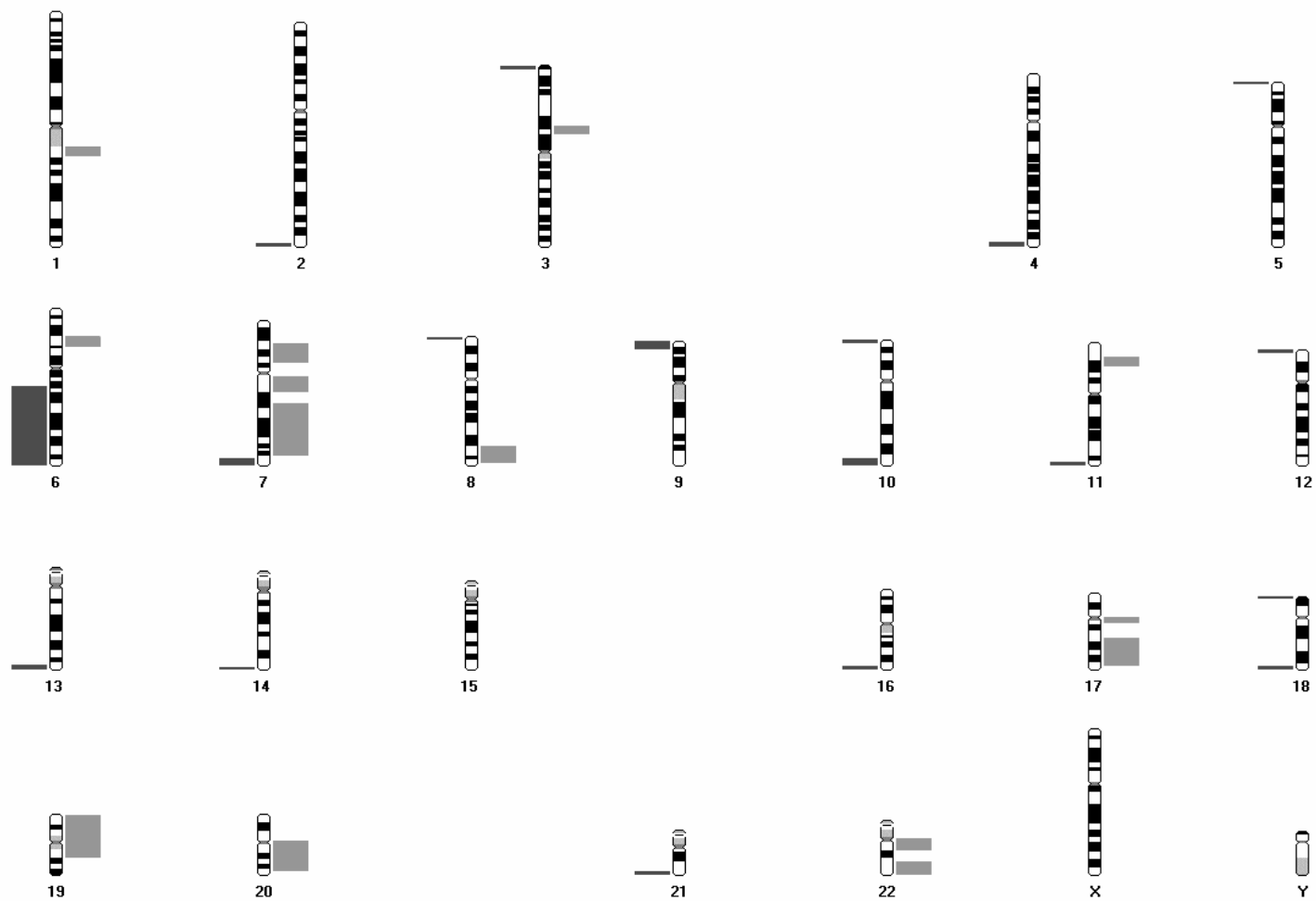


Figure 20. Minimal Common Regions of Gain and Loss Distilled from CGH Mean Profile Data of Ten Uveal Melanoma Cell Lines. The light gray bars to the right of the ideogram represent gain, and dark gray bars to the left of the ideogram represent regions of loss, common among at least 50% of the cell lines. These minimal common regions may denote chromosomal regions related to the development and progression of uveal melanoma. Only autosomes are considered in our analysis.

Table 2. A Comparison of Gains Seen in Ten Uveal Melanoma Cell Lines Compared with Previously Reported Chromosomal Abnormalities in Uveal Melanoma.

Gains Observed in the Current Study ^a		Cell Lines ^b	Gains Reported by CGH ^a		Reference	Gains Reported by Classical Cytogenetics ^a		Reference
1q21.1 - q21.2	(60%)	1,2,3,6,7,8	1q	(9.1%)	Speicher <i>et al.</i> , 1994			
1q21.2	(60%)	1,3,4,6,7,8						
3p13 - p14.1	(50%)	2,5,6,7,10						
6p21.2 - p21.3	(50%)	1,2,7,9,10	6p	(45.5%)	Speicher <i>et al.</i> , 1994	6p	(46.3%)	White <i>et al.</i> , 1998b
			6p	(57%)	Ghazvini <i>et al.</i> , 1996	6p	(25%)	Wiltshire <i>et al.</i> , 1993
			6p	(42%)	"	6p12 - 6pter	(25%)	"
			6p	(40%)	Gordon <i>et al.</i> , 1994			
			6p21 - pter	(54.5%)	Speicher <i>et al.</i> , 1994			
7p13 - p15.2	(50%)	2,3,6,7,9						
7q11.21 - q11.23	(50%)	1,3,4,9,10	7q	(70%)	Gordon <i>et al.</i> , 1994			
7q21.2 - q21.3	(60%)	1,2,3,7,8,9						
7q21.3 - q22.1	(60%)	1,2,5,7,8,9						
7q22.1 - q31.1	(70%)	1,2,5,6,7,8,9						
7q31.1 - q31.3	(50%)	2,5,7,8,9						
7q31.3 - q33	(60%)	2,5,6,7,8,9						
7q34 - q35	(50%)	1,5,6,8,9						
8q24.1 - q24.2	(60%)	1,2,4,5,8,10	8q	(54.5%)	Speicher <i>et al.</i> , 1994	8q	(48.1%)	White <i>et al.</i> , 1998b
8q24.2 - q24.3	(60%)	1,2,5,6,8,10	8q	(100%, fresh)	Ghazvini <i>et al.</i> , 1996	8	(25%)	Wiltshire <i>et al.</i> , 1993
8q24.3	(60%)	1,2,5,8,10	8q	(57%, fixed)	"	8q	(50%)	"
			8q	(100%)	Gordon <i>et al.</i> , 1994	8q13.1 - 8qter	(25%)	"
			8q24 - qter	(63.6%)	Speicher <i>et al.</i> , 1994			
11p14 - p15.1	(50%)	3,4,5,7,8	11p	(9.1%)	"			

^aThe percentage in parentheses is the frequency of occurrence for a given gain.

^bSee cell line key.

Table 2 (cont'd). A Comparison of Gains Seen in Ten Uveal Melanoma Cell Lines Compared with Previously Reported Chromosomal Abnormalities in Uveal Melanoma.

Gains Observed in the Current Study ^a		Cell Lines ^b	Gains Reported by CGH ^a		Reference	Gains Reported by Classical Cytogenetics ^a	Reference
17q11.1 - q11.2	(50%)	3,4,5,6,8	17	(18.2%)	Speicher <i>et al.</i> , 1994		
17q21.3 - q22	(50%)	1,5,6,7,8					
17q22 - q24	(80%)	1,2,5,6,7,8,9,10					
17q24	(70%)	1,2,5,6,8,9,10					
17q24 - q25	(60%)	1,2,6,8,9,10					
19p13.3 - q12	(50%)	1,3,6,7,10					
19q12 - q13.1	(60%)	1,3,6,7,8,10					
19q13.1 - q13.2	(50%)	3,6,7,8,10					
20p11.1 - q11.1	(50%)	1,3,6,7,9	20	(14%)	Ghazvini <i>et al.</i> , 1996		
20q11.1 - q11.2	(70%)	1,3,5,6,7,9,10					
20q11.2 - q13.1	(60%)	3,5,6,7,9,10					
20q13.1 - q13.3	(50%)	3,5,6,7,9					
22q11.1 - q11.2	(80%)	1,2,4,5,6,7,8,10	22	(9.1%)	Speicher <i>et al.</i> , 1994		
22q11.2 - q12.1	(90%)	1,2,4,5,6,7,8,9,10	22q	(9.1%, fresh)	Ghazvini <i>et al.</i> , 1996		
22q13.2	(50%)	1,6,7,8,10	22q	(42%, fixed)	"		
22q13.3 - qter	(50%)	1,6,7,8,10					

^aThe percentage in parentheses is the frequency of occurrence for a given gain.

^bSee cell line key.

Table 3. A Comparison of Losses Seen in Ten Uveal Melanoma Cell Lines Compared with Previously Reported Chromosomal Abnormalities in Uveal Melanoma.

Losses Observed in the Current Study ^a		Cell Lines ^b	Losses Reported by CGH ^a		Reference	Losses Reported by Classical Cytogenetics ^a		Reference
2q37.3 - qter	(50%)	2,5,8,9,10						
3p26 - pter	(50%)	3,4,6,7,8	3	(45.5%)	Speicher <i>et al.</i> , 1994	3	(80%)	White <i>et al.</i> , 1998a
			3	(57%, fresh)	Ghazvini <i>et al.</i> , 1996	3	(50%)	White <i>et al.</i> , 1998b
			3	(85%, fixed)	"	3	(100%)	Wiltshire <i>et al.</i> , 1993
			3	(70%)	Gordon <i>et al.</i> , 1994			
			3	(57%)	Prescher <i>et al.</i> , 1996			
4q35 - 4qter	(90%)	1,2,3,4,6,7,8,9,10	4q	(14%)	Ghazvini <i>et al.</i> , 1996			
5p15.3 - pter	(50%)	2,4,6,7,10						
6q14 - q21	(50%)	1,2,6,7,10	6q	(45.5%)	Speicher <i>et al.</i> , 1994	6q	(46.3%)	White <i>et al.</i> , 1998b
6q21 - q22.2	(60%)	1,2,3,6,7,10	6q	(42%, fresh)	Ghazvini <i>et al.</i> , 1996	6q	(25%)	Wiltshire <i>et al.</i> , 1993
6q22.2 - q23.3	(60%)	1,2,6,7,9,10	6q	(28%, fixed)	"	6q12 - 6qter	(25%)	"
6q23.3 - q25.2	(70%)	1,2,3,6,7,9,10						
6q25.2 - q26	(60%)	1,2,3,7,9,10						
6q26 - q27	(70%)	1,2,3,7,8,9,10						
6q27 - qter	(90%)	1,2,3,4,5,7,8,9,10						
7q36 - qter	(60%)	2,3,4,7,8,10						
8p23.3 - pter	(50%)	3,4,6,7,10	8p	(28%)	"	8p	(25%)	Wiltshire <i>et al.</i> , 1993
9p23 - p24	(50%)	6,7,8,9,10	9p21 - pter	(27.3%)	Speicher <i>et al.</i> , 1994	9p	(25%)	"
9p24 - pter	(90%)	1,2,4,5,6,7,8,9,10	"	"	"	9p23 - 9pter	(25%)	"
10p15.1 - pter	(70%)	2,3,4,6,7,8,10						
10q26.2 - qter	(60%)	2,4,7,8,9,10						
11q25 - qter	(80%)	1,2,5,6,7,8,9,10	11q23 - qter, 11q	(18.2%) (42%)	" Ghazvini <i>et al.</i> , 1996			

^aThe percentage in parentheses is the frequency of occurrence for a given loss.

^bSee cell line key.

Table 3 (cont'd). A Comparison of Losses Seen in Ten Uveal Melanoma Cell Lines Compared with Previously Reported Chromosomal Abnormalities in Uveal Melanoma.

Losses Observed in the Current Study ^a		Cell Lines ^b	Losses Reported by CGH ^a		Reference	Losses Reported by Classical Cytogenetics ^a	Reference
12p13.3 - pter	(80%)	1,2,3,4,6,7,8,10	12p	(9.1%)	Speicher <i>et al.</i> , 1994		
13q34 - qter	(50%)	2,4,6,7,8					
14q32.3 - qter	(60%)	2,3,5,7,8,9					
16q24 - qter	(50%)	2,7,8,9,10	16q	(18.2%)	"		
18p11.31 - pter	(80%)	2,3,4,6,7,8,9,10					
18q23 - qter	(70%)	1,2,4,7,8,9,10					
21q22.3 - qter	(50%)	2,7,8,9,10					

^aThe percentage in parentheses is the frequency of occurrence for a given loss.

^bSee cell line key.

Table 4. A Correlation of Copy Number Abnormalities in Ten Uveal Melanoma Cell Lines and Genes Associated with Uveal Melanoma or its Predisposing Factors.

Gain/Loss Observed in Current Study ^a	Cell Lines ^b	Gene	Locus ^c	Function	Source ^{c,d}
+1q21.1 - 1q21.2 (60%)	1,2,3,6,7,8	TNFSF6	1q23	tumor necrosis factor ligand	OMIM
+1q21.2 (60%)	1,3,4,6,7,8				
-2q31 - q32 (20%)	9,10	alpha4 integrin subunit gene, CAT gene	2q31 - q32	transcriptional regulator of alpha4 integrin subunit gene in metastasis, alpha4 promoter fused to CAT gene	Larouche <i>et al.</i> , 1998
+6p21.2 - p21.3 (50%)	1,2,7,9,10	HLA-G	6p21.3	histocompatibility antigen	OMIM
-6q14 - q21 (50%)	1,2,6,7,10	?	6q12 - q21	putative tumor suppressor gene	Copeman, 1992
-6q21 - q22.2 (60%)	1,2,3,6,7,10	AIM1	6q21	absent in melanoma	OMIM
+7q21.2 - q21.3 (60%)	1,2,3,7,8,9	MDR1	7q21.1 - q21.2	produces P-gp pump protein, causes drug resistance in cancer cells	Dunne <i>et al.</i> , 1998
+8q24.1 - q24.2 (60%)	1,2,4,5,8,10	c-myc	8q24	oncogene	Blom <i>et al.</i> , 1997
+8q24.2 - q24.3 (60%)	1,2,5,6,8,10	"	"	"	Chana <i>et al.</i> , 1999
+8q24.3 (50%)	1,2,5,8,10				
-9p23 - p24 (50%)	6,7,8,9,10	CDKN2 (p16)	9p21	tumor suppressor, involved in FAM-M and Li-Fraumeni	Singh <i>et al.</i> , 1996a
-9p24 - pter (90%)	1,2,4,5,6,7,8,9,10	FCM critical region	9p13 - p22	familial cutaneous melanoma critical region	Houlston and Damato, 1999
					Merbs and Sidransky, 1999
		CMM2	9p21	cutaneous malignant melanoma, also involved in FAM-M	Singh <i>et al.</i> , 1996b
		TYRP1	9p23	tyrosinase-related protein 1	OMIM

^aThe percentage in parentheses is the frequency of occurrence for a given abnormality.

^bSee cell line key.

^cLoci without an OMIM reference were pinpointed using the International RH Mapping Consortium - GeneMap '99 at <http://www.ncbi.nlm.nih.gov/genemap99>. A number of these loci are not identical to those identified in the current study. The International RH Mapping Consortium recognizes the presence of positional discrepancies in the published map. Therefore, we have chosen to list these loci due to their linkage with uveal melanoma and their general proximity to the copy number abnormalities identified in this study.

^dAll references to OMIM refer to Online Mendelian Inheritance in Man, <http://www.ncbi.nlm.nih.gov/Omim/> and were collected by doing a keyword search of "uveal melanoma" and "melanoma."

Table 4 (cont'd). A Correlation of Copy Number Abnormalities in Ten Uveal Melanoma Cell Lines and Genes Associated with Uveal Melanoma or its Predisposing Factors.

Gain/Loss Observed in Current Study ^a	Cell Lines ^b	Gene	Locus ^c	Function	Source ^{c,d}
-10q26.2 qter (60%)	2,4,7,8,9,10	DMBT1	10q25.3 - q26.1	deleted in malignant brain tumors	OMIM
+11p14 - p15.1 (50%)	3,4,5,7,8	HRAS "	11p15.5 "	v-Ha-Ras oncogene "	Singh <i>et al.</i> , 1996a OMIM
-11q25 - qter (80%)	1,2,5,6,7,8,9,10	tyrosinase	11q13.5 - q14.1	melanoma associated antigen	Luyten <i>et al.</i> , 1998
-12p13.3 - pter (80%)	1,2,3,4,6,7,8,10	KRAS "	12p12.1 "	v-Ki-Ras 2 oncogene "	Singh <i>et al.</i> , 1996a OMIM
-13q34 - qter (50%)	2,4,6,7,8	BRCA2	13q12.2 - q12.3	breast cancer susceptibility locus	Houlston and Damato, 1999
-16q24 - qter (50%)	2,7,8,9,10	MC1R	16q24.3	melanocortin 1 receptor	OMIM
-17p13 - pter (30%)	2,9,10	p53	17p13.1	tumor suppressor, involved in Li-Fraumeni	Singh <i>et al.</i> , 1996a
+17q11.1 - q11.2 (50%)	3,4,5,6,8	NF1	17q11.2	neurofibromatosis	OMIM
+17q21.3 - q22 (50%)	1,5,6,7,8	BRCA1	17q21	breast cancer	OMIM
+17q22 - q24 (80%)	1,2,5,6,7,8,9,10	PRKCA	17q22 - q23.2	protein kinase C	OMIM
+19p13.3 - q12 (50%)	1,3,6,7,10	STK11	19p13.3	serine/threonine protein kinase II	OMIM
+19q12 - q13.1 (60%)	1,3,6,7,8,10	MEL	19p13.2 - cen	oncogene MEL, Ras-associated protein	OMIM
+19q13.1 - q13.2 (50%)	3,6,7,8,10	MIA	19q13.32 - q13.33	melanoma inhibitory activity	OMIM
+22q11.2 - q12.1 (90%)	1,2,4,5,6,7,8,9,10	EWSR1 LFS NF2	22q12 22q12.1 22q12.2	Ewing sarcoma breakpoint Li-Fraumeni neurofibromatosis	OMIM OMIM OMIM

^aThe percentage in parentheses is the frequency of occurrence for a given abnormality.

^bSee cell line key.

^cLoci without an OMIM reference were pinpointed using the International RH Mapping Consortium - GeneMap '99 at <http://www.ncbi.nlm.nih.gov/genemap99>. A number of these loci are not identical to those identified in the current study. The International RH Mapping Consortium recognizes the presence of positional discrepancies in the published map. Therefore, we have chosen to list these loci due to their linkage with uveal melanoma and their general proximity to the copy number abnormalities identified in this study.

^dAll references to OMIM refer to Online Mendelian Inheritance in Man, <http://www.ncbi.nlm.nih.gov/Omim/> and were collected by doing a keyword search of "uveal melanoma" and "melanoma."

3 as a whole. Gains were also seen on 6p and distal 8q, while consistent losses were found on 6q (Fig. 16). A thorough evaluation of chromosomes 3, 6, and 8 was critical because they are frequently reported as aberrant in uveal melanoma. The cell line MEL285 approached monosomy 3, as a prominent loss extended from the p-terminus to 3q21, but the remainder of the chromosome traced the normal midline of the CGH profile. Loss of distal 3p was seen in the quantitative comparison data (QCD) (Fig. 19) for MEL290, OCM3, OCM8, and OM431. Several cell lines exhibited tendencies toward loss of portions of chromosome 3, including 92-1, MEL290, OCM-3, OCM-8, and OM431. These tendencies did not exceed the threshold for loss. The trend seen in 92-1 was toward a loss of 3q, whilst the others were for loss of 3p. The p-arm of chromosome 6 was gained in 92-1, MEL270, OMM-1, and OMM-2.3, while 6q was lost in 92-1, MEL270, MEL285, OCM-3, OCM-8, OMM-1, and OMM-2.3. Three cell lines showed loss on both 6q and distal 3p (MEL285, OCM-3, and OM431). A focal gain at 8q24 was also seen in 5 of the 10 cell lines (92-1, MEL290, OCM-1, OCM-3, and OM431). The entire chromosome 8 was gained in MEL270, while only 8q was gained in OMM-2.3.

Spectral Karyotyping.

SKY identified numerical and structural aberrations on a per-cell basis in each of the cell lines. For our SKY analysis, a total of 2,334 chromosome structures were analyzed, with the percent of aberrations ranging from 0% for the Y chromosome to 62.96% for chromosome 1 (Table 5). Chromosomes 1, 3, 8 and X contained aberrations in all of the cell lines. Chromosomes 1, 3, 7, 12, 17 and 20 were aberrant more than 50% of the time collectively across all cell lines. Frequent structural and numerical aberrations were tabulated as those that occurred across 3 or more cell lines (Table 5).

The high frequency of these aberrations suggests that chromosomes 1, 3, 7, 12, 17 and 20 may contain genes of significance in the establishment and/or progression of uveal malignant melanoma. Chromosomes 1, 3, 8, 17, 19, 20, and 22 were often involved in numerical aberrations (Table 5). Complex aberrations involving more than 2 chromosomes were seen frequently in MEL290, OCM-1, OCM-3, and OCM-8 (Fig. 21).

Partially deleted, or truncated, copies of chromosome 3 were seen in OCM-3, OCM-8, and OM431. There were multiple copies of marker chromosomes in OCM-1 and OM431 that SKY classified as chromosome 3 material. Additional copies of 6p were found in MEL270 and OCM-8, and additional copies of 8q were found in OCM-3 and OCM-8. There were no (3;6) or (3;8) rearrangements in any of the cell lines.

Five chromosomal aberrations were observed across multiple cell lines (Fig. 22). The most prevalent abnormalities were +der(1)t(1;10)(q10;q10) (92-1, OCM-8, OM431, OCM-3, and MEL285) and +der(2)t(2;12)(p10;q10) (92-1, OCM-8, OM431, OCM-3, and OCM-1), each evidenced in 5 cell lines. Other interactions, including +der(20)t(X;20)(?;q?) (OCM-8, OCM-3, OCM-1, and OMM-2.3) and the persistent reciprocal t(3;10)(p25;q25) (OCM-8, OM431, OMM-2.3, and MEL270), were each seen in four cell lines. Three distinct rearrangements were seen between chromosomes 3 and 7, but poor banding quality prevented clarification beyond +der(3)t(3;7)(?;?) or +der(7)t(3;7)(?;?) for these non-reciprocal translocations. These rearrangements between chromosomes 3 and 7 were seen in OCM-8, OM431, OCM-1, and OMM-1. Note that the cell line OCM-8 was the only line evidencing some form of all five of these interactions.

Table 5. Summary of Aberrations Identified by SKY in Ten Uveal Melanoma Cell Lines

Chromosome	Range Percent Aberrations ^a	Mean Percent Aberrations	Lines with Aberrations	Structural Aberrations ^b	Frequent Aberrations ^{b,c,d}
1	25 - 100	62.96	10	t, dic, del, ins, mr	der(1;10) [5] t(1;2) [3] der(1;7) [3] der(1;16) [3]
2	0 - 100	49.29	7	t, dic, del, ins, mr	der(2;12) [5]
3	16.67 - 66.67	51.43	10	t, dic, del, ins, mr	der(3;7)/t(3;7) [5] t(3;10) [4]
4	0 - 52.63	22.73	7	t, del	
5	0 - 88.89	42.54	7	t, del, i	dup(5p) [3]
6	0 - 66.67	37.84	8	t, del, i	
7	0 - 90.63	59.90	9	t, dic, del, mr	t(7;17) [3]
8	8.33 - 75	47.17	10	t, del, i, mr	der(8;11) [3]
9	0 - 66.67	25.24	6	t	
10	0 - 80	44.74	8	t, ins, del	
11	0 - 75	43.65	7	t, ins, del	
12	0 - 85.71	61.81	8	t, ins, del	dup(12p) [3] dup(12q) [3]
13	0 - 50	22.99	7	t	
14	0 - 50	12.64	4	t, mr, R	
15	0 - 66.67	27.45	4	t, mr	
16	0 - 72.73	49.59	8	t, mr	der(16;17) [3]
17	0 - 100	57.81	8	t, mr	
18	0 - 46.67	14.94	3	t, mr	
19	0 - 75	30.36	7	t, mr	
20	0 - 100	57.45	6	t, mr	der(20;X) [4]
21	0 - 100	15.15	8	t	
22	0 - 57.89	18.10	5	t, i	
X	11.11 - 100	46.51	10	t, del	
Y	0 - ND ^e	0	0		

^aThe range of percent aberrations is determined by the number of aberrant copies of a given chromosome in all SKY spreads for a cell line compared to the number of normal copies of that same chromosome in that same cell line

^bdel = deletion, der = derivative, dic = dicentric, dup = duplication, i = isochromosome, ins = insertion, mr = multiple rearrangement, R = Robertsonian translocation, t = translocation. All nomenclature, except "mr," according to ISCN 1995.

^cThe number in brackets is the number of cell lines in which the particular aberration was identified.

^dRedundancies in the data set have been eliminated.

^eThe notation "ND" indicates that there were no observations, normal or aberrant, for that chromosome. There was no data in 92-1, MEL270, MEL285, MEL290, OCM-1, OCM-3, OM431, and OMM1 for chromosome Y.

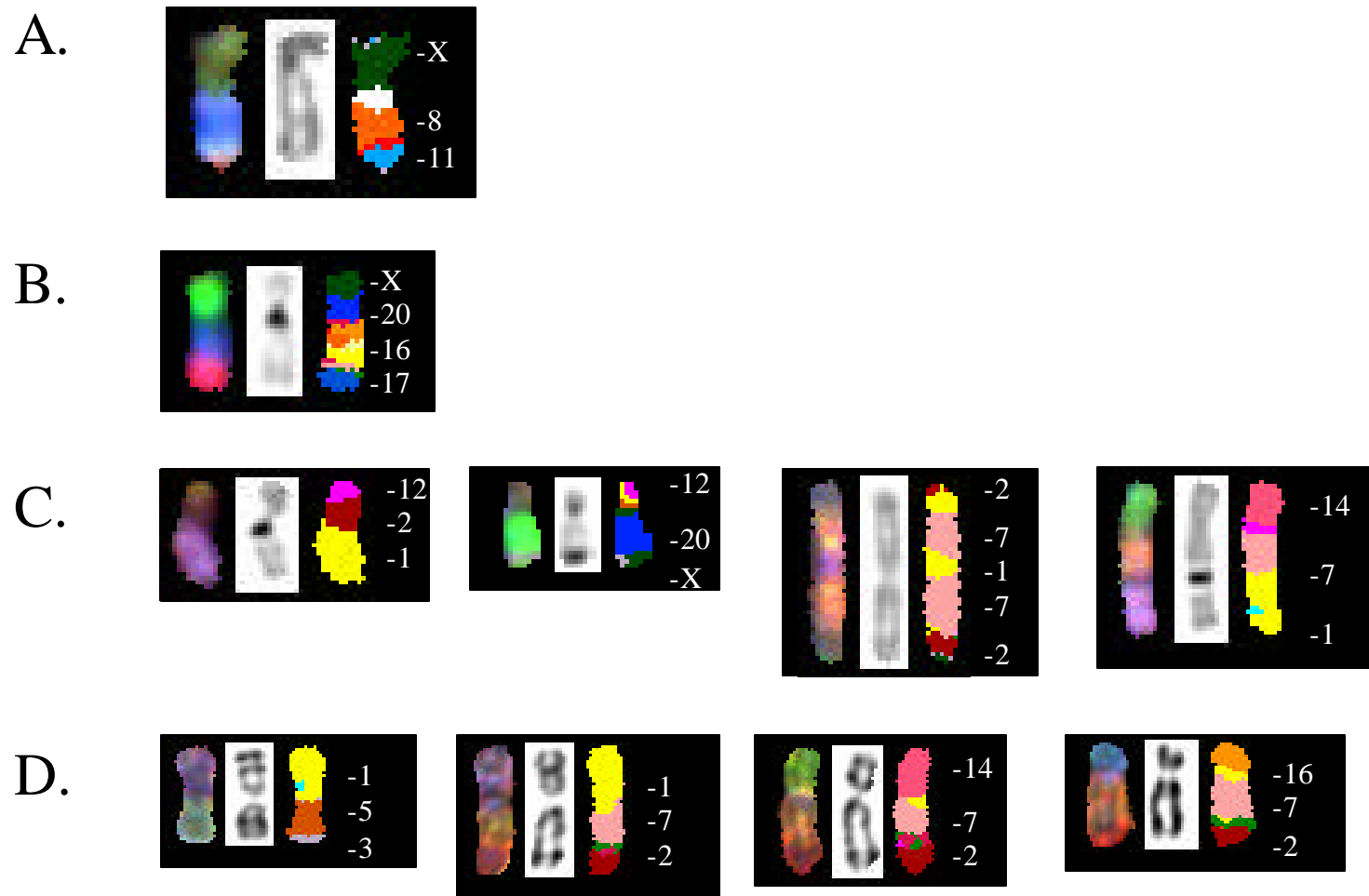


Figure 21. Complex Aberrations Detected by Spectral Karyotyping. SKY employs 24 distinctly labeled chromosome-specific probes, thus allowing for the identification of all the chromosomes involved in complex rearrangements. SKY was performed on 10 uveal melanoma cell lines and revealed complex chromosomal rearrangements in 4 of the lines: (A) MEL290, (B) OCM-1, (C) OCM-3 and (D) OCM-8.

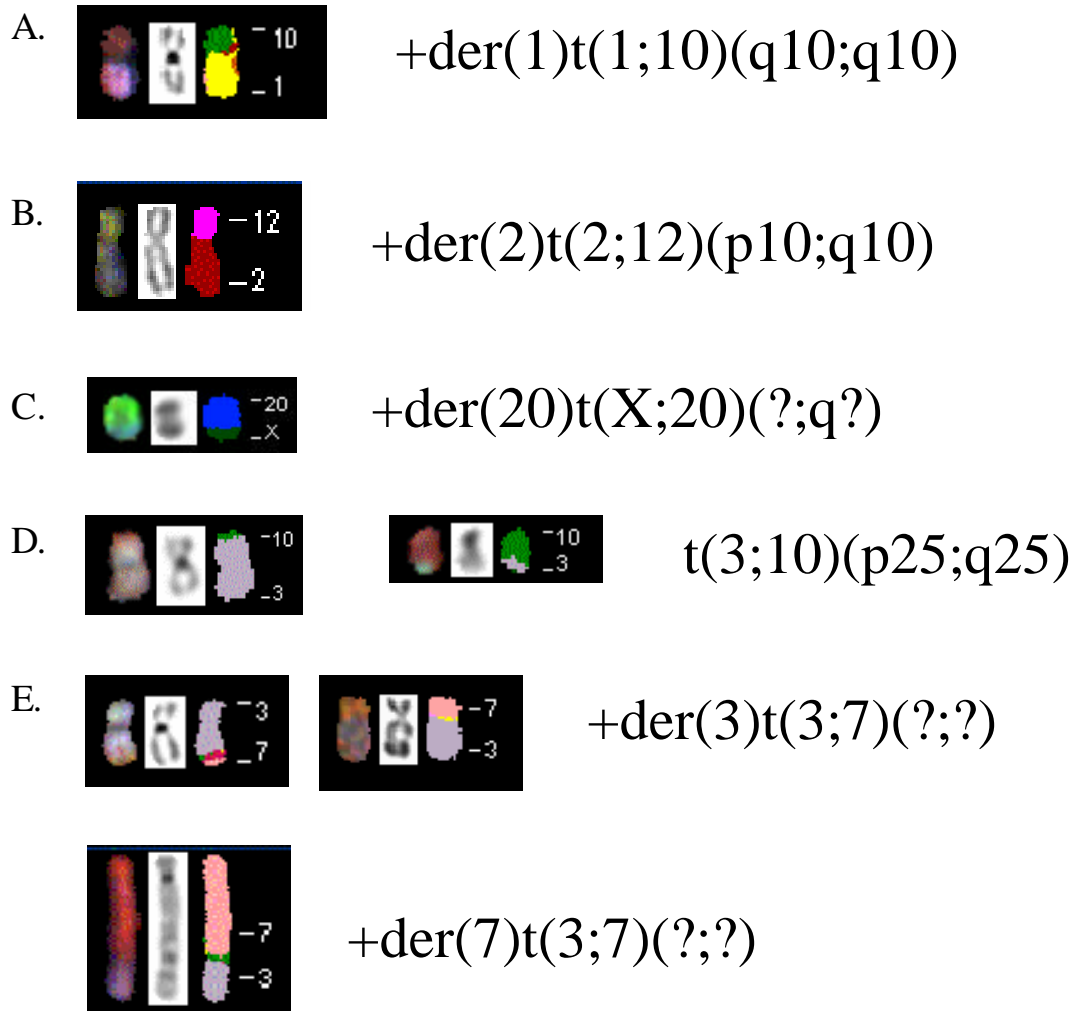


Figure 22. Chromosome Rearrangements Seen Across Ten Uveal Melanoma Cell Lines. (A) A +der(1)t(1;10)(q10;q10) was seen in 92-1, OCM-3, OCM-8, OM431 and MEL285. (B) A +der(2)t(2;12)(p10;q10) was seen in 92-1, OCM-1, OCM-3, OCM-8 and OM431. Note that these interactions were observed in 5 cell lines each. (C) The cell lines OCM-1, OCM-3, OCM-8 and OMM2.3 all evidenced a +der(20)t(X;20)(?,q?). (D) Four cell lines (MEL270, OCM-8, OM431 and OMM2.3) exhibited the reciprocal t(3;10)(p25;q25). (E) Additional interactions involving chromosome 3, all between chromosomes 3 and 7, were seen as 2 distinct +der(3)t(3;7)(?,?) and a +der(7)t(3;7)(?,?) that were not elucidated by banding analyses. These interactions all occurred in OCM-1, OCM-8, OM431 and OMM1. Note that the only cell line containing some form of all five of these interactions was OCM-8. Interactions observed in multiple cell lines, such as these, are likely linked to the development of their associated cell line, and warrant further study. These interactions are also likely associated with copy number abnormalities in the genome, which lead to enhanced or diminished gene products during development.

Interphase Fluorescence *in situ* Hybridization.

Locus-specific FISH probes for 3p, 3q, and 3cen allowed further study of chromosome 3 in the cell lines (Table 6). Two hundred nuclei were scored at random for each probe and each cell line. In the diploid control, 86% of the normal male nuclei analyzed had 2 signals for 3cen. Our cell lines were heterogeneous in chromosome 3 complement according to centromeric-FISH, showing 0 to 6 copies of 3cen (Table 6), and averaging 0.99 to 1.53 copies per cell. The percentage of 3cen loss (0 or 1 copies present) was highest in MEL285 (72.5%) and lowest in OCM-1 (49.5%). The dominant population in each cell line had one 3cen hybridization signal per nucleus (ranging from 34% of cells for 92-1 to 45.5% of cells for MEL285). Meanwhile, gain of signal (≥ 2 copies) ranged from 2.5% (OMM-1) to 19% (OCM-3) by centromeric-FISH.

Results for the telomere probes of the diploid control showed that 93% of cells had 2 signals for both 3p and 3q. However, we saw a broad range of signals for 3p (0 to 10 copies) and 3q (0 to 12) in individual cells across all cell lines (Table 6). In contrast to the FISH findings for 3cen, no more than 16% of nuclei had one 3p signal and no more than 4% had one 3q signal (both seen in MEL290). Four cell lines had at least two 3p and/or two 3q signals in every cell scored (Table 6).

Comparison of Techniques.

A quantitative analysis was used to determine the relationship between CGH, SKY and FISH. Measurements of relative balance were generated from pixel quantification in CGH and SKY to show the association between the 2 techniques for all chromosomes (Fig. 23). Regression analysis of this data revealed significant association

Table 6. Chromosome 3 FISH Signals for Ten Uveal Melanoma Cell Lines

Cell Line	3cen \pm SE	3cen Range ^a	3p \pm SE	3p Range ^a	3q \pm SE	3q Range ^a	FISH RCE ^b \pm SE
Control	2.04 \pm 0.03	0 - 4	1.99 \pm 0.02	1 - 3	1.96 \pm 0.02	0 - 3	1.99 \pm 0.01
92-1	1.23 \pm 0.07	0 - 4	4.14 \pm 0.05	2 - 6	3.76 \pm 0.04	2 - 5	3.05 \pm 0.06
MEL270	1.12 \pm 0.07	0 - 3	3.10 \pm 0.07	0 - 6	3.21 \pm 0.06	0 - 7	2.48 \pm 0.05
MEL285	1.06 \pm 0.06	0 - 3	2.41 \pm 0.06	0 - 6	3.08 \pm 0.05	0 - 8	2.18 \pm 0.05
MEL290	1.53 \pm 0.07	0 - 4	2.03 \pm 0.06	0 - 6	2.26 \pm 0.04	1 - 5	1.94 \pm 0.04
OCM-1	1.50 \pm 0.06	0 - 4	4.90 \pm 0.07	1 - 10	5.45 \pm 0.07	3 - 11	3.95 \pm 0.08
OCM-3	1.50 \pm 0.08	0 - 5	2.96 \pm 0.06	0 - 7	4.37 \pm 0.08	0 - 9	2.94 \pm 0.06
OCM-8	1.21 \pm 0.07	0 - 6	3.29 \pm 0.06	2 - 7	4.64 \pm 0.09	2 - 12	3.05 \pm 0.07
OM431	1.31 \pm 0.07	0 - 6	3.98 \pm 0.04	2 - 6	5.51 \pm 0.07	0 - 11	3.60 \pm 0.08
OMM1	0.99 \pm 0.06	0 - 3	3.03 \pm 0.04	1 - 6	3.04 \pm 0.05	0 - 7	2.35 \pm 0.05
OMM2.3	1.13 \pm 0.06	0 - 5	4.34 \pm 0.07	2 - 9	4.22 \pm 0.07	2 - 9	3.23 \pm 0.07

^a The range provided for 3p, 3q, and 3cen is the span of total hybridization signals observed in each of the cell lines and the control.

^b FISH RCE was calculated by averaging the values in the 3cen, 3p and 3q columns for each cell line.

between CGH RB and SKY RB for all 22 autosomes across the 9 analyzable cell lines ($R = 0.6146$, $p = 6.513 \times 10^{-21}$). Correlation of CGH and SKY was also seen visually, wherein gain and loss in the CGH profile mirrored specific numerical and structural aberrations in SKY (Fig. 24, note chromosomes 3, 6 and 8).

Of particular interest, were the CGH and SKY correlations in chromosomes 3, 6 and 8, as well as SKY and FISH correlations for chromosome 3 (Fig. 25 and Table 7). Correlation of SKY RCE and FISH RCE for chromosome 3 demonstrated good agreement between the two measurements of copy number ($R = 0.7370$, $p = 0.0235$) (Fig. 25A), and further correlation of FISH and SKY was also evident visually in the cell line OCM-1 (Fig. 26). The CGH RB:SKY RB comparison for chromosome 3 also showed significant correlation ($R = 0.6775$, $p = 0.0449$) (Fig. 25B). Correlations for chromosome 6 ($R = 0.6825$, $p = 0.0428$) and chromosome 8 ($R = 0.8242$, $p = 0.0063$) were both significant (Figs. 25C and D).

TUMOR STUDY.

Comparative Genomic Hybridization.

Eighty-two of the 100 cases (46 male, 36 female) were successfully extracted, labeled via DOP-PCR, hybridized, and analyzed. Probe constructs from the remaining 18 DNA isolates were unsuccessful in yielding results, due to a failure to either amplify or hybridize appropriately.

Results for all 82 tumors were evaluated by comparison of the mean ratio profiles; numerous consistencies were found throughout the data and used to derive the minimal common regions as a means of simplifying the data set (Figs. 27, 28 and 29). These

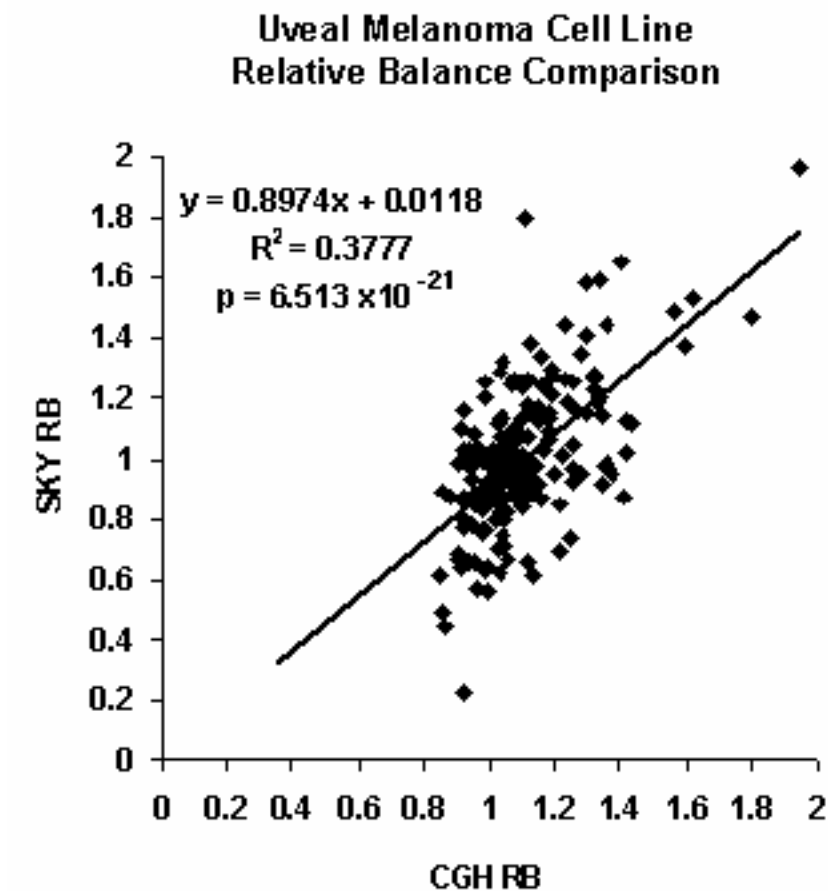
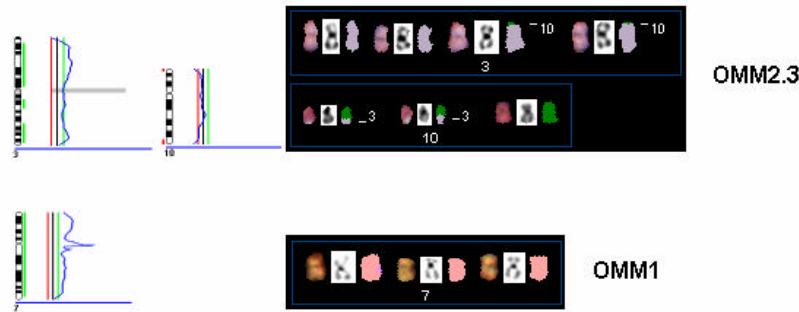


Figure 23. Overall Comparison of Calculated CGH RB and SKY RB Values for the 22 Autosomes in Nine Cell Lines. OCM-3 was excluded from this analysis due to inadequate SKY data. The equation for the regression line is provided in the upper left hand corner with the R^2 -value and p-value immediately below. The y-axis reflects the transformation of internally normalized SKY data into SKY RB values, which converts them from an absolute measure of copy number to a more relative measure comparable to CGH. Transformed CGH data (CGH RB) is plotted on the x-axis. Deviation from the regression line is partially explainable by the inherent difference between the two techniques, as CGH is a genomic average from a pooling of cells and SKY analysis is performed on per-cell basis with results taken from a few metaphase spreads.

A. Numerical Chromosome Aberrations



B. Structural Chromosome Aberrations

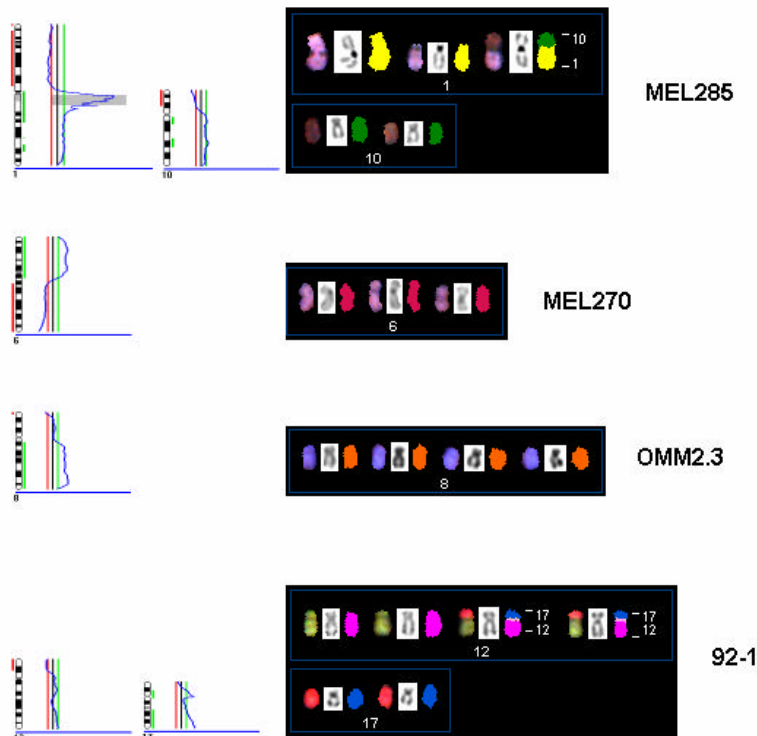


Figure 24. Visual Comparison of CGH and SKY. **(A)** These examples show how the numerical aberrations in SKY (right) correspond to whole chromosome amplification in CGH (left). Balanced structural aberrations such as the t(3;10) in OMM2.3 essentially result in a numerical aberration leading to additional complete copies of chromosome 3. Addition of an entire chromosome, as seen in chromosome 7 from OMM1 (a pseudodiploid cell line), also result in amplification along the length of the CGH ratio profile. **(B)** These examples demonstrate correlation between CGH mean ratio profiles and unbalanced structural aberrations in SKY. The presence of a normal chromosome 1, a 1q, and a der(1;10q) result in gain of 1q and loss of 1p in CGH of MEL285. The der(1;10q) adds additional 10q material mirrored by the relative loss of 10p and gain of 10q in CGH. In the next example the gain of 6p and loss of 6q in CGH are mirrored by the 2 normal chromosomes 6 (left) and an iso(6p) (right) in SKY. Two normal chromosomes 8 (first 2) accompanied by 2 copies of 8q (second 2) as seen in SKY, result in a relative deficit of 8p and a gain of 8q by CGH in OMM2.3. In the final example, SKY reveals 2 normal copies each of chromosomes 12 and 17, and 2 copies of a der(12q;17q) that explain the amplification of 17q and loss of 12p seen in the CGH profile of cell line 92-1.

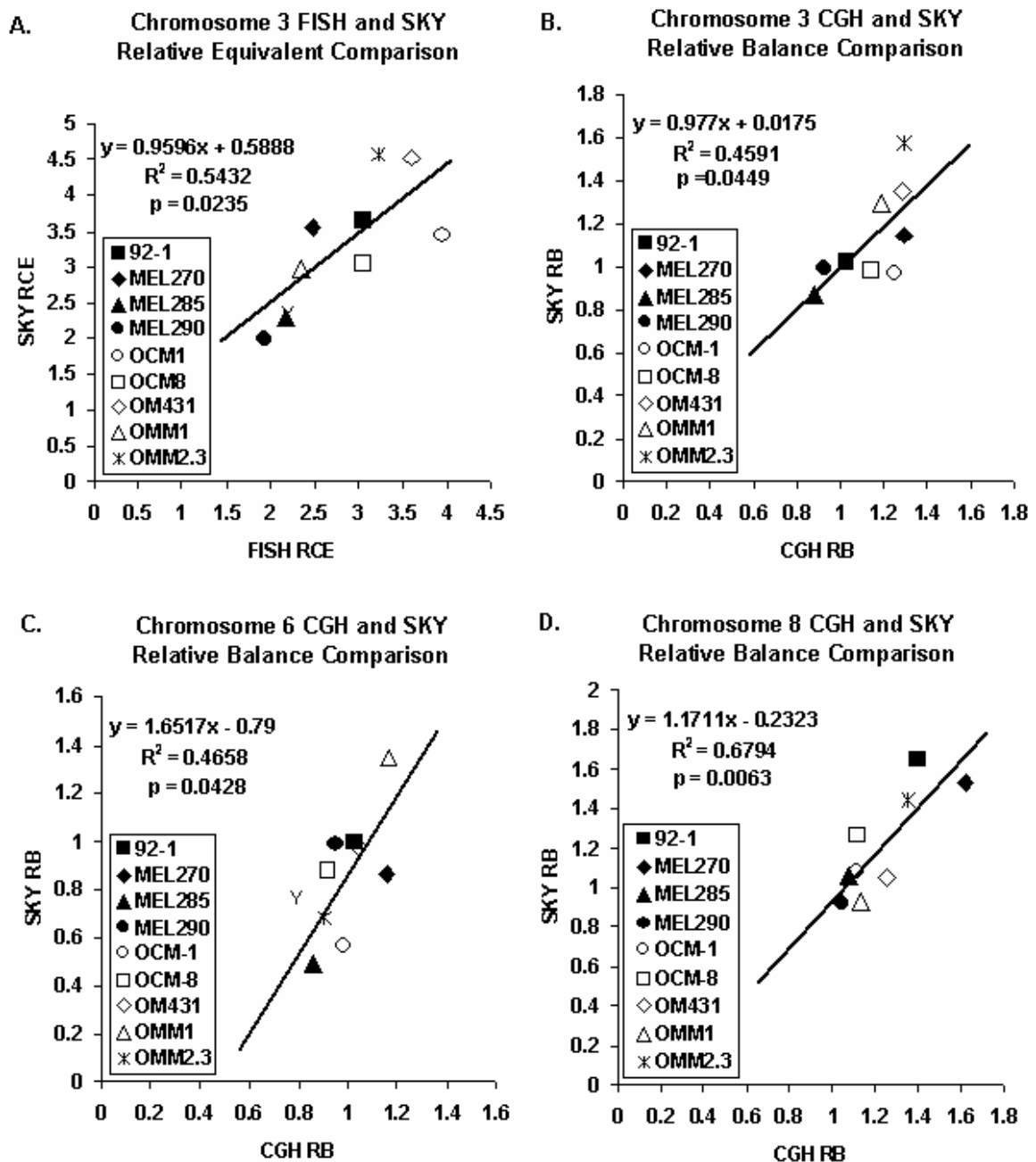


Figure 25. Comparisons of FISH, SKY and CGH Results for Chromosomes 3, 6, and 8, the Three Chromosomes Most Frequently Implicated in Uveal Melanoma. These plots, with trendlines, resulted from the analysis of 9 cell lines, as the cell line OCM-3 was not available for analysis due to a hardware failure during archiving of the data. The regression equations, R^2 -values, and p-values for each correlation are provided in the upper left-hand corner of each plot. (A) This plot depicts the correlation of SKY RCE and FISH RCE for chromosome 3. Copy number values are read directly from the axes for each technique. (B) This plot represents the correlation calculated between SKY RB and CGH RB values for chromosome 3. Similar correlations between SKY RB and CGH RB are shown for chromosomes 6 (C) and 8 (D).

Table 7. Comparison of CGH, SKY and FISH in Relative Balance (RB) and Relative Chromosome Equivalents (RCE) for Chromosomes 3, 6 and 8

Cell Line	Chromosome 3				Chromosome 6		Chromosome 8	
	CGH RB	SKY RB	SKY RCE	FISH RCE	CGH RB	SKY RB	CGH RB	SKY RB
92-1	1.03 ± 0.06	1.02 ± 0.11	3.66 ± 0.58	3.05 ± 0.06	1.03 ± 0.03	1.00 ± 0.05	1.40 ± 0.06	1.65 ± 0.08
MEL270	1.29 ± 0.05	1.15 ± 0.03	3.57 ± 0.14	2.48 ± 0.05	1.16 ± 0.03	0.86 ± 0.09	1.62 ± 0.05	1.53 ± 0.06
MEL285	0.88 ± 0.04	0.87 ± 0.10	2.30 ± 0.25	2.18 ± 0.05	0.86 ± 0.03	0.49 ± 0.08	1.08 ± 0.03	1.06 ± 0.10
MEL290	0.93 ± 0.03	0.99 ± 0.06	1.99 ± 0.12	1.94 ± 0.04	0.95 ± 0.02	0.99 ± 0.05	1.05 ± 0.02	0.92 ± 0.03
OCM-1	1.25 ± 0.03	0.97 ± 0.04	3.45 ± 0.13	3.95 ± 0.08	0.99 ± 0.02	0.56 ± 0.01	1.12 ± 0.02	1.08 ± 0.02
OCM-3	1.20 ± 0.04	ND ^a	ND ^a	2.94 ± 0.06	0.96 ± 0.02	ND ^a	1.17 ± 0.06	ND ^a
OCM-8	1.14 ± 0.04	0.98 ± 0.06	3.05 ± 0.15	3.05 ± 0.07	0.92 ± 0.02	0.87 ± 0.05	1.12 ± 0.05	1.27 ± 0.03
OM431	1.28 ± 0.05	1.35 ± 0.07	4.52 ± 0.26	3.60 ± 0.08	1.04 ± 0.02	0.98 ± 0.09	1.25 ± 0.05	1.05 ± 0.11
OMM1	1.19 ± 0.08	1.30 ± 0.03	2.97 ± 0.06	2.35 ± 0.05	1.16 ± 0.07	0.67 ± ND ^a	1.13 ± 0.04	0.93 ± 0.15
OMM2.3	1.29 ± 0.05	1.58 ± 0.06	4.56 ± 0.17	3.23 ± 0.07	0.91 ± 0.02	0.68 ± 0.08	1.35 ± 0.06	1.44 ± 0.15

^a ND indicates “No Data.” OCM-3 was the cell line eliminated from the SKY analysis. This value is also given as the standard error for chromosome 6 in OMM1, because there was only one spread bearing a chromosome 6 for that cell line.

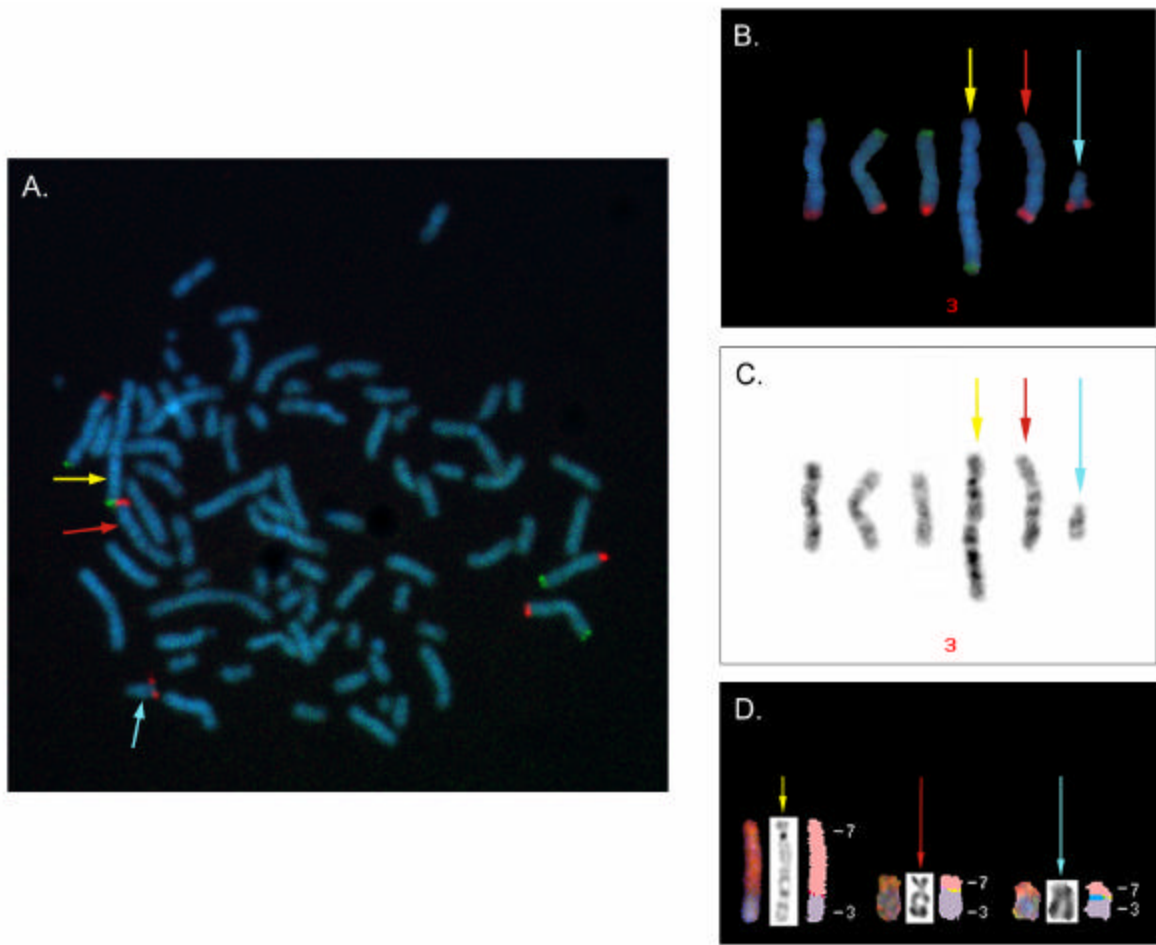


Figure 26. Visual Comparison of FISH and SKY. During the scoring of telomere probes (3p = green, 3q = red) in interphase FISH of OCM-1, we happened upon a metaphase spread that was particularly illustrative regarding the amount and the arrangement of chromosome 3 telomere material. **(A)** A digital image of the metaphase spread, where the yellow, red, and blue arrows indicate the 3 aberrant chromosomes. **(B)** All of the chromosome 3 material in the metaphase spread is grouped following image processing. **(C)** Inversion of the DAPI images for the chromosomes in **(B)** revealed a banding pattern that allowed accurate determination that these examples from FISH and SKY **(D)** were equivalent. Analysis reveals there are 2 normal copies of chromosome 3, a third potentially abnormal copy, a der(3p;7) (yellow arrow), a der(3q;7) (red arrow), and a truncated copy of 3q (blue arrow).

regions were those copy number abnormalities identified in greater than 30% but fewer than 70% of all tumor cases. Any copy number abnormality seen in less than 30% of the cases is likely not a strong indicator of prognosis. Conversely, those abnormalities present in greater than 70% of the cases are not of prognostic significance, since they are likely commonalities among all cases of uveal melanoma rather than predictive of outcome.

Within the minimal common regions, differential gain and loss was observed between male and female cases on the sex chromosomes (Figs. 28 and 29). The data was further subdivided into minimal common regions for those who survived 9 years or more post-diagnosis, and those that succumbed to the disease in that time frame (Figs. 30 and 31). Additionally, the sex chromosomes were evaluated independently for male and female subsets within the live and dead cohorts (Fig. 32). The 25 male patients who succumbed to the disease evidenced a +Xq21 not seen in the 21 male patients who survived beyond 9 years post-diagnosis, but no difference was seen on the X chromosome in the female cases (Fig. 32).

Statistical comparison of the live and dead data sets revealed six chromosomal regions that correlated strongly with a poor prognosis; five evidenced gain (18q11.2, 6q16, 21q11.2, 9q12 and 3q12), and one showed a loss (1p33). Overall, the strongest correlation with prognosis was associated with gain of 18q11.2 ($p = 0.0037$) (Fig. 33). Gain of 18q11.2 and concomitant loss of 1p33 was the strongest multivariate predictor of prognosis ($p = 0.0028$) (Fig. 34).

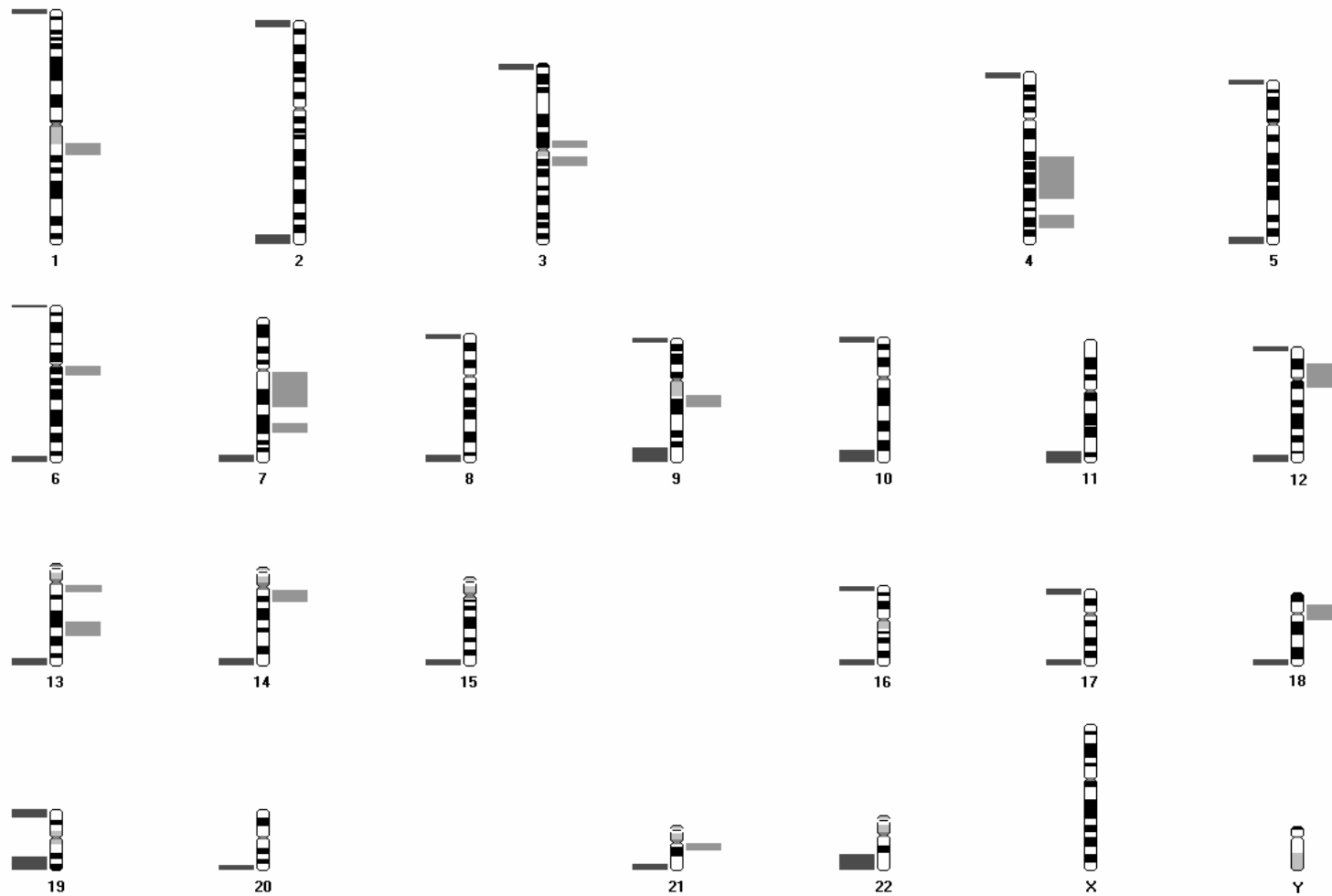
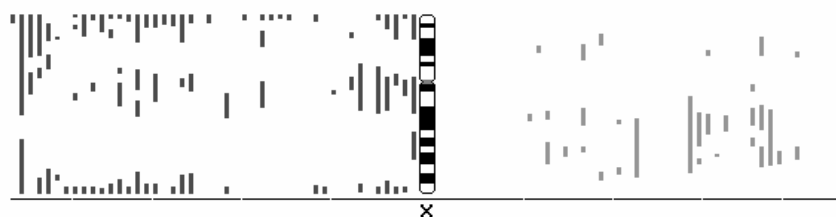


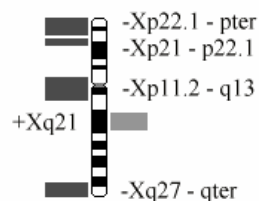
Figure 27. Minimal Common Regions of Gain and Loss Distilled from CGH Mean Profile Data of 82 FFPE Uveal Melanoma Cases. The light gray bars to the right of the ideogram represent gain, and dark gray bars to the left of the ideogram represent regions of loss, common between more than 30% and less than 70% of the archival cases. These minimal common regions may denote chromosomal regions related to the development and progression of uveal melanoma. Minimal common regions for the sex chromosomes are provided in Figs. 28, 29 and 32.

MALE SEX CHROMOSOME DATA

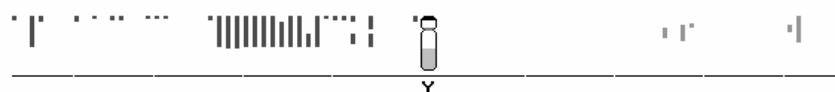
A. Chromosome X Data for 46 cases



Chromosome X MCR



B. Chromosome Y Data for 46 Cases



Chromosome Y MCR

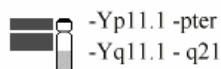


Figure 28. Quantitative Comparison Data and Minimal Common Regions for the Sex Chromosomes of the Male Archival Cases. **(A)** The QPD for the X chromosome is shown above the minimal common regions for that chromosome. Regions of gain and loss, possibly those having prognostic significance, are shown in the minimal common regions. **(B)** The QPD and the minimal common regions are shown for the Y chromosome.

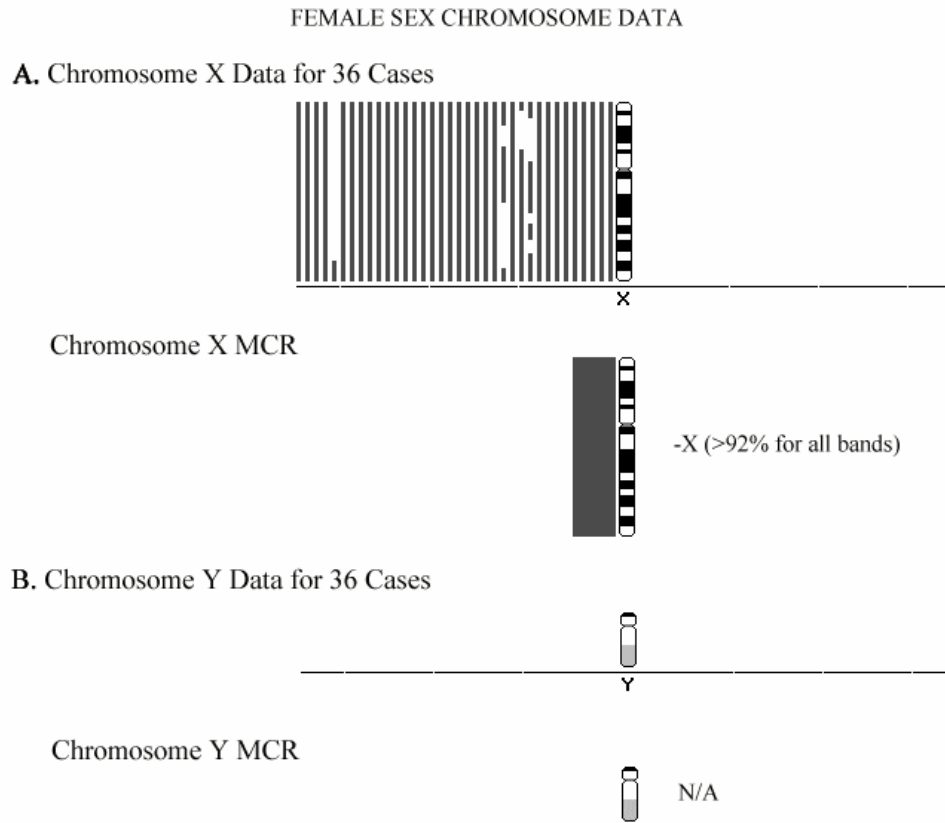


Figure 29. Quantitative Comparison Data and Minimal Common Regions for the Sex Chromosomes of the Female Archival Cases. **(A)** The QPD for the X chromosome is shown above the minimal common regions for that chromosome. In greater than 92% of the cases, the entire X chromosome was lost, eliminating it from having any prognostic significance. **(B)** The QPD and the minimal common regions reveal no gains or losses, as expected, in the female cases.

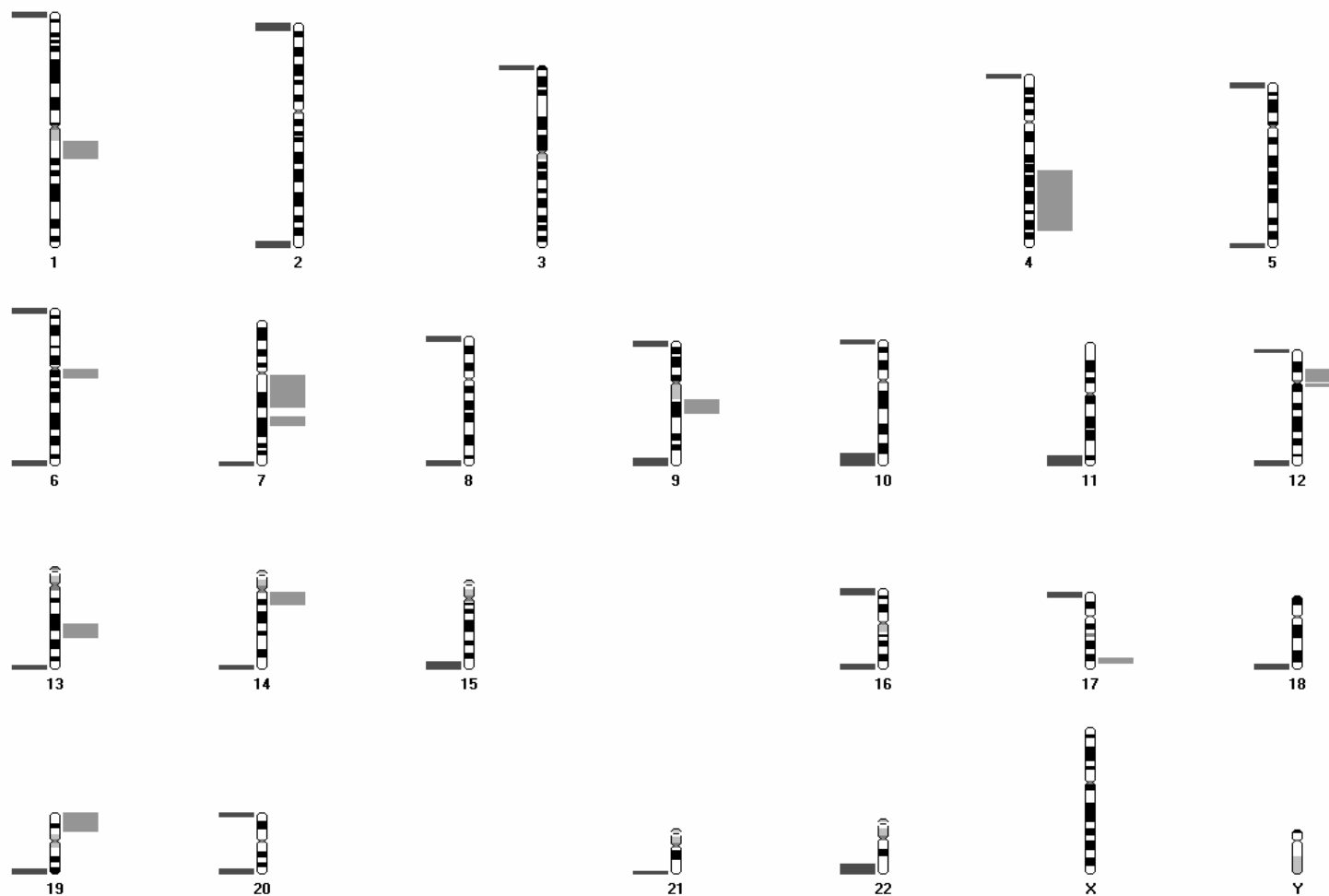


Figure 30. Minimal Common Regions of Gain and Loss Distilled from CGH Mean Profile Data of 51 FFPE Uveal Melanoma Cases, Representing Those Patients that Survived Beyond 9 Years Post-diagnosis. The light gray bars to the right of the ideogram represent gain, and dark gray bars to the left of the ideogram represent regions of loss, common among more than 30% and less than 70% of the archival cases. These minimal common regions may denote chromosomal regions related to a more favorable prognosis in uveal melanoma. Minimal common regions for the sex chromosomes are provided in Figs. 28, 29 and 32.

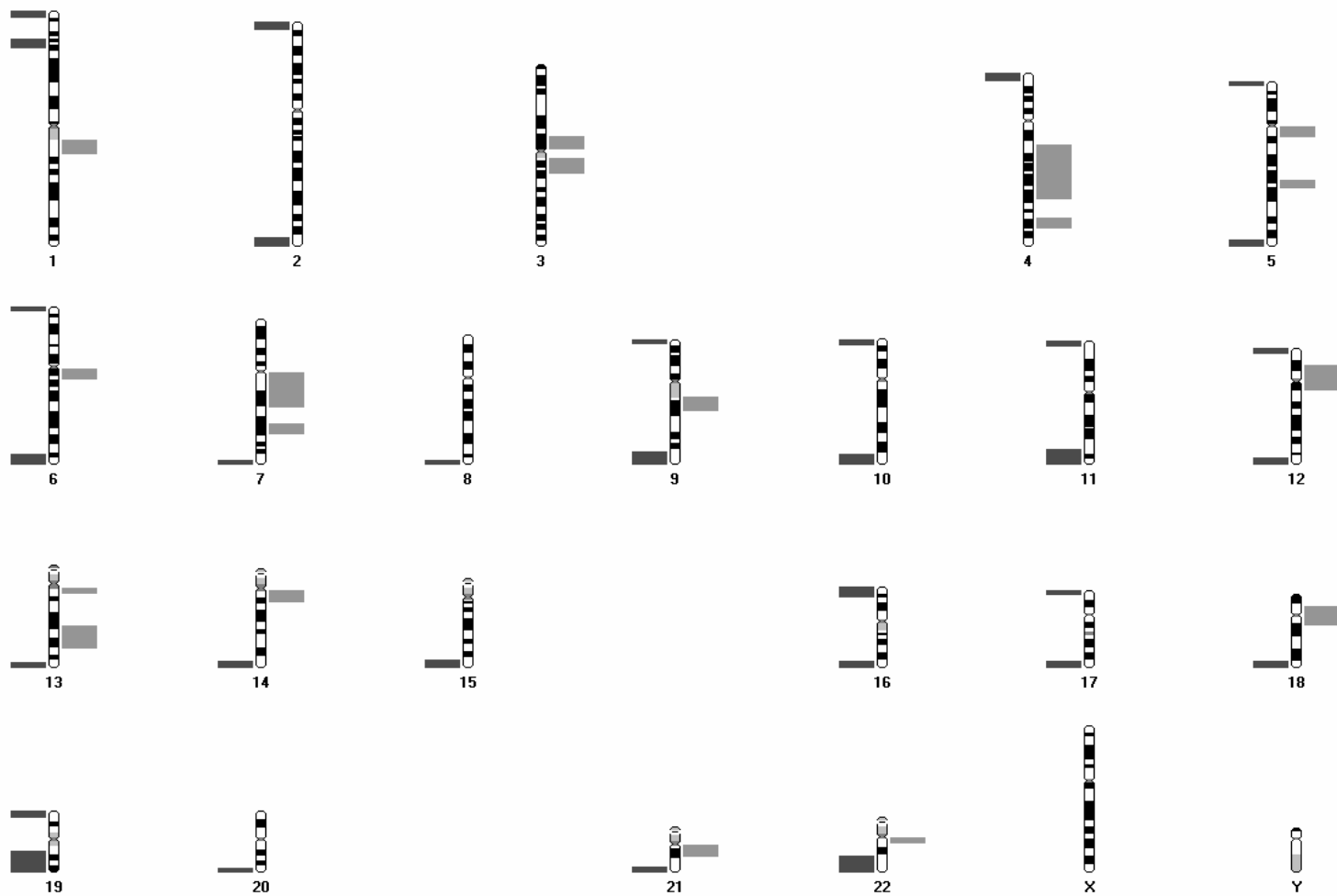


Figure 31. Minimal Common Regions of Gain and Loss Distilled from CGH Mean Profile Data of 49 FFPE Uveal Melanoma Cases, Representing Those Patients that Succumbed to Hematogenous Metastasis. The light gray bars to the right of the ideogram represent gain, and dark gray bars to the left of the ideogram represent regions of loss, common between more than 30% and less than 70% of the archival cases. These minimal common regions may denote chromosomal regions related to a poor prognosis in uveal melanoma. Minimal common regions for the sex chromosomes are provided in Figs. 28, 29 and 32.

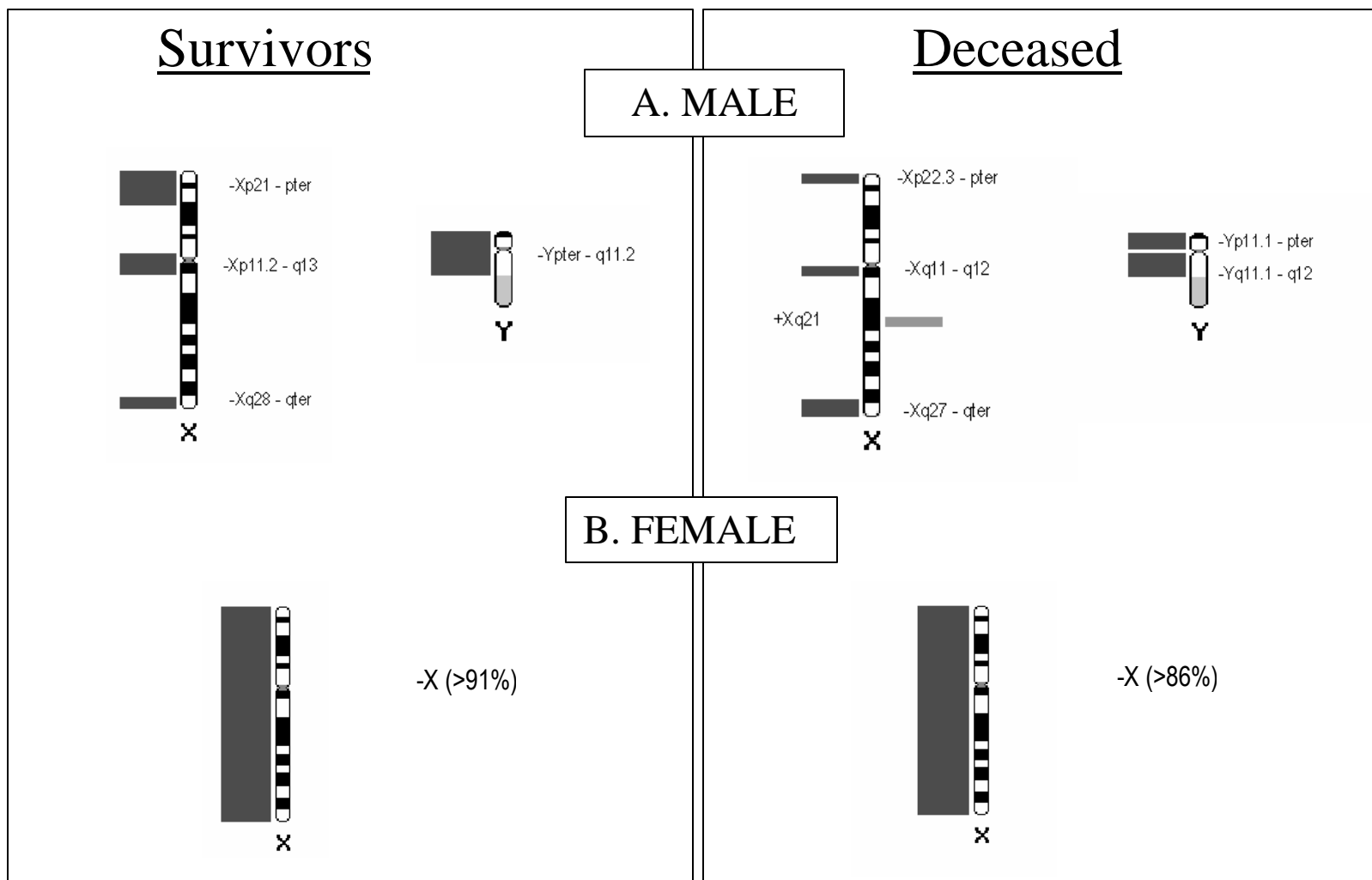


Figure 32. Minimal Common Regions for the Sex Chromosomes, Separated by Gender and Survival. **(A)** The sex chromosomes for males that survived beyond 9 years with uveal melanoma (23 cases) are compared with the male cases that succumbed to hematogenous metastasis (29 cases). **(B)** The X chromosome is compared for the female cases that survived beyond 9 years (28 cases) and those females that succumbed to the disease within that time period (20 cases).

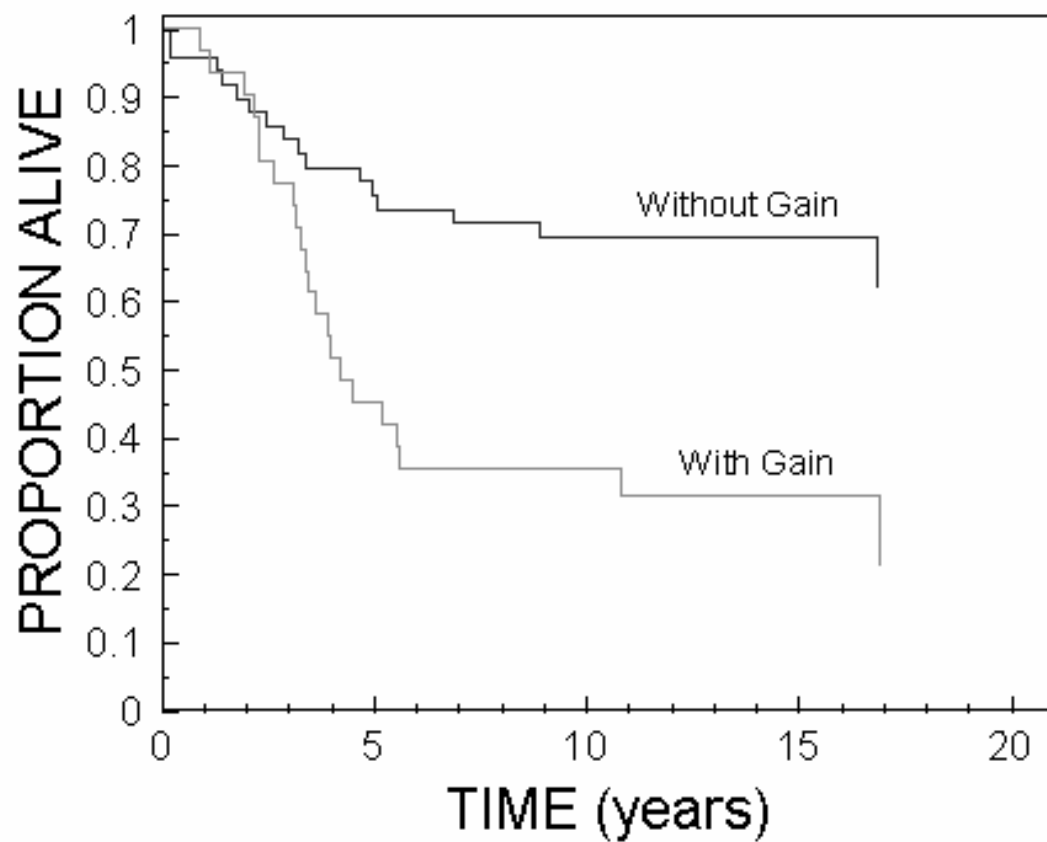


Figure 33. Univariate Kaplan-Meier Cause Specific Survival Correlation Curve. This comparative plot shows the two-fold negative effect on survival that is conferred by the gain of 18q11.2. This plot was generated from results comprised of all 82 FFPE archival cases in our CGH analysis.

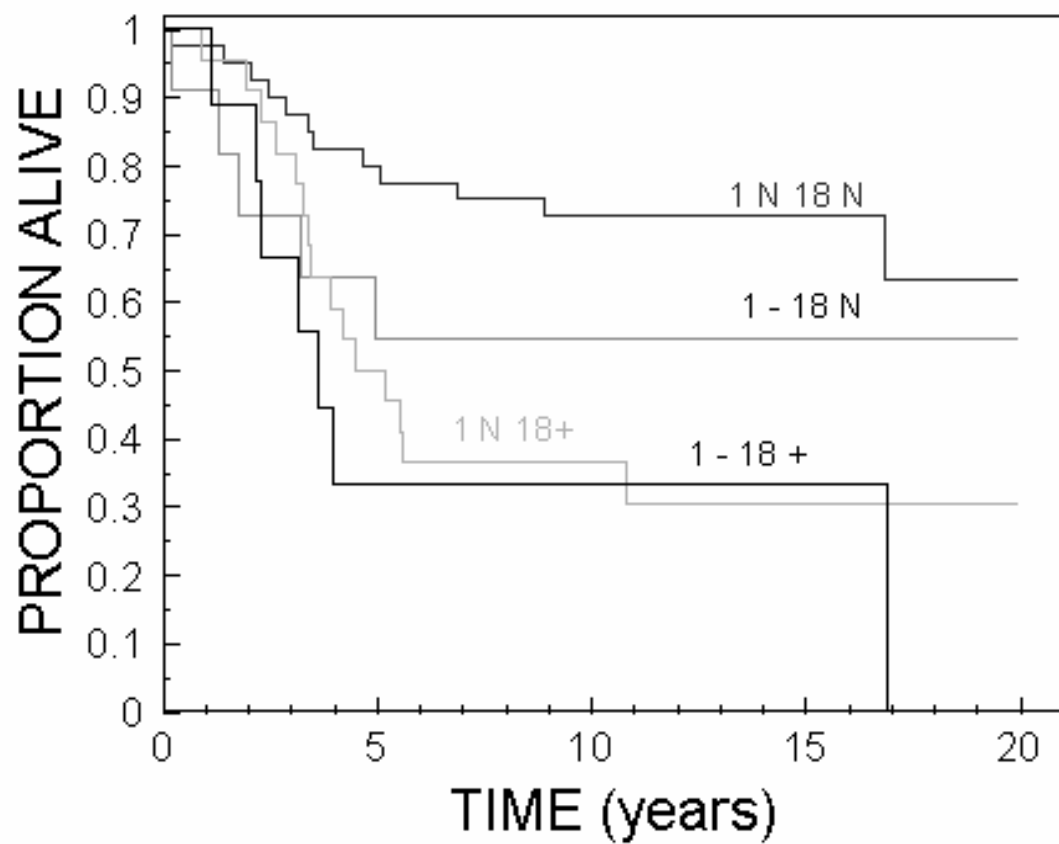


Figure 34. Multivariate Kaplan-Meier Cause Specific Survival Correlation Curve. This comparative plot shows the cumulative negative effect on survival that is conferred by the gain of 18q11.2 and concomitant loss of 1p33. This plot was generated from results comprised of all 82 FFPE archival cases in our CGH analysis.

DISCUSSION

Chromosomal rearrangements, both numerical and structural, are often correlated with morphology, tumor stage, and the aggressive potential of the tumor; therefore, such aberrations are often of prognostic value (Rothmann *et al.*, 1998). Some of the chromosomal rearrangements associated with uveal melanoma have been identified, but often without being linked to a particular cellular function. Furthermore, the majority of studies thus far have looked at relatively small populations, and employed cytogenetic techniques with fairly low resolution. There remains a need for large-scale profiling of the genomic changes in uveal melanoma, using higher resolution methodologies, in order to increase and better define the catalogue of cytogenetic aberrations associated with the disease. Complete cytogenetic characterization of uveal melanoma is a critical step toward gene-specific investigation of malignancy.

To that end, we fully characterized 10 uveal melanoma cell lines and 82 archival FFPE tumors using molecular cytogenetic techniques. In our cell line study, CGH revealed genomic imbalances, and SKY provided insight into numerical and structural abnormalities that contribute to these imbalances in the genome. The tandem application of CGH and SKY, and the associated synthesis of the results, allowed for a comprehensive analysis of chromosomal abnormalities in the genome and insight into the mechanisms of chromosomal aberrations that have accumulated during clonal divergence (Veldman *et al.*, 1997; Macville *et al.*, 1999). We applied a third technique, FISH, to our cell lines to assay three specific loci as a practical means of chromosome 3 enumeration. In our archival tissue study, a thorough evaluation of 82 primary uveal melanoma tumors, culled from the tissue archives of the AFIP, revealed the specific genomic imbalances

associated with each tumor, and helped determine regions predictive of prognosis. These 2 studies helped to more fully understand the underlying cytogenetic events of uveal melanoma development and progression.

CELL LINE STUDY.

Our research demonstrated that synthesis of CGH and SKY techniques develops an integrated data set comprised of numerical and structural alterations. Utilizing this approach, copy number aberrations were localized in chromosomal regions of the 10 cell lines. These specific regions are likely to contain genes differentially expressed in uveal melanoma.

CGH provided a comparison of the cell line genomes through evaluation of mean profile data (Fig. 19), and revealed commonalties in the data set, recorded as minimal common regions (Fig. 20). These regions are either gained or lost in 50% or more of the cell lines, and are likely of significance in uveal melanoma. It is thought that within these regions are the genes that, when their copy number is altered, contribute to the establishment and/or progression of uveal melanoma.

The definitive numerical and structural composition of individual cell line genomes was revealed by SKY, and evidence of rearrangement was present within the chromosome complement of each cell that was analyzed. Reconciliation of multiple single cell analyses in our SKY results provided an adequate representation of the genome of each cell line. Comparison of SKY results between the cell lines identified five common chromosomal abnormalities, each seen in a minimum of four cell lines (Fig. 22). The prevalence of these aberrations suggests that they are of import to uveal melanoma development or progression. Our comprehensive SKY analysis revealed

extensive numerical changes and structural rearrangements in each cell line, which resulted in aneuploidy, instances of mosaicism, aneusomy and partial chromosome amplifications and deletions.

Before we could interpret our findings from CGH and SKY, we needed to determine the correlation between the two techniques. However, there was a caveat to our interpretation of the CGH and SKY results. A known limitation of CGH is the inability to elucidate structural information, as only numerical data are gleaned from the compilation and analysis of mean ratio profiles. Similarly, SKY can not be expected to reveal all permutations of structural and numerical rearrangement in a cell line, as the analysis is based on a few analyzable metaphase spreads. With that in mind, we were able to isolate multiple visual examples where CGH and SKY showed agreement regarding chromosomal aberrations within a given cell line (Fig. 23). SKY results strongly demonstrate that the gains and losses identified by CGH are not exclusively due to numerical chromosome aberrations. Instead, it is clear that structural rearrangement of the genome also significantly contributes to amplification and deletion of DNA sequences. Complementation between SKY and CGH data is exemplified in the formation of an isochromosome 6p and concomitant loss of a 6q in MEL270, which yielded four copies of 6p and only 2 copies of the 6q arm (Fig. 24). This was mirrored in the CGH results that show a gain of 6p and loss of 6q for that cell line. Also shown in Figure 24, are additional examples in which genomic imbalances detected by CGH are mirrored in the SKY analysis from the same cell lines.

An additional feature of SKY, is its ability to resolve complex chromosomal rearrangements (Fig. 21). While these more complex rearrangements also affect copy

number, it is not possible to resolve this by a simple visual inspection of results. Therefore, we developed mathematical calculations of genomic balance for CGH and SKY that could be statistically correlated. This quantitative approach for comparing techniques also served as an independent confirmation of the visual correlation seen between CGH and SKY.

While visual confirmation of the link between CGH and SKY was intriguing, demonstration of statistical correlation between the 2 techniques would lend credence to our observations. Unfortunately, SKY results for OCM-3 were compromised in the data recovery process, and were omitted from statistical analysis. Comparison of the relative balance for the 9 remaining cell lines, analyzed by both CGH and SKY, showed significant correlation across the entire genome, as determined by the associated R^2 - and p-values (Fig. 23). Additionally, chromosome-specific correlations were drawn from CGH and SKY results for the chromosomes previously reported as having prognostic value for uveal melanoma (Fig. 25B-D and Table 7). The strength of these quantitative comparisons confirmed our visual correlations between the two independent *in situ* hybridization techniques, and validated our molecular cytogenetic characterizations of the cell line genomes.

The correlation established between CGH and SKY permitted further interpretation of the data sets. Several chromosomes (6, 7, 17q and 20q) that showed imbalance of large continuous sections by CGH in at least half of the cell lines were also involved in frequent numerical or structural aberrations revealed by SKY (Fig. 20 and Table 5). The involvement of chromosomes 6 and 7 in uveal melanoma is well documented in the literature (Gordon *et al.*, 1994; Speicher *et al.*, 1994; Ghazvini *et al.*,

1996; White *et al.*, 1998b). Our CGH and SKY results show copy number alteration events on other chromosomes similar to those in the literature (Tables 2 and 3) (Wiltshire *et al.*, 1993; Gordon *et al.*, 1994; Speicher *et al.*, 1994; Ghazvini *et al.*, 1996; Prescher *et al.*, 1996; White *et al.*, 1998a and b). It should be noted that both CGH and SKY identified alterations of 17q and 20q, neither of which has been previously implicated in uveal melanoma. We suggest that these chromosomes warrant further study to determine their significance. The comparison of our data with the published literature suggests our demonstrated lack of monosomy 3 by CGH or SKY is most noteworthy and requires explanation.

Application of FISH in a confirmatory capacity following CGH or SKY is a very powerful application of the technique (Macville *et al.*, 1999). We used human chromosome 3-specific centromere and telomere FISH probes on interphase preparations of all 10 cell lines to confirm our CGH and SKY results for chromosome 3. Our 3cen hybridizations seemed to indicate loss of chromosome 3, as the dominant population in each cell line had a single 3cen hybridization signal per nucleus, but the range spanned from 0 to 6 signals. In contrast, the number of telomere probe hybridization signals ranged from 0 to 12 signals, with a tendency for 3 or more signals per telomere in each nucleus. These results indicated a high degree of heterogeneity in the cell lines, and vastly different chromosome 3 complements than our diploid control (Table 6). Heterogeneity was also observed in cell line karyotypes from our SKY analyses. The lack of a major clone in the cell line populations, coupled with the high degree of heterogeneity observed by SKY and FISH, is suggestive of mosaicism in these cell lines. The signal variation and enhanced copy numbers for the centromere and telomere probes,

suggested the presence of enhanced copies of portions of chromosome 3. This is also shown in the CGH profiles for each cell line, and the numerous rearrangements bearing chromosome 3 material in our SKY analyses (Figs. 19 and 22E). The distribution of chromosome 3 material observed in SKY and the partial chromosome 3 gains in CGH, when considered alongside the FISH results, point toward rearrangement as playing a key role in chromosome 3 involvement. Visual confirmation of the role of rearrangement came from a comparison between FISH and SKY findings that show enhanced copy number for chromosome 3 and define specific rearrangements associated with OCM-1 (Fig. 26). Further, chromosome-specific correlations show that chromosome 3 rearrangement contributes to copy number enhancement (Fig. 25A and B). Ideally, all three probes (3cen, 3p and 3q) would have been simultaneously hybridized to determine the precise assortment of each signal. This would have provided more insight into the precise mechanism(s) of rearrangement, and also definitively pinpointed mosaicism, but the hybridization was not technically feasible.

Although monosomy 3 has been heavily reported as a hallmark for uveal melanoma, our findings for chromosome 3, confirmed using FISH following independent CGH and SKY analyses, clearly indicate there was no loss of a whole chromosome 3 in these cell lines. In contrast to our methodologies, the majority of uveal melanoma analysis published in the literature is derived from classical cytogenetic evaluations (Horsman *et al.*, 1990; Sisley *et al.*, 1990; Prescher *et al.*, 1990; Horsthemke *et al.*, 1992; Sisley *et al.*, 1992; Horsman and White, 1993; Wiltsire *et al.*, 1993; Singh *et al.*, 1994; Prescher *et al.*, 1994; Prescher *et al.*, 1995; Prescher *et al.*, 1996; White *et al.*, 1998b; Parada *et al.*, 1999; Sisley *et al.*, 2000; Tschentscher *et al.*, 2001). However, other

studies have used molecular cytogenetic methods in their determination of monosomy 3, which indicates that our findings are not linked to our methodologies (Ghazvini *et al.*, 1996; Prescher *et al.*, 1996; McNamara *et al.*, 1997; Sisley *et al.*, 1997; Tschentscher *et al.*, 2001). The absence of chromosome 3, 6, and 8 abnormalities in some cases, suggests there are additional pathways of malignant transformation (Singh *et al.*, 1996a). Thus, there were indications that there could be alternate explanations for our findings on chromosome 3.

The search for alternative explanations for our lack of monosomy 3, led to an examination of cell line origin. Monosomy 3 is frequently reported in tumors of the ciliary body, whereas a normal or polysomic complement of chromosome 3 is typically reported in choroidal melanoma (Sisley *et al.*, 1993; McNamara *et al.*, 1997). Our information regarding cell line origin is incomplete (Table 1), but available information shows only one cell line (MEL270) was established from a ciliary body tumor. A second cell line (OMM2.3) was established from a metastasis of the same primary tumor. Neither MEL270 nor OMM-2.3 evidenced any loss on chromosome 3 by CGH, while OMM-2.3 actually demonstrated significant gains on chromosome 3. In fact, only one cell line (MEL285) demonstrated a considerable loss of chromosome 3 material, and three other lines (MEL290, OCM-3 and OCM-8) lost only distal 3p material (Fig. 19). The origin of these four cell lines was indeterminate, which effectively prevented further correlation between CGH results and cell line origin. SKY results revealed truncated or partially deleted copies of chromosome 3 in at least three of our cell lines (OCM-3, OCM-8 and OM431), in addition to normal copies of chromosome 3. The retention of abnormal copies of chromosome 3 precludes the designation of monosomy to any of

these cell lines. Further, FISH results indicate different mean signal counts for each probe within a cell line, which is not congruent with a determination of monosomy (Table 6).

Additional investigation regarding the original karyotype, specifically a closer look at chromosome 3, demonstrated strong parallels between our findings and those published at the time of establishment. Although establishment karyotypes were only available for a subset of the cell lines, this investigation was warranted because our cell lines were of an indeterminate number of passages, and verification of our findings strengthened any conclusions regarding chromosome 3. The published karyotype for OCM-1 includes add(3)(q12) and +del(3)(q13q23) (Luyten *et al.*, 1996). The majority of chromosome 3 was demonstrated to be gained in OCM-1 via CGH, with the exception of 3q13-q23 and distal 3p (Fig. 19). Also, multiple truncated copies of chromosome 3 were found in our SKY results for OCM-1. The karyotype for OMM-1 indicated a +3[50%] at the time of establishment, but our CGH results revealed only a 3p gain, and SKY revealed an apparent trisomy 3 or possibly an isochromosome 3p (Luyten *et al.*, 1996). Meanwhile, the cell line 92-1 had no known chromosome 3 abnormalities at the time the cell line was established (DeWaard-Siebinga *et al.*, 1995). There was evidence of a very small focal 3q13.3 gain in 92-1, and no losses reported along the length of the chromosome (Fig. 19). Our findings for chromosome 3 demonstrate minimal divergence from the original karyotype for these 3 cell lines, and the strength of our quantitative analyses suggests the same would hold true for the remainder of the cell lines (Figs. 23 and 25).

No explanation for the lack of monosomy 3 was found in the cell line origin, and there were no indications were that our cell lines had significantly diverged while in culture. Based on the strength of the correlations determined for our three techniques, we sought to reevaluate the literature to elucidate possible discrepancies in data interpretation between our study and others. Some published reports in the literature, based upon CGH analyses, have noted a “decreased copy number” for chromosome 3 in lieu of monosomy. These results provide evidence of a copy number below 1, but the profile does not cross the loss threshold (Gordon *et al.*, 1994; Ghazvini *et al.*, 1996). Others have alluded to two tumor suppressor loci, one on the p- and a second on the q-arm of the chromosome, which result in focal deletions on chromosome 3 instead of whole chromosome loss (Sisley *et al.*, 1993; White *et al.*, 1998a; Parella *et al.*, 1999; Myatt *et al.*, 2000; Tschentscher *et al.*, 2001). In one LOH study, two purported tumor suppressor loci were defined in terms of the smallest region of overlap (SRO), one within band 3p25 and the other on the q-arm between 3q24-q26 (Tschentscher *et al.*, 2001). A second study implicated only 3p24.3 by LOH (Sisley *et al.*, 1993). Two more LOH studies demonstrated isodisomy of chromosome 3, which may lead to functional monosomy (White *et al.*, 1996; White *et al.*, 1998a). Comparison of results from CGH and LOH studies typically results in a high degree of concordance (Ried *et al.*, 1997). Therefore, the alignment of our findings with those of LOH studies is not surprising. Elsewhere in the literature, a GTG-banding study reported loss of 3p13 (Blasi *et al.*, 1999). A later study by Naus and colleagues, who also applied CGH, SKY and FISH to characterize uveal melanoma, failed to find monosomy 3 but were able to define 3q13-q21 as a region of loss (Naus *et al.*, 2001). The findings of Blasi *et al.* (1999) and Naus

et al. (2001) suggest a region near band 3q13 may potentially harbor a tumor suppressor gene. Other findings in the literature, including trisomy 3 and even tetrasomy 3 as reported by McNamara and colleagues, are supportive of our CGH, SKY and FISH results that indicate gains on chromosome 3 (Figs. 16, 22 and 23, Tables 6 and 7) (McNamara *et al.*, 1997). This review of the literature revealed indications that there are explanations for the involvement of chromosome 3 other than whole chromosome loss.

Another finding of note was the consistent involvement of several specific chromosomes in structural rearrangements as seen by SKY, which suggests a redundant mechanism for this occurrence (Fig. 22, Table 5). Our cell lines were shown to have minimally diverged in culture, therefore cell culture artifacts only account for a small proportion of these findings. Each of the five common chromosomal interactions observed across multiple cell lines, which include several chromosome 3 interactions, involved chromosomes with deletions in one or both telomeric regions of the chromosome (Figs. 19 and 22). Other telomeric deletions in specific cell lines were related to increased structural rearrangement of those same chromosomes in SKY analysis, and these deletions on the distal p- or q-arms were consistent with the rearrangement observed in the SKY karyotypes. In general, chromosomes shown to evidence telomeric deletion in the minimal common regions, also revealed higher frequencies of structural rearrangements by SKY (Fig. 20 and Table 5). This suggests that telomeric loss may facilitate structural rearrangement, but further study would be required to accurately determine the significance of this finding in the uveal melanoma cell lines.

CGH and SKY represent distinct approaches that reveal complementary information on cytogenetic features of uveal melanoma. Utilizing a combination of CGH, FISH and SKY we confirmed the absence of monosomy 3 in these ten cell lines, and demonstrated alternative manifestations of chromosome 3 in this tumor. Our findings do not refute the occurrence of monosomy 3 reported by others, but instead we postulate that frequent rearrangement of chromosome 3 may have an equally important contribution in the mechanisms driving uveal melanoma. The portion of the study that followed, a study of archival tissue by CGH, was expected to enhance resolution of the critical chromosomal regions throughout the genome and ultimately aid in the determination of specific gene involvement in uveal melanoma.

TUMOR STUDY.

Classification of tumors based on histopathology and tumor grading is subjective and qualitative, based on a two-dimensional image analysis (Rothmann *et al.*, 1998). Classical cytogenetic studies, while useful in elucidating structural abnormalities, are time consuming and require fresh tissue. Furthermore, classical cytogenetic analysis is compromised when dealing with solid tumor preparations due to low mitotic indices, poor growth in culture, *etc.* (Joos *et al.*, 1994; Houldsworth and Chaganti, 1994; Isola *et al.*, 1994; Macville *et al.*, 1997; Veldman *et al.*, 1997; Ried *et al.*, 1997; Rothmann *et al.*, 1998). Techniques such as CGH are expected to yield more information. Our large-scale CGH study, aimed at determining a set of prognostic indicators in uveal melanoma, identified specific regions of gain and loss (Figs. 27, 28 and 29). These regions were initially derived irrespective of the survival correlation portion of the study, thus indicating regions that may contain genes leading to development of uveal melanoma.

The CGH data was further subdivided based upon survival correlation (Figs. 30, 31 and 32). Regions containing genes associated with malignancy were revealed in the survival correlation and associated minimal common regions, and are presumed to be indicators of prognosis. Statistical analyses confirmed 6 regions of import with regard to survival. Of these, the most potent predictor of prognosis identified in this study was 18q11.2 (Fig. 33). Multivariate analyses revealed that gain of 18q11.2 combined with the loss of 1p33 had the most drastic effect on prognosis (Fig. 34).

Application of a Bonferroni correction obfuscates the statistical significance of our findings. This includes both conservative and rigorous applications of this correction. This is likely attributable to a relatively small sample size, further subdivided for survival correlation analysis, for such an application.

There is evidence that suggests gender may be involved in uveal melanoma susceptibility, as males are slightly more susceptible than females (McLean and Gamel, 1996). CGH results revealed very different regions of gain and loss on the X chromosome in a comparison of male and female cases (Figs. 28 and 29). The minimal common regions revealed that +Xq21 is unique to male patients who succumbed to uveal malignant melanoma (Figs. 28, 29 and 32). This region was not statistically significantly different in the analysis, because of the reduction of the sample size required to simultaneously analyze survival and gender (Fig. 32), but may warrant further study.

Due to the high frequency with which chromosome 3 loss is reported in uveal melanoma, data interpretation of CGH becomes critical in evaluation of chromosome 3. A closer look at the published literature revealed some inconsistencies. In some reports, CGH research has noted a decrease in copy number of chromosome 3 instead of whole

chromosome loss (Gordon *et al.*, 1994; Ghazvini *et al.*, 1996). In such instances, the ratio profile indicates a copy number ratio below 1, but does not exceed the loss threshold in all cases. These results indicate a tendency toward loss, rather than monosomy 3 as reported (Gordon *et al.*, 1994; Ghazvini *et al.*, 1996). Chromosome 3 findings in previously published uveal melanoma studies have revealed contributions of chromosome 3 other than monosomy. LOH studies have demonstrated loss on either the p- or q-arm of the chromosome, but not complete loss along the length of the chromosome (White *et al.*, 1996; White *et al.*, 1998a; Parella *et al.*, 1999). Other LOH studies have localized various regions of loss to 3p24.3, 3p13, 3p22 (TGFbetaR2 gene locus), 3p25, and 3q24-q26 (Sisley *et al.*, 1993; Blasi *et al.*, 1999; Myatt *et al.*, 2000; Tschentscher *et al.*, 2001).

We did not find any instances where the entire CGH ratio profile exceeded the threshold for loss. All partial chromosome losses, or tendencies toward loss, were recorded on interstitial portions of the p- and q-arms. Any observations in the most proximal and most distal bands of chromosome 3 were not included in this segment of the analysis, due in large part to the variability in hybridization near the centromere or telomere. The observed regions of interstitial loss fall within 3p13-p25 and 3q12-q28. Findings in other studies, particularly involving LOH of chromosome 3, align with our findings.

A drawback to large-scale CGH is the potential to mask critical chromosomal regions present in a low frequency within a given sample or within a collection of samples, and a similar drawback is realized in the distillation of minimal common regions. However, correlation of CGH with patient follow-up, using a variety of

established prognostic factors, has more utility. Using this approach, we have found six regions shown to be of significance to prognosis, including 18q11.2, 6q16, 21q11.2, 9q12, 3q12, and 1p33. We also identified a region on the X chromosome that seemed to correlate with a poor prognosis in males, but was not confirmed as statistically significant. All seven of these regions warrant further study.

SUMMARY

Our complete characterization of 10 cell lines, and analysis of copy number imbalances in 82 archival specimens, represents the most extensive and comprehensive cytogenetic characterization of uveal melanoma to date. In our cell lines, we catalogued numerous numerical and structural chromosomal aberrations. Many of these aberrations were suggested by the genomic imbalances revealed in the study of cell line and archival material. Chromosomes 1, 3, 7, 12, 17 and 20 were most frequently involved in numerical or structural aberrations in our SKY analysis, and CGH confirmed substantial genomic imbalance on each of these chromosomes, suggesting an integral role for these chromosomes in uveal melanoma. We were able to determine the involvement of chromosome 3 in our cell lines, and confirmed that rearrangement of that chromosome is more prevalent than whole chromosome loss in our samples. Our tumor study identified several chromosomal regions associated with prognosis, including 18q11.2, 6q16, 21q11.2, 9q12, 3q12, and 1p33. Together, our studies are aimed at directing further gene-specific study of malignancy in uveal melanoma.

REFERENCES

- Albert DM, Ruzzo MA, McLaughlin MA, Robinson NL, Craft JL, Epstein J: Establishment of cell lines of uveal melanoma. Methodology and characteristics. Invest Ophthalmol Vis Sci 1984, 25:1284-1299.
- Bauman JG, Wiegant J, Borst P, van Duijn P: A new method for fluorescence microscopical localization of specific DNA sequences by *in situ* hybridization of fluorochrome labelled RNA. Exp Cell Res 1980, 128:485-490.
- Bayani J and Squire JA: Advances in the detection of chromosomal aberrations using spectral karyotyping. Clin Genet 2001, 59:65-73.
- Bayani JM and Squire JA: Applications of SKY in cancer cytogenetics. Cancer Invest 2002, 20:373-386.
- Blasi MA, Roccella F, Balestrazzi E, Del Porto G, De Felice N, Roccella M, Rota R, Grammatico P: 3p13 region: a possible location of a tumor suppressor gene involved in uveal melanoma. Cancer Genet Cytogenet 1999, 108:81-83.
- Blom DJ, Mooy CM, Luyten GP, Kerkvliet S, Ouwerkerk I, Zwinderman AH, Schrier PI, Jager MJ: Inverse correlation between expression of HLA -B and c-myc in uveal melanoma. J Pathol 1997, 181:75-79.
- Callender GR: Malignant melanotic tumors of the eye: a study of histologic types in 111 cases. Transact Amer Acad Ophthalmol Otolaryngol 1931, 36:131-142.
- Carpenter NJ: Molecular cytogenetics. Semin Pediatr Neurol 2001, 8:135-146.
- Carter NP: Cytogenetic analysis by chromosome painting. Cytometry 1994, 18:2-10.
- Casperson T, Farber S, Folley G, Kudynowski J, Modest E, Simonsson E, Wash U, Zech L: Chemical differentiation along metaphase chromosomes. Exp Cell Res 1968, 49:219-222.
- Chana JS, Wilson GD, Cree IA, Alexander RA, Myatt N, Neale M, Foss AJ, Hungerford JL: c-myc, p53, and Bcl-2 expression and clinical outcome in uveal melanoma. Br J Ophthalmol 1999, 83:110-114.
- Chang SS and Mark HF: Emerging molecular cytogenetic technologies. Cytobios 1997, 90:7-22.

Chen PW, Murray TG, Uno T, Salgaller ML, Reddy R, Ksander BR: Expression of MAGE genes in ocular melanoma during progression from primary to metastatic disease. Clin Exp Metastasis 1997, 15:509-518.

Cohen IJ, Issakov J, Avigad S, Stark B, Meller I, Zaizov R, Bar-Am I: Synovial sarcoma of bone delineated by spectral karyotyping. Lancet 1997, 350:1679-1680.

Copeman, MC: The putative melanoma tumor-suppressor gene on human chromosome 6q. Pathology 1992, 24:307-309.

Cremer T, Landegent J, Bruckner A, Scholl HP, Schardin M, Hager HD, Devilee P, Pearson P, van der Ploeg M: Detection of chromosome aberrations in the human interphase nucleus by visualization of specific target DNAs with radioactive and non-radioactive *in situ* hybridization techniques: diagnosis of trisomy 18 with probe L1.84. Hum Genet 1986, 74:346-352.

Cremer T, Lichter P, Borden J, Ward DC, Manuelidis L: Detection of chromosome aberrations in metaphase and interphase tumor cells by *in situ* hybridization using chromosome-specific library probes. Hum Genet 1988, 80:235-246.

Dauwerse JG, Wiegant J, Raap AK, Breuning MH, van Ommen GJ: Multiple colors by fluorescence *in situ* hybridization using ratio-labelled DNA probes create a molecular karyotype. Hum Mol Genet 1992, 1:593-598.

De Waard-Siebinga I, Blom DJ, Griffioen M, Schrier PI, Hoogendoorn E, Beverstock G, Danen EH, Jager MJ: Establishment and characterization of an uveal-melanoma cell line. Int J Cancer 1995, 62:155-161.

Demetrick DJ: Gone FISHin' for genes. CMAJ 1999, 161:1138.

Devilee P, Thierry RF, Kievits T, Kolluri R, Hopman AH, Willard HF, Pearson PL, Cornelisse CJ: Detection of chromosome aneuploidy in interphase nuclei from human primary breast tumors using chromosome-specific repetitive DNA probes. Cancer Res 1988, 48:5825-5830.

Dolin PJ, Foss AJ, Hungerford JL: Uveal melanoma: is solar ultraviolet radiation a risk factor? Ophthalmic Epidemiol 1994, 1:27-30.

du Manoir S, Speicher MR, Joos S, Schröck E, Popp S, Dohner H, Kovacs G, Robert-Nicoud M, Lichter P, Cremer T: Detection of complete and partial chromosome gains and losses by comparative genomic *in situ* hybridization. Hum Genet 1993, 90:590-610.

du Manoir S, Kallioniemi OP, Lichter P, Piper J, Benedetti PA, Carothers AD, Fantes JA, Garcia-Sagredo JM, Gerdes T, Giollant M, Hemery B, Isola J, Maahr J, Morrison H, Perry P, Stark M, Sudar D, van Vliet LJ, Verwoerd N, Vrolijk J: Hardware and software requirements for quantitative analysis of comparative genomic hybridization. *Cytometry* 1995a, 19:4-9.

du Manoir S, Schröck E, Bentz M, Speicher MR, Joos S, Ried T, Lichter P, Cremer T: Quantitative analysis of comparative genomic hybridization. *Cytometry* 1995b, 19:27-41.

Dunne BM, McNamara M, Clynes M, Shering SG, Larkin AM, Moran E, Barnes C, Kennedy SM: MDR1 expression is associated with adverse survival in melanoma of the uveal tract. *Hum Pathol* 1998, 29:594-598.

Eastmond DA and Pinkel D: Aneuploidy detection by analysis of interphase nuclei using fluorescence *in situ* hybridization with chromosome-specific probes. *Prog Clin Biol Res* 1989, 318:277-284.

Egan KM, Seddon JM, Glynn RJ, Gragoudas ES, Albert DM: Epidemiologic aspects of uveal melanoma. *Surv Ophthalmol* 1988, 32:239-251.

Fidler IJ: Critical factors in the biology of human cancer metastasis: twenty-eighth G.H.A. Clowes memorial award lecture. *Cancer Res* 1990, 50:6130-6138.

Forozan F, Karhu R, Kononen J, Kallioniemi A, Kallioniemi OP: Genome screening by comparative genomic hybridization. *Trends Genet* 1997, 13:405-409.

Gall JG and Pardue ML: Formation and detection of RNA-DNA hybrid molecules in cytological preparations. *Proc Natl Acad Sci USA* 1969, 63:378-383.

Garini, Y., Macville, M., du Manoir, S., Buckwald, R.A., Lavi, M., Katzir, N., Wine, D., Bar-Am, I., Schröck, E., Cabib, D., Ried, T: Spectral karyotyping. *Bioimaging* 1996, 4:65-72.

Garini Y, Gil A, Bar-Am I, Cabib D, Katzir N: Signal to noise analysis of multiple color fluorescence imaging microscopy. *Cytometry* 1999, 35:214-226.

Genetics of Cancer Resource Center, "G-banded metaphase spread of a normal female somatic cell." 2001, World Wide Web URL: <http://www.intouchlive.com/cancergenetics/Images/b-banded-metaphase.jpg>.

Ghazvini S, Char DH, Kroll S, Waldman FM, Pinkel D: Comparative genomic hybridization analysis of archival formalin-fixed paraffin-embedded uveal melanomas. *Cancer Genet Cytogenet* 1996, 90:95-101.

Gordon KB, Thompson CT, Char DH, O'Brien JM, Kroll S, Ghazvini S, Gray JW: Comparative genomic hybridization in the detection of DNA copy number abnormalities in uveal melanoma. *Cancer Res* 1994, 54:4764-4768.

Griffin CA, Long PP, Schachat AP: Trisomy 6p in an ocular melanoma. *Cancer Genet Cytogenet* 1988, 32:129-132.

Herrington CS, Cooper K, McGee JO: Interphase cytogenetics: analysis of numerical chromosome aberrations in isolated cells. *J Pathol* 1995, 175:283-295.

Holly EA, Aston DA, Char DH, Kristiansen JJ, Ahn DK: Uveal melanoma in relation to ultraviolet light exposure and host factors. *Cancer Res* 1990, 50:5773-5777.

Hopman AH, Ramaekers FC, Raap AK, Beck JL, Devilee P, van der Ploeg M, Vooijs GP: *In situ* hybridization as a tool to study numerical chromosome aberrations in solid bladder tumors. *Histochemistry* 1988, 89:307-316.

Horsman DE, Sroka H, Rootman J, White VA: Monosomy 3 and isochromosome 8q in a uveal melanoma. *Cancer Genet Cytogenet* 1990, 45:249-253.

Horsman DE and White VA: Cytogenetic analysis of uveal melanoma. Consistent occurrence of monosomy 3 and trisomy 8q. *Cancer* 1993, 71:811-819.

Horsthemke B, Prescher G, Bornfeld N, Becher R: Loss of chromosome 3 alleles and multiplication of chromosome 8 alleles in uveal melanoma. *Genes Chromosomes Cancer* 1992, 4:217-221.

Houldsworth J and Chaganti RS: Comparative genomic hybridization: an overview. *Am J Pathol* 1994, 145:1253-1260.

Houlston RS and Damato BE: Genetic predisposition to ocular melanoma. *Eye* 1999, 13:43-46.

Hsu TC: Mammalian chromosomes in vitro. I. The karyotype of man. *J Hered* 1952, 43:167-172.

Hungerford DA, Donnelly AJ, Nowell PC, Beck S: The chromosome constitution of a human phenotypic intersex. *Am J Hum Genet* 1959; 11:215-236.

Hungerford J: Uveal melanoma. *Eur J Cancer* 1993, 29A:1365-1368.

Institut für Pathologie, University Hospital Charité, "CGH Protocols." 1996, World Wide Web URL: <http://amba.charite.de/cgh/protocol/02/prot02.html>.

International RH Mapping Consortium, "GeneMap '99." 1999, World Wide Web URL: <http://www.ncbi.nlm.nih.gov/genemap99>.

ISCN (1995): An International System for Human Cytogenetic Nomenclature, Mitelman F (ed); S. Karger, Basel, 1995.

Isola J, DeVries S, Chu L, Ghazvini S, Waldman F: Analysis of changes in DNA sequence copy number by comparative genomic hybridization in archival paraffin-embedded tumor samples. *Am J Pathol* 1994, 145:1301-1308.

John HA, Birnstiel ML, Jones KW: RNA-DNA hybrids at the cytological level. *Nature* 1969, 223:582-587.

Joos S, Fink TM, Ratsch A, Lichter P: Mapping and chromosome analysis: the potential of fluorescence *in situ* hybridization. *J Biotechnol* 1994, 35:135-153.

Kallioniemi A, Kallioniemi OP, Sudar D, Rutovit D, Gray J, Waldman F, Pinkel D: Comparative genomic hybridization for molecular cytogenetic analysis of solid tumors. *Science* 1992, 258:818-821.

Kallioniemi OP, Kallioniemi A, Sudar D, Rutovitz D, Gray JW, Waldman F, Pinkel D: Comparative genomic hybridization: a rapid new method for detecting and mapping DNA amplification in tumors. *Semin Cancer Biol* 1993, 4:41-46.

Kallioniemi OP, Kallioniemi A, Piper J, Isola J, Waldman FM, Gray JW, Pinkel D: Optimizing comparative genomic hybridization for analysis of DNA sequence copy number changes in solid tumors. *Genes Chromosomes Cancer* 1994, 10:231-243.

Kan-Mitchell J, Mitchell MS, Rao N, Liggett PE: Characterization of uveal melanoma cell lines that grow as xenografts in rabbit eyes. *Invest Ophthalmol Vis Sci* 1989, 30:829-834.

Kincaid MC: Uveal Melanoma. *Cancer Control* 1998, 5:299-309.

Langer PR, Waldrop AA, Ward DC: Enzymatic synthesis of biotin-labeled polynucleotides: novel nucleic acid affinity probes. *Proc Natl Acad Sci USA* 1981, 78:6633-6637.

Larouche N, Larouche K, Beliveau A, Leclerc S, Salesse C, Pelletier G, Guerin SL: Transcriptional regulation of the alpha 4 integrin subunit gene in the metastatic spread of uveal melanoma. *Anticancer Res* 1998, 18:3539-3547.

Lawrence JB, Villnave CA, Singer RH: Sensitive, high-resolution chromatin and chromosome mapping *in situ*: presence and orientation of two closely integrated copies of EBV in a lymphoma line. *Cell* 1988, 52:51-61.

Lee C, Gisselsson D, Jin C, Nordgren A, Ferguson DO, Blennow E, Fletcher JA, Morton CC: Limitations of chromosome classification by multicolor karyotyping. *Am J Hum Genet* 2001, 68:1043-1047.

Lichter P, Cremer T, Borden J, Manuelidis L, Ward DC: Delineation of individual human chromosomes in metaphase and interphase cells by *in situ* suppression hybridization using recombinant DNA libraries. *Hum Genet* 1988a, 80:224-234.

Lichter P, Cremer T, Tang CJ, Watkins PC, Manuelidis L, Ward DC: Rapid detection of human chromosome 21 aberrations by *in situ* hybridization. *Proc Natl Acad Sci USA* 1988b, 85:9664-9668.

Logani S, Cho AS, Ali BH, Withers HR, McBride WH, Kozlov KL, Hall MO, Lee DA, Straatsma BR: Single-dose compared with fractionated-dose radiation of the OM431 choroidal melanoma cell line. *Am J Ophthalmol* 1995a, 120:506-510.

Logani S, Cho AS, Su LD, Withers HR, McBride WH, Hall MO, Lee DA, Milani JK, Straatsma BR: Effects of gamma radiation on the OM431 human ocular melanoma cell line. *Exp Eye Res* 1995b, 60:603-605.

Luke S and Shepelsky M: FISH: recent advances and diagnostic aspects. *Cell Vis* 1998, 5:49-53.

Lundsteen C, Maahr J, Christensen B, Bryndorf T, Bentz M, Lichter P, Gerdes T: Image analysis in comparative genomic hybridization. *Cytometry* 1995, 19:42-50.

Luyten GP, Naus NC, Mooy CM, Hagemeijer A, Kan-Mitchell J, Van Drunen E, Vuzevski V, De Jong PT, Luiders TM: Establishment and characterization of primary and metastatic uveal melanoma cell lines. *Int J Cancer* 1996, 66:380-387.

Luyten GP, van der Spek CW, Brand I, Sintnicolaas K, de Waard-Siebinga I, Jager MJ, de Jong PT, Schrier PI, Luiders TM: Expression of MAGE, gp100 and tyrosinase genes in uveal melanoma cell lines. *Melanoma Res* 1998, 8:11-16.

Lynch HT, Anderson DE, Krush AJ: Heredity and intraocular malignant melanoma. Study of two families and review of forty-five cases. *Cancer* 1968, 21:119-125.

Macville M, Veldman T, Padilla-Nash H, Wangsa D, O'Brien P, Schröck E, Ried T: Spectral karyotyping, a 24-colour FISH technique for the analysis of chromosomal rearrangements. *Histochem Cell Bio* 1997, 108:299-305.

Macville M, Schröck E, Padilla-Nash H, Keck C, Ghadimi BM, Zimonjic D, Popescu N, Ried T: Comprehensive and definitive molecular cytogenetic characterization of HeLa cells by spectral karyotyping. *Cancer Res* 1999, 59:141-150.

McLean IW, Foster WD, Zimmerman LE: Prognostic factors in small malignant melanomas of choroid and ciliary body. *Arch Ophthalmol* 1977, 95:48-58.

McLean IW, Foster WD, Zimmerman LE, Gamel JW: Modifications of Callender's classification of uveal melanoma at the Armed Forces Institute of Pathology. *Am J Ophthalmol* 1983, 96:502-509.

McLean IW: The biology of haematogenous metastasis in human uveal malignant melanoma. *Virchows Arch A Pathol Anat Histopathol* 1993, 422:433-437.

McLean, IW: Prognostic Features of Uveal Malignant Melanoma. *Ophthalmol Clin North Am* 1995, 8:143-153.

McLean, W and Gamel JW: Uveal (intraocular) melanoma. *Cancer J* 1996, 9:20-25.

McNamara M, Felix C, Davison EV, Fenton M, Kennedy SM: Assessment of chromosome 3 copy number in ocular melanoma using fluorescence *in situ* hybridization. *Cancer Genet Cytogenet* 1997, 98:4-8.

McNicol AM and Farquharson MA: *In situ* hybridization and its diagnostic applications in pathology. J Pathol 1997 Jul, 182:250-261.

Merbs SL and Sidransky D: Analysis of p16 (CDKN2/MTS-1/INK4A) alterations in primary sporadic uveal melanoma. Invest Ophthalmol Vis Sci 1999, 40:779-783.

Myatt N, Aristodemou P, Neale MH, Foss AJ, Hungerford JL, Bhattacharya S, A Cree I: Abnormalities of the transforming growth factor-beta pathway in ocular melanoma. J Pathol 2000, 192:511-518.

Naus NC, van Drunen E, de Klein A, Luyten GP, Paridaens DA, Alers JC, Ksander BR, Beverloo HB, Slater RM: Characterization of complex chromosomal abnormalities in uveal melanoma by fluorescence *in situ* hybridization, spectral karyotyping, and comparative genomic hybridization. Genes Chromosomes Cancer 2001, 30:267-273.

Naus NC, Verhoeven AC, van Drunen E, Slater R, Mooy CM, Paridaens DA, Luyten GP, de Klein A: Detection of genetic prognostic markers in uveal melanoma biopsies using fluorescence *in situ* hybridization. Clin Cancer Res 2002, 8:534-539.

Nederlof PM, Robinson D, Abuknesha R, Wiegant J, Hopman AH, Tanke HJ, Raap AK: Three-color fluorescence *in situ* hybridization for the simultaneous detection of multiple nucleic acid sequences. Cytometry 1989, 10:20-27.

Nederlof PM, van der Flier S, Wiegant J, Raap AK, Tanke HJ, Ploem JS, van der Ploeg M: Multiple fluorescence *in situ* hybridization. Cytometry 1990, 11:126-131.

Online Mendelian Inheritance in Man, OMIM™. McKusick-Nathans Institute for Genetic Medicine, Johns Hopkins University (Baltimore, MD) and National Center for Biotechnology Information, National Library of Medicine (Bethesda, MD), 2000. World Wide Web URL: <http://www.ncbi.nlm.nih.gov/omim>.

Parada LA, Maranon A, Hallen M, Tranberg KG, Stenram U, Bardi G, Johansson B: Cytogenetic analyses of secondary liver tumors reveal significant differences in genomic imbalances between primary and metastatic colon carcinomas. Clin Exp Metastasis 1999, 17:471-479.

Parrella P, Sidransky D, Merbs SL: Allelotype of posterior uveal melanoma: implications for a bifurcated tumor progression pathway. Cancer Res 1999, 59:3032-3037.

Pereira F, Burnier MN Jr, Shibata H, Wang B, Carey W: Cytomorphometric parameters and the metastatic potential of cutaneous and uveal melanoma: a comparison with prognostic factors. *Am J Dermatopathol* 2001, 23:304-307.

Pinkel D, Straume T, Gray JW: Cytogenetic analysis using quantitative, high-sensitivity, fluorescence hybridization. *Proc Natl Acad Sci USA* 1986a, 83:2934-2938.

Pinkel D, Gray JW, Trask B, van den Engh G, Fuscoe J, van Dekken H: Cytogenetic analysis by *in situ* hybridization with fluorescently labeled nucleic acid probes. *Cold Spring Harb Symp Quant Biol* 1986b, 51 Pt 1:151-157.

Pinkel D, Landegent J, Collins C, Fuscoe J, Segraves R, Lucas J, Gray J: Fluorescence *in situ* hybridization with human chromosome-specific libraries: detection of trisomy 21 and translocations of chromosome 4. *Proc Natl Acad Sci USA* 1988, 85:9138-9142.

Piper J, Rutovitz D, Sudar D, Kallioniemi A, Kallioniemi OP, Waldman FM, Gray JW, Pinkel D: Computer image analysis of comparative genomic hybridization. *Cytometry* 1995, 19:10-26.

Prescher G, Bornfeld N, Becher R: Nonrandom chromosomal abnormalities in primary uveal melanoma. *J Natl Cancer Inst* 1990, 82:1765-1769.

Prescher G, Bornfeld N, Becher R: Two subclones in a case of uveal melanoma. Relevance of monosomy 3 and multiplication of chromosome 8q. *Cancer Genet Cytogenet* 1994, 77:144-146.

Prescher G, Bornfeld N, Friedrichs W, Seeber S, Becher R: Cytogenetics of twelve cases of uveal melanoma and patterns of nonrandom anomalies and isochromosome formation. *Cancer Genet Cytogenet* 1995, 80:40-46.

Prescher G, Bornfeld N, Hirche H, Horsthemke B, Jockel K, Becher R: Prognostic implications of monosomy 3 in uveal melanoma. *Lancet* 1996, 347:1222-1225.

Raap T: Cytometry for CGH. *Cytometry* 1995, 19:1-3.

Raap AK: Advances in fluorescence *in situ* hybridization. *Mutat Res* 1998, 400:287-298.

Regan S, Judge HE, Gragoudas ES, Egan KM: Iris color as a prognostic factor in ocular melanoma. *Arch Ophthalmol* 1999, 117:811-814.

Ried T, Baldini A, Rand TC, Ward DC: Simultaneous visualization of seven different DNA probes by *in situ* hybridization using combinatorial fluorescence and digital imaging microscopy. Proc Natl Acad Sci USA 1992a, 89:1388-1392.

Ried T, Landes G, Dackowski W, Klinger K, Ward DC: Multicolor fluorescence *in situ* hybridization for the simultaneous detection of probe sets for chromosomes 13, 18, 21, X and Y in uncultured amniotic fluid cells. Hum Mol Genet 1992b, 1:307-313.

Ried T, Liyanage M, du Manoir S, Heselmeyer K, Auer G, Macville M, Schröck E: Tumor cytogenetics revisited: comparative genomic hybridization and spectral karyotyping. J Mol Med 1997, 75:801-814.

Rosenberg C, Schut TB, Mostert MC, Tanke HJ, Raap AK, Oosterhuis JW, Looijenga LH: Comparative genomic hybridization in hypotriploid/hyperdiploid tumors. Cytometry 1997, 29:113-121.

Rothmann C, Bar-Am I, Malik Z: Spectral imaging for quantitative histology and cytogenetics. Histol Histopathol 1998, 13:921-926.

Rudkin GT and Stollar BD: High resolution detection of DNA-RNA hybrids *in situ* by indirect immunofluorescence. Nature 1977, 265:472-473.

Schröck E, du Manoir S, Veldman T, Schoell B, Wienberg J, Ferguson-Smith MA, Ning Y, Ledbetter DH, Bar-Am I, Soenksen D, Garini Y, Ried T: Multicolor spectral karyotyping of human chromosomes. Science 1996, 273:494-497.

Schröck E, Veldman T, Padilla-Nash H, Ning Y, Spurbeck J, Jalal S, Shaffer LG, Papenhausen P, Kozma C, Phelan MC, Kjeldsen E, Schonberg SA, O'Brien P, Biesecker L, du Manoir S, Ried T: Spectral karyotyping refines cytogenetic diagnostics of constitutional chromosomal abnormalities. Hum Genet 1997, 101:255-262.

Schröck E and Padilla-Nash H: Spectral karyotyping and multicolor fluorescence *in situ* hybridization reveal new tumor-specific chromosomal aberrations. Semin Hematol 2000, 37:334-347.

Singh AD, Boghosian-Sell L, Wary KK, Shields CL, De Potter P, Donoso LA, Shields JA, Cannizzaro LA: Cytogenetic findings in primary uveal melanoma. Cancer Genet Cytogenet 1994, 72:109-115.

Singh AD, Wang MX, Donoso LA, Shields CL, De Potter P, Shields JA: Genetic aspects of uveal melanoma: a brief review. Semin Oncol 1996a, 23:768-772.

Singh AD, Donoso LA, Jackson L, Shields CL, De Potter P, Shields JA: Familial uveal melanoma: absence of constitutional cytogenetic abnormalities in 14 cases. *Arch Ophthalmol* 1996b, 114:502-503.

Singh AD, Shields CL, Shields JA: Prognostic factors in uveal melanoma. *Melanoma Res* 2001, 11:255-263.

Sisley 1990 Sisley K, Rennie IG, Cottam DW, Potter AM, Potter CW, Rees RC: Cytogenetic findings in six posterior uveal melanomas: involvement of chromosomes 3, 6, and 8. *Genes Chromosomes Cancer* 1990, 2:205-209.

Sisley K, Cottam DW, Rennie IG, Parsons MA, Potter AM, Potter CW, Rees RC: Non-random abnormalities of chromosomes 3, 6, and 8 associated with posterior uveal melanoma. *Genes Chromosomes Cancer* 1992, 5:197-200.

Sisley K, Curtis D, Rennie IG, Rees RC: Loss of heterozygosity of the thyroid hormone receptor B in posterior uveal melanoma. *Melanoma Res* 1993, 3:457-461.

Sisley K, Rennie IG, Parsons MA, Jacques R, Hammond DW, Bell SM, Potter AM, Rees RC: Abnormalities of chromosomes 3 and 8 in posterior uveal melanoma correlate with prognosis. *Genes Chromosomes Cancer* 1997, 19:22-28.

Sisley K, Parsons MA, Garnham J, Potter AM, Curtis D, Rees RC, Rennie IG: Association of specific chromosome alterations with tumour phenotype in posterior uveal melanoma. *Br J Cancer* 2000, 82:330-338.

Speicher MR, du Manoir S, Schröck E, Holtgreve-Grez H, Schoell B, Lengauer C, Cremer T, Ried T: Molecular cytogenetic analysis of formalin-fixed, paraffin-embedded solid tumors by comparative genomic hybridization after universal DNA-amplification. *Hum Mol Genet* 1993, 2:1907-1914.

Speicher MR, Prescher G, du Manoir S, Jauch A, Horsthemke B, Bornfeld N, Becher R, Cremer T: Chromosomal gains and losses in uveal melanomas detected by comparative genomic hybridization. *Cancer Res* 1994, 54:3817-3823.

Speicher MR, Gwyn Ballard S, Ward DC: Karyotyping human chromosomes by combinatorial multi-fluor FISH. *Nat Genet* 1996, 12:368-375.

Telenius H, Pelmeur AH, Tunnacliffe A, Carter NP, Behmel A, Ferguson-Smith MA, Nordenskjöld M, Pfragner R, Ponder BA: Cytogenetic analysis by chromosome painting using DOP-PCR amplified flow-sorted chromosomes. *Genes Chromosomes Cancer* 1992a, 4:257-263.

Telenius H, Carter NP, Bebb CE, Nordenskjöld M, Ponder BA, Tunnacliffe A: Degenerate oligonucleotide-primed PCR: general amplification of target DNA by a single degenerate primer. *Genomics* 1992b, 13:718-725.

Thompson CT and Gray JW: Cytogenetic profiling using fluorescence *in situ* hybridization (FISH) and comparative genomic hybridization (CGH). *J Cell Biochem Suppl* 1993, 17G:139-143.

Tjio JH and Levan A: The chromosome number of man. *Hereditas* 1956, 42:1-6.

Tonon G, Roschke A, Stover K, Shou Y, Kuehl WM, Kirsch IR: Spectral karyotyping combined with locus-specific FISH simultaneously defines genes and chromosomes involved in chromosomal translocations. *Genes Chromosomes Cancer* 2000, 27:418-423.

Trask BJ: Fluorescence *in situ* hybridization: applications in cytogenetics and gene mapping. *Trends Genet* 1991, 7:149-154.

Tschentscher F, Prescher G, Horsman DE, White VA, Rieder H, Anastassiou G, Schilling H, Bornfeld N, Bartz-Schmidt KU, Horsthemke B, Lohmann DR, Zeschneck M: Partial deletions of the long and short arm of chromosome 3 point to two tumor suppressor genes in uveal melanoma. *Cancer Res* 2001, 61:3439-3442.

Tucker JD, Lee DA, Ramsey MJ, Briner J, Olsen L, Moore DH 2nd: On the frequency of chromosome exchanges in a control population measured by chromosome painting. *Mutat Res* 1994, 313:193-202.

Tucker MA, Shields JA, Hartge P, Augsburger J, Hoover RN, Fraumeni JF Jr: Sunlight exposure as risk factor for intraocular malignant melanoma. *N Engl J Med* 1985, 313:789-792.

University of Michigan Health System, "DNA Denaturation/Renaturation." 1998, World Wide Web URL: <http://www.seqcore.brcf.med.umich.edu/doc/educ/dnapr/pg2.html>.

Veldman T, Vignon C, Schröck E, Rowley JD, Ried T: Hidden chromosome abnormalities in haematological malignancies detected by multicolour spectral karyotyping. *Nat Genet* 1997, 15:406-410.

Watson JD and Crick FH: Molecular structure of nucleic acids: a structure for deoxyribose nucleic acid. Nature 1953, 4356:737-738.

White VA, McNeil BK, Thiberville L, Horsman DE: Acquired homozygosity (isodisomy) of chromosome 3 during clonal evolution of a uveal melanoma: association with morphologic heterogeneity. Genes Chromosomes Cancer 1996, 15:138-143.

White VA, McNeil BK, Horsman DE: Acquired homozygosity (isodisomy) of chromosome 3 in uveal melanoma. Cancer Genet Cytogenet 1998a, 102:40-45.

White VA, Chambers JD, Courtright PD, Chang WY, Horsman DE: Correlation of cytogenetic abnormalities with the outcome of patients with uveal melanoma. Cancer 1998b, 83:354-359.

Wiltshire RN, Elner VM, Dennis T, Vine AK, Trent JM: Cytogenetic analysis of posterior uveal melanoma. Cancer Genet Cytogenet 1993, 66:47-53.

APPENDIX A

BUFFERS, REAGENTS AND SOLUTIONS

Cell Culture

RPMI 1640

1 package powdered RPMI 1640 media (Invitrogen Life Technologies, Carlsbad, CA)
2g NaHCO₃
1000ml sterile or autoclaved dH₂O

Add powdered media and approximately 900ml sterile/autoclaved dH₂O to 1000ml volumetric flask. Add 2g NaHCO₃, and add a stir bar. When dissolved, pH to 0.2-0.3 below final desired pH (7.0-7.4). Remove stir bar, and add remainder of dH₂O to reach 1000ml. Using suction filtration, divide flask into two 500ml sterile bottles. Incomplete media can be stored at -20°C until needed.

To complete media (each 500ml bottle):

50ml FBS (Sigma Co., St. Louis, MO)
5ml NEAA (Sigma Co., St. Louis, MO)
5ml HEPES Buffer (Sigma Co., St. Louis, MO)
0.5ml gentamicin (Invitrogen Life Technologies, Carlsbad, CA)
0.5-1ml Fungizone (Invitrogen Life Technologies, Carlsbad, CA)
1-2ml penicillin/streptomycin (100U/ml and 100µg/ml, respectively) (Invitrogen Life Technologies, Carlsbad, CA)

Store completed media at 4°C in the dark.

DMEM

1 bottle powdered DMEM media (Sigma Co., St. Louis, MO)
3.7g NaHCO₃
1000ml sterile or autoclaved dH₂O

Add powdered media and approximately 900ml sterile/autoclaved dH₂O to 1000ml volumetric flask. Add 3.7g NaHCO₃, and add a stir bar. When dissolved, pH to 0.2-0.3 below final desired pH (7.0±0.3). Remove stir bar, and add remainder of dH₂O to reach 1000ml. Using suction filtration, divide flask into two 500ml sterile bottles. Incomplete media can be stored at -20°C until needed.

To complete media (each 500ml bottle):

50ml FBS
5ml NEAA
5ml HEPES Buffer
0.5ml gentamycin
0.5-1ml Fungizone
1-2ml penicillin/streptomycin

Store completed media at 4°C in the dark.

Ham's F-12

1 package powdered Ham's F-12 media (Invitrogen Life Technologies, Carlsbad, CA)
1.176g NaHCO₃
1000ml sterile or autoclaved dH₂O

Add powdered media and approximately 900ml sterile/autoclaved dH₂O to 1000ml volumetric flask. Add 1.176g NaHCO₃, and add a stir bar. When dissolved, pH to 0.2-0.3 below final desired pH (7.6-7.9). Remove stir bar, and add remainder of dH₂O to reach 1000ml. Using suction filtration, divide flask into two 500ml sterile bottles. Incomplete media can be stored at -20°C until needed.

To complete media (each 500ml bottle):

50ml FBS

5ml NEAA

5ml HEPES Buffer

0.5ml gentamycin

0.5-1ml Fungizone

1-2ml penicillin/streptomycin

Store completed media at 4°C in the dark.

Metaphase Chromosome Preparation

Carnoy's Fixative

75ml absolute methanol, HPLC grade (Fisher Scientific, Inc., Pittsburgh, PA)

25ml glacial acetic acid, tracenmetal grade (Fisher Scientific, Pittsburgh, PA)

Make 3:1 mixture as needed. Use only when fresh (first day).

75mM KCl

5.6g KCl

1000ml dH₂O

Dissolve KCl in dH₂O. Store at room temperature.

DNA Isolation

100mM Tris/Cl pH 8.5

2.21g Tris-HCl (Sigma Co., St. Louis, MO)

4.36g Trizma Base (Sigma Co., St. Louis, MO)

Add Tris-HCL, Trizma base and ~450ml dH₂O to a 500ml volumetric flask with a magnetic stir bar. After contents are completely dissolved, remove stir bar and fill flask the remainder of the way to the 500ml mark with dH₂O. Adjust pH to 8.5 and autoclave. Store at room temperature.

Cell Lysis Buffer

20ml 100mM Tris-HCl pH 8.5

2ml 0.5M EDTA pH 8.0 (Digene, Gaithersburg, MD)

4ml 10% SDS (Fisher Scientific, Pittsburgh, PA)

8ml 5M NaCl

165ml dH₂O

Makes 199ml. Store at room temperature.

TE Buffer pH 7.0

5ml 1M Tris-HCl pH 7.0 (Quality Biological, Inc., Gaithersburg, MD)

1ml 0.5M EDTA pH 8.0

494ml dH₂O

Adjust to pH 7.0 and autoclave. Store at room temperature.

RNase A

100mg RNase A, lyophilized (Roche Molecular Biochemicals, Indianapolis, IN)

5ml sterile H₂O (DNase free, RNase free)

To dissolve, boil for 15 minutes, and then cool to room temperature. Aliquot 20mg/ml solution, and store at -20°C. See also "Pretreatment of Slides for CGH, SKY and FISH."

Nick Translation

NT Buffer

500 µl 0.5M Tris HCl, pH 8.0 (Quality Biological, Inc., Gaithersburg, MD)
100µl 50mM MgCl₂
50µl 0.5mg/ml BSA (Sigma Co., St. Louis, MO)
350µl sterile H₂O (DNase free, RNase free) (Sigma Co., St. Louis, MO)

Makes 1ml. Aliquot and store at -20°C.

DNase I (1mg/ml)

10mg DNase I (Roche Molecular Biochemicals, Indianapolis, IN)
1.5ml 0.15M NaCl (Quality Biological, Inc., Gaithersburg, MD)
5ml 50% Glycerol (Fisher Scientific, Pittsburgh, PA)
10ml sterile H₂O (DNase free, RNase free)

Aliquot and store at -20°C. Make 1:1000 dilution for use in nick translation reactions.

dNTP Mixture

5µl each of 100mM dATP, dCTP, and dGTP (Promega, Madison, WI)
1µl of 100mM dTTP (Promega, Madison, WI)
984µl sterile H₂O (DNase free, RNase free)

Makes 0.5mM dATP/dCTP/dGTP and 0.05mM dTTP. Aliquot and store at -20°C.

0.1M β-Mercaptoethanol

34.7µl of 99% (14.4M) solution (Sigma Co., St. Louis, MO)
Sterile H₂O (DNase free, RNase free) to make 5ml

Aliquot and store at -20°C.

50µl Nick Translation Reaction

xµl (1µg) DNA (volume variable)
5µl 10xNT Buffer
5µl dNTP mixture
5µl 0.1M β-Mercaptoethanol
2µl biotin- or digoxigenin-11-dUTP
33-xµl sterile H₂O (DNase free, RNase free)

DOP-PCR

DOP-PCR Primer

Resuspend DOP-PCR CGH primer, 5' - GAT CAA GCT NNN NNN ATG TGG - 3' (Integrated DNA Technologies, Inc., Coralville, IA) in 1223.7µl sterile H₂O (DNase free, RNase free) to make 100mM primer stock.

Dilute primer stock 1:5 in sterile H₂O (DNase free, RNase free) to make 20mM primer.

Biotin- or dig-dNTP Mixture

3.04µl dATP

3.04µl dCTP

3.04µl dGTP

1.26µl dTTP

25µl biotin- or dig-dUTP (Roche Molecular Biochemicals, Indianapolis, IN)

117µl sterile H₂O (DNase free, RNase free)

Makes 152µl dNTP mix. Make fresh as needed.

DOP-PCR Polymerase

250U AmpliTaq Gold Polymerase stock, 5U/µl (Roche Applied Biosystems, Foster City, CA)

50µl sterile H₂O (DNase free, RNase free)

Make 1:1 dilution (2.5U/µl) of AmpliTaq Gold Polymerase before use, by adding 50µl sterile H₂O to 50µl AmpliTaq Gold stock.

DOP-PCR Master Mix (MM)

10µl 10xBuffer II (Roche Applied Biosystems, Foster City, CA)

10µl 20mM DOP Primer (Integrated DNA Technologies, Inc., Coralville, IA)

24µl 25mM MgCl₂ (Roche Applied Biosystems, Foster City, CA)

5µl biotin- or dig-dUTP mixture

39µl sterile H₂O (DNase free, RNase free)

2µl AmpliTaq Gold Polymerase

Makes 90µl MM, which is enough for a single DOP-PCR reaction. Scale as needed, allowing for a single extra reaction in case of error. Make fresh as needed and keep on ice.

100µl DOP-PCR Reaction

10µl DNA

90µl DOP-PCR MM

Reaction Conditions:

95°C for 10 minutes, initial soak

15 cycles:

94°C for 1 minute

30°C for 1 minute

72°C for 1 minute

60 cycles (with a 1 second per cycle addition to each step in the 60 cycles):

94°C for 30 seconds

52°C for 30 seconds

72°C for 1 minute

Final extension of 72°C for 10 minutes

Hold at 4°C.

Electrophoresis

1.7% Agarose Gel

0.85g low melting point agarose powder (Invitrogen Life Technologies, Carlsbad, CA)

50ml 1x TBE buffer (Invitrogen Life Technologies, Carlsbad, CA)

Microwave (boil) until dissolved. Cool to ~65°C in a water bath and mix in 2.5ml of a 10mg/ml ethidium bromide solution. Pour gel or store at 4°C in the dark.

Gel-Loading Buffer III (6x)

0.025g bromophenol blue (Sigma Co., St. Louis, MO)

0.025g xylene cyanol (Sigma Co., St. Louis, MO)

3ml glycerol

6.95ml dH₂O

Final solution is 0.25% bromophenol blue, 0.25% xylene cyanol, and 30% glycerol in dH₂O. Store at 4°C.

Pretreatment for CGH, SKY and FISH

2xSSC

10ml 20xSSC (Fisher Scientific, Pittsburgh, PA)

90ml dH₂O

Store at room temperature.

1xPBS

10ml 10xPBS (w/o MgCl₂ or CaCl₂) (Invitrogen Life Technologies, Carlsbad, CA)

90ml dH₂O

Store at room temperature.

1M MgCl₂

203.3g MgCl₂•6H₂O (Fisher Scientific, Pittsburgh, PA)

1000ml dH₂O

Add MgCl₂•6H₂O and ~800ml dH₂O to a 1000ml volumetric flask with a stir bar. Remove stir bar and fill flask to 1000ml. Aliquot and autoclave. Store at room temperature.

1x PBS/MgCl₂

50ml 1M MgCl₂

950ml 1xPBS (w/o MgCl₂ or CaCl₂)

Store at room temperature.

RNase A

100mg RNase A, lyophilized (Roche Molecular Biochemicals, Indianapolis, IN)

5ml sterile H₂O (DNase free, RNase free)

To dissolve, boil for 15 minutes, and then cool to room temperature. Aliquot 20mg/ml solution, and store at -20°C. Make 1:200 dilution in 2xSSC for slide pretreatment.

Pepsin stock solution

100mg pepsin (Sigma Co., St. Louis, MO)

1ml sterile H₂O (DNase free, RNase free)

Dissolve, keep on ice. Make 50µl aliquots of 100mg/ml stock solution, and store at -20°C.

0.01M HCl

1ml 1M HCl (Fisher Scientific, Pittsburgh, PA)

99ml dH₂O

Store at room temperature.

Pepsin/HCl

15µl pepsin stock solution
100ml 0.01M HCl

Make fresh as needed with HCl pre-warmed to 37°C.

1% Formaldehyde in 1xPBS/MgCl₂

2.7ml of 37% Formaldehyde solution (Fisher Scientific, Pittsburgh, PA)
100ml 1xPBS/MgCl₂

Store at room temperature.

Hybridization for CGH, SKY and FISH

Master Mix (MM)

1g dextran sulfate sodium salt (Biotech grade) (Fisher Scientific, Pittsburgh, PA)
5ml 2xSSC

Dissolve dextran sulfate in 2xSSC at 70°C for several hours. Once dissolved, cool to room temperature and adjust to pH 7.0. Aliquot, store at -20°C.

70% FA/SSC for CGH slide denaturation

7ml formamide, molecular grade (Fisher Scientific, Pittsburgh, PA)
1ml 20xSSC
2ml sterile H₂O (DNase free, RNase free)

Adjust to pH 7.2-7.3. Store at -20°C.

70% FA/SSC for FISH slide denaturation

35ml formamide, molecular grade
5ml 20xSSC
10ml sterile H₂O (DNase free, RNase free)

Adjust to pH 7.0. Store at 4°C for up to 3 weeks.

Probe Precipitation for CGH

30µl each (tumor and reference) DOP-PCR product
60µl human Cot-1 DNA (Invitrogen Life Technologies, Carlsbad, CA)
1µl salmon testes DNA (Sigma Co., St. Louis, MO)
12.1µl 3M sodium acetate
400µl absolute ethanol, ice cold

Detection for CGH, SKY and FISH

50% FA/SSC

30ml 20xSSC
120ml dH₂O
150ml formamide, molecular grade

Make one day before needed. Adjust to pH ~7.25.

4xSSC/0.1% Tween 20 for CGH

100ml 20xSSC

400ml dH₂O

0.5ml Tween 20 (Sigma Co., St. Louis, MO)

Store at room temperature.

4xSSC/0.05% Tween 20 for FISH

100ml 20xSSC

400ml dH₂O

0.25ml Tween 20

Store at room temperature.

1xSSC for SKY

25ml 20xSSC

Add 475ml dH₂O to make 500ml

0.1xSSC

2.5ml 20xSSC

Add dH₂O (~497.5ml) to make 500ml

0.4xSSC

10ml 20xSSC

Add dH₂O (490ml) to make 500ml

Store at room temperature.

3% BSA for CGH

0.3g bovine serum albumin (BSA) powder (Sigma Co., St. Louis, MO)

10ml 4xSSC/0.1% Tween 20

Dissolve BSA in 4xSSC/Tween 20 to make 3% blocking solution. Store at 4°C.

1% BSA for Antibody Layering in CGH

Dilute 3% BSA 2:1 in 4xSSC/0.1% Tween 20

Used in antibody dilution for detection layers in CGH. Store at 4°C.

3% NFDM for FISH

1 bottle lyophilized NFDM (Sigma Co., St. Louis, MO)

100ml dH₂O

0.2% sodium azide

Reconstitute NFDM in dH₂O. Add 200μl sodium azide as a preservative. Makes 3% blocking solution. Also used in antibody dilution for detection layers in FISH. Store at 4°C.

Antibody Layers for CGH

- 1) avidin-FITC (1:200), mouse anti-dig (1:100), in 1% BSA
- 2) anti-avidin (1:200), rabbit anti-mouse TRITC (1:200), in 1% BSA
- 3) avidin-FITC (1:200), in 1% BSA
- 4) goat anti-rabbit TRITC (1:200), in 1% BSA

1% BSA is dilution of 3% BSA blocking solution for CGH. Prepare 200μl of each layer per slide. Make fresh.

Antibody Layers for FISH

- 1) avidin-FITC (1:400), avidin-Rhodamine (1:400), in 3% NFDM
- 2) anti-avidin (1:100), in 3% NFDM
- 3) avidin-FITC (1:400), avidin-Rhodamine (1:400), in 3% NFDM

3% NFDM is also used in blocking layer for FISH. Prepare 200µl of each layer per slide. Make fresh.

DAPI

2mg DAPI (Roche Molecular Biochemicals, Indianapolis, IN)
10ml 2xSSC

Dissolve DAPI in 2xSSC to make 2mg/ml DAPI stock solution. Working solution is 80ng/ml. To make working solution, add 4µl DAPI stock solution to 50ml 2xSSC.

0.5M carbonate buffer

6.2g Na₂CO₃·H₂O or 5.3g Na₂CO₃ (Sigma Co., St. Louis, MO)
autoclaved dH₂O to complete 100ml

Dissolve to make 100ml of 0.5M Na₂CO₃.

0.5M bicarbonate buffer

4.2g NaHCO₃ (Sigma Co., St. Louis, MO)
autoclaved dH₂O to complete 100ml

Dissolve to make 100ml of 0.5M NaHCO₃.

0.5M carbonate-bicarbonate buffer

10ml 0.5M Na₂CO₃
90ml 0.5M NaHCO₃

Adjust to pH 9.0. Store at room temperature.

Antifade

100mg phenylenediamine dihydrochloride (Sigma Co., St. Louis, MO)
10ml 1xPBS (w/o MgCl₂ or CaCl₂)
90ml glycerol

Dissolve phenylenediamine dihydrochloride in 1xPBS, and sterile filter solution. Adjust pH to 8.0 with 0.5M carbonate-bicarbonate buffer (pH 9.0), and add 90ml glycerol for a total volume of approximately 110ml. Store at -20°C in the dark (may be useful to wrap bottle in aluminum foil to avoid degradation when using it at room temperature).

APPENDIX B

MOLECULAR CYTOGENETICS

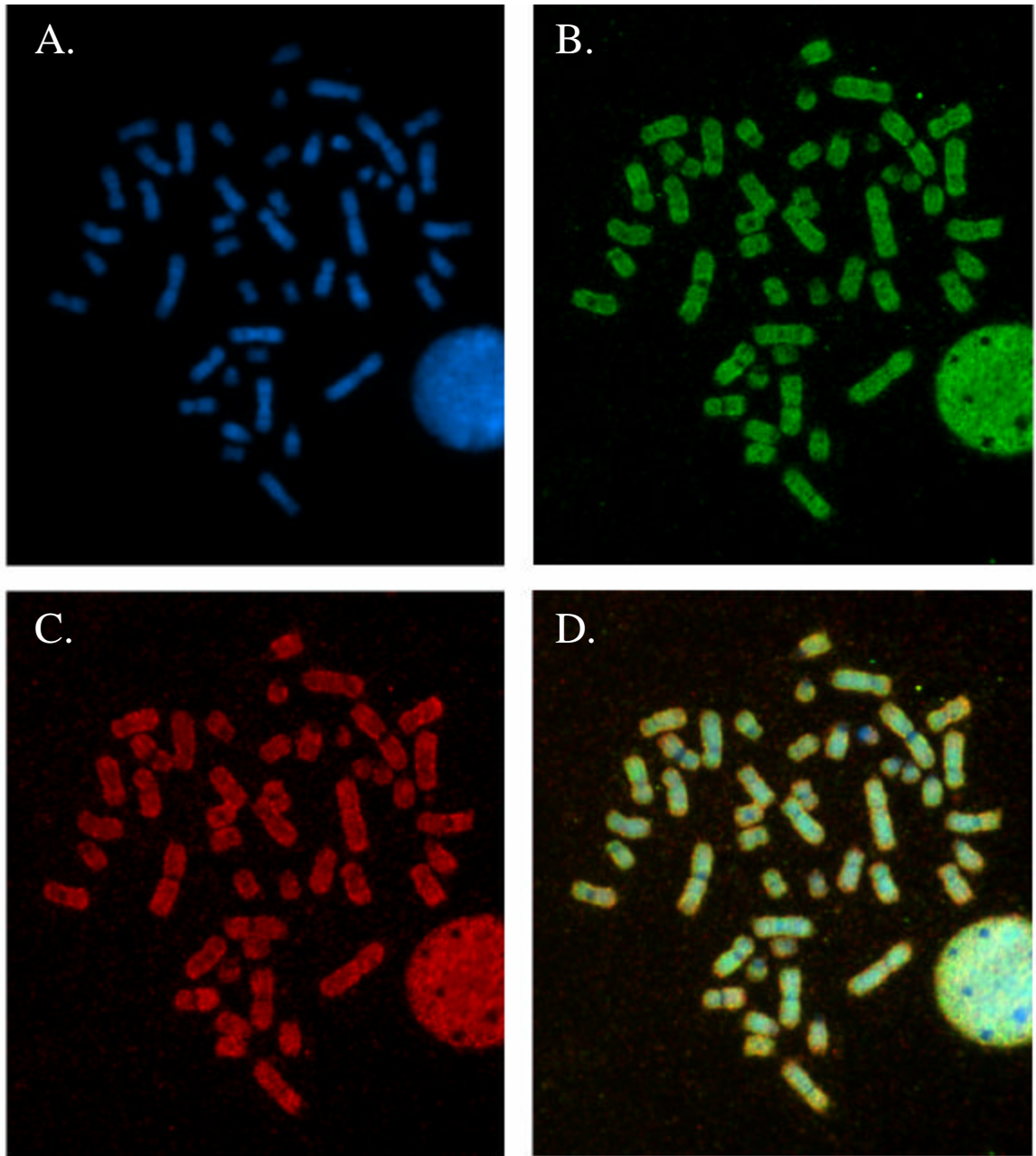


Figure 35. Image Capture for CGH Analysis from an Archival Uveal Melanoma Case. Each of these images is the identical normal male metaphase spread detected with three different fluorescent filters. **(A)** The metaphase chromosomes counterstained with DAPI. Biotinylated tumor DNA and dig-11-dUTP-labelled normal DNA signals were detected with avidin-conjugated fluorescein isothiocyanate (FITC) and tetramethylrhodamine isothiocyanate (TRITC) conjugated antibodies. **(B)** The FITC image, and **(C)** The TRITC image. These three fluorescent images **(A, B and C)** combine to form the completed CGH image seen in **(D)**. This newly combined image is suitable for CGH analysis; the image is classified and karyotyped, followed by the generation of CGH profiles to illustrate the amplifications and deletions present within the tumor genome.

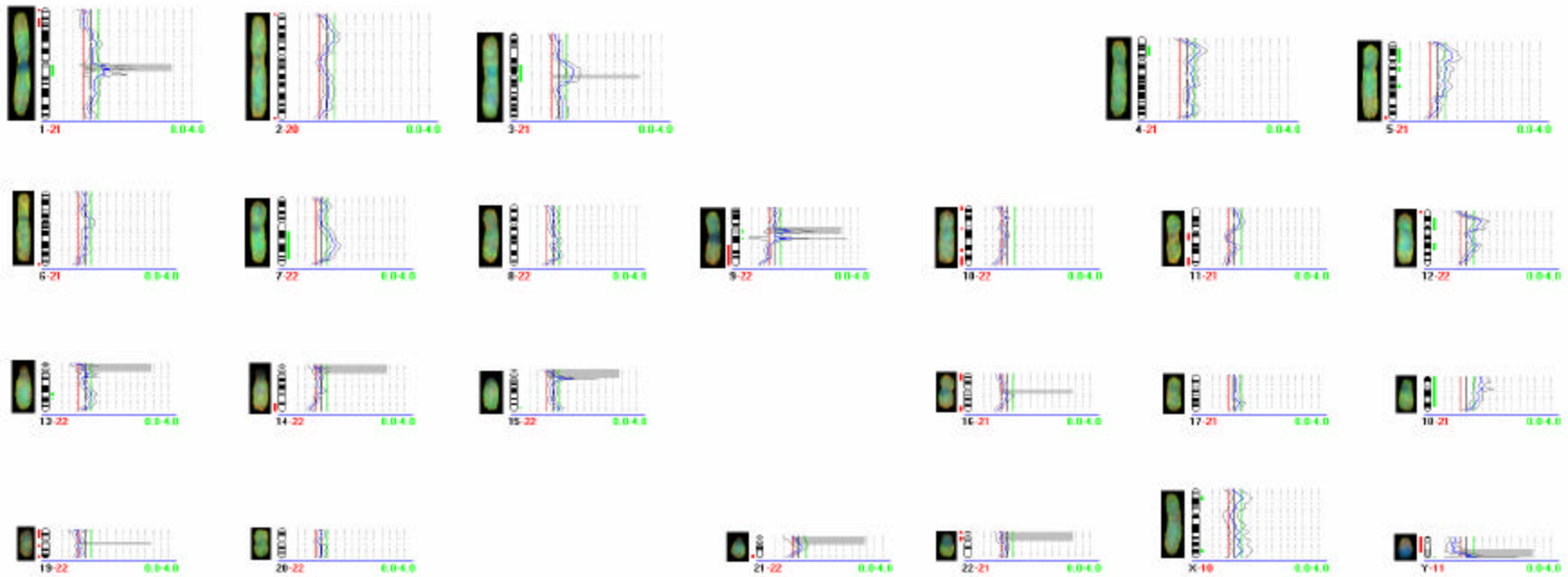


Figure 36. An Example of CGH Profile Data. The Leica image analysis software (Leica Inc., Exton, PA) generates 95% confidence intervals for mean CGH profile data once each metaphase has been appropriately karyotyped. This profile data is from case 39, a male patient. A minimum of ten metaphase spreads were collated to generate the mean data for each of the cases. Using the profiles from each of the spreads that combine to form the mean for each case, the software is able to calculate these confidence intervals for the mean profile data. The color chromosome image to the left of each ideogram (from Fig. 35D) was generated using the combination of all three fluorescent filters seen in Figs. 35A, B, and C. It should be noted that in the case data represented above, the profile data for the chromosomes have relatively narrow confidence intervals, which lends credence to the values of the mean. Simplified, the less variation (width) in the confidence interval, the greater certainty that can be assigned to the relative copy numbers in the data. This kind of data is generated for the mean profile data for the data set of each case during analysis.

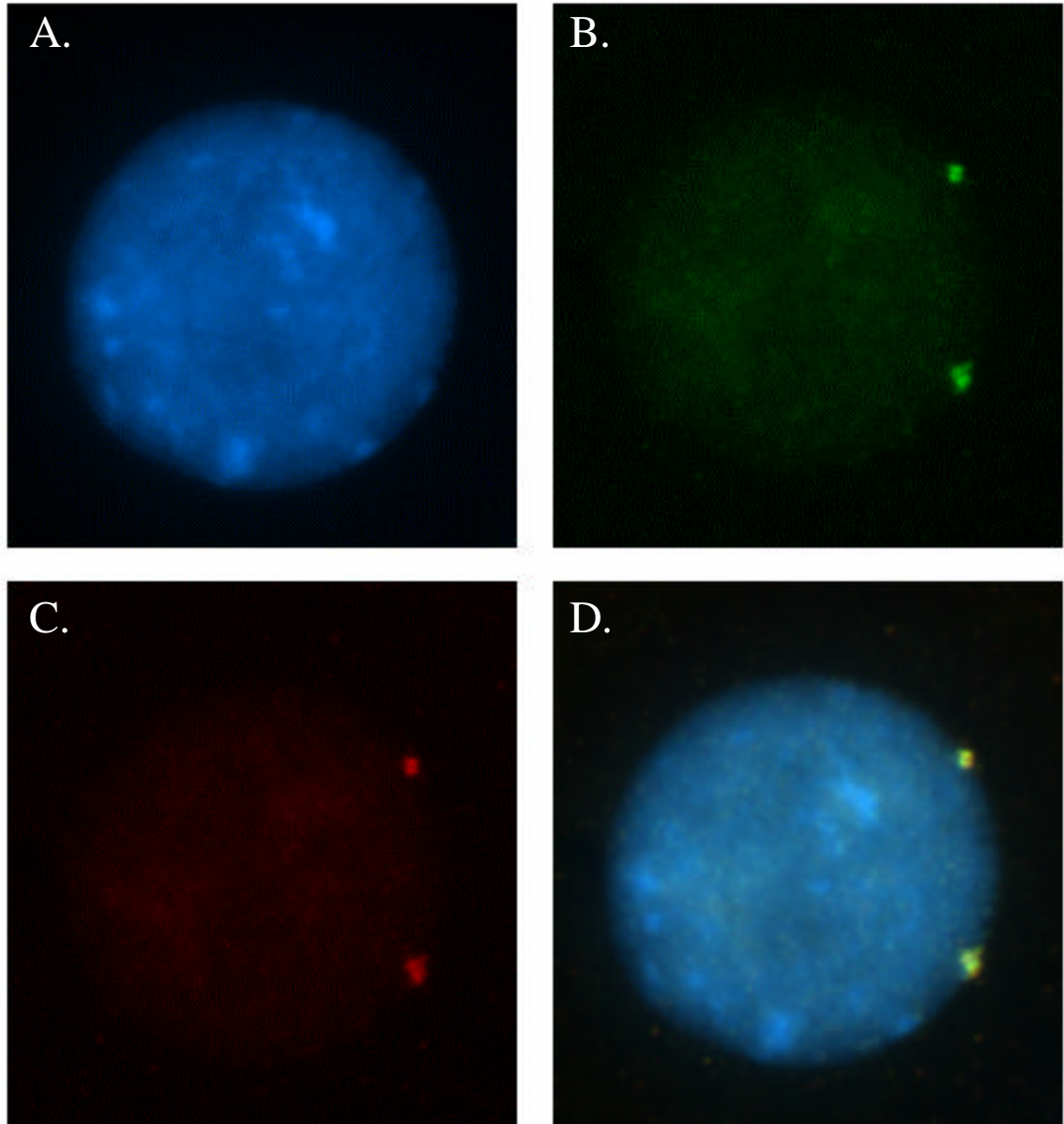


Figure 37. Interphase FISH Control Using Centromere Probe for Chromosome 3. **(A)** The isolated nucleus is counterstained with DAPI. **(B)** The FITC and **(C)** the TRITC images represent the dual-color fluorescence visualization of the centromere probe, ensuring distinction of the signal from the background. **(D)** The overlay shows 2 yellow signals that confirm the 2 signals visualized are in fact the centromere probe and not background noise. The overlay also confirms that the control nucleus in this image is in fact normal.

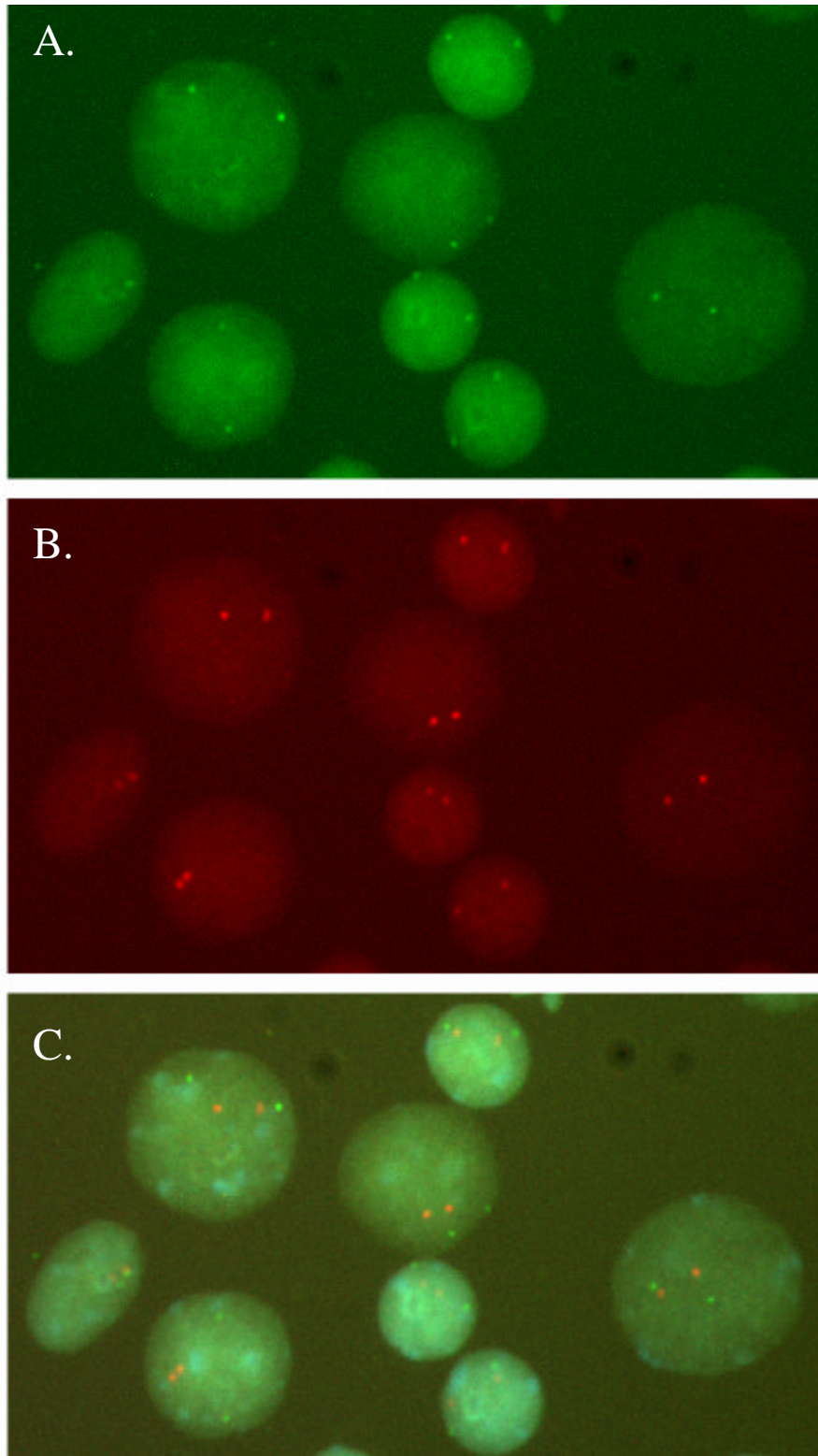


Figure 38. Interphase FISH Control Using Telomere Probes for 3p and 3q. (A) The 3p probes are visualized with FITC. (B) The 3q probes are visualized with TRITC. (C) The overlay of FITC and TRITC probes on a DAPI counterstain confirms 2 signals per cell for the control nuclei.

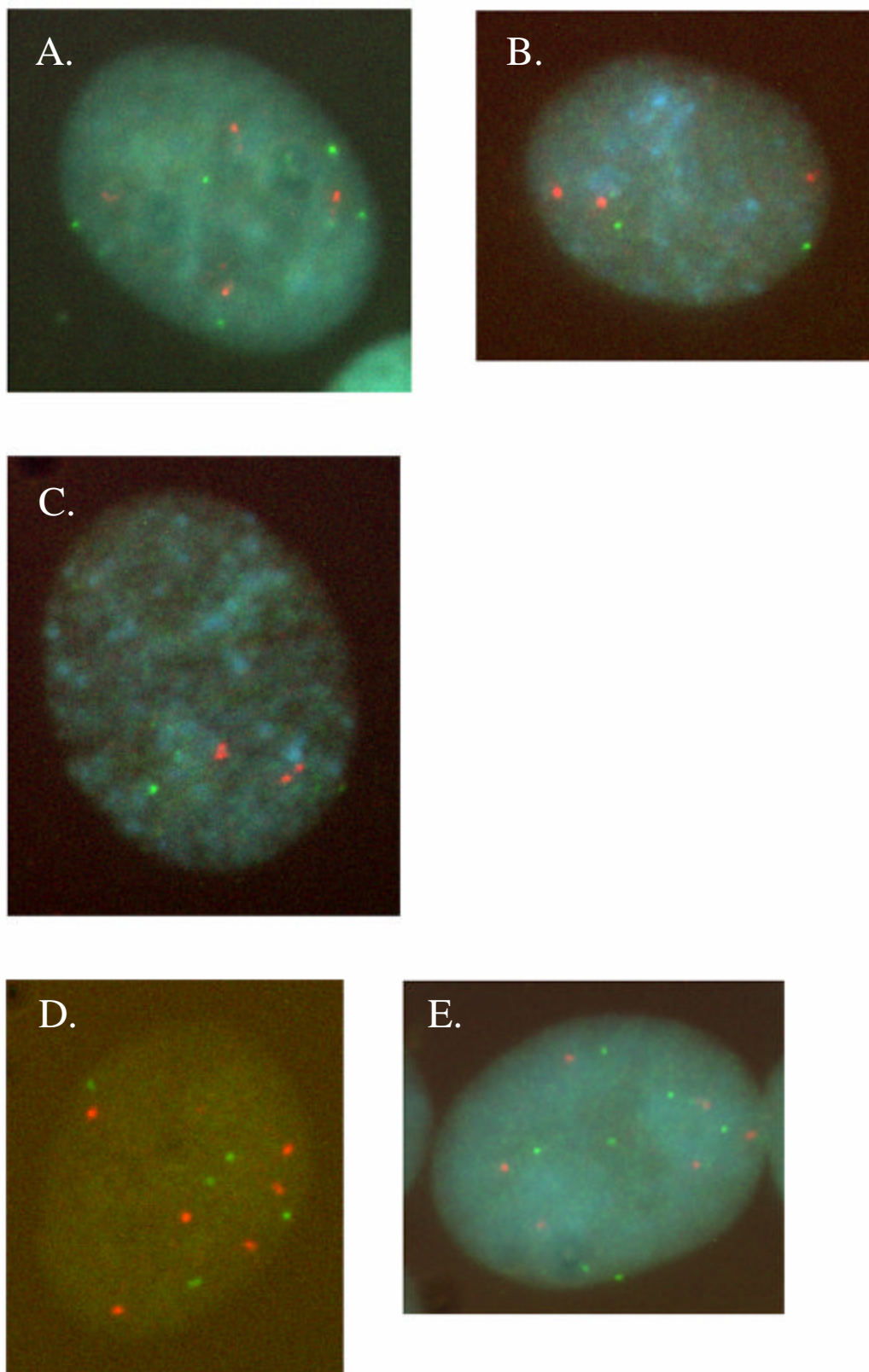


Figure 39. Telomere Probe Signals (3p and 3q) in Uveal Melanoma Cell Lines. Examples from the cell line (A) MEL270; (B) MEL285 ; (C) MEL290; (D) OCM-1; (E) OCM-3.

CURRICULUM VITAE

Jason Scott White
9926 Woodburn Road
Silver Spring, MD 20901

EDUCATION

West Virginia University, Morgantown, WV	Ph.D.	Genetics	2003
Franklin and Marshall College, Lancaster, PA	B.A.	Biology	1998

PROFESSIONAL EXPERIENCE

2001-2002	Student Intern, Division of Quantitative Pathology, Armed Forces Institute of Pathology, Washington, D.C.
2000	Research Biologist, Student Intern, American Registry of Pathology, Armed Forces Institute of Pathology, Washington, D.C.
2000	Teaching Assistant, Department of Biology, West Virginia University, Morgantown, WV
1999	Research Biologist, American Registry of Pathology, Armed Forces Institute of Pathology, Washington, D.C.
1998-1999	Teaching Assistant, Department of Biology, West Virginia University, Morgantown, WV

AWARDS AND HONORS

2001-2002	Nathaniel F. Rodman, Jr. Fellowship in Genetics and Developmental Biology, West Virginia University, Morgantown, West Virginia.
2001	Genetic Toxicology Association Student Travel Award, 32 nd Environmental Mutagen Society Meeting, San Diego, California.
2001	West Virginia University Doctoral Student Travel Award for the 32 nd Environmental Mutagen Society Meeting, San Diego, California.
2000	Outstanding Student Poster Award, 31 st Environmental Mutagen Society Meeting, New Orleans, Louisiana.
2000	West Virginia University Doctoral Student Travel Award for the 31 st Environmental Mutagen Society Meeting, New Orleans, Louisiana.

PROFESSIONAL ACTIVITIES

1999-2002	Member of the Environmental Mutagen Society.
-----------	--

RELEVANT GRADUATE COURSE WORK

Advanced Biochemical Genetics
Basic Concepts of Modern Genetics
Biochemistry
Cytogenetics
Human Genetics
Population Genetics

DEMONSTRATED SKILLS

Cell culture of human cell lines.
Peripheral blood culture (human).
Metaphase chromosome preparation from peripheral blood (human).
Nuclei isolation and cytospin preparation from fresh and archival tissue.
Fluorescence *in situ* Hybridization (FISH), including interphase FISH applications on fresh and archival tissue.
Tyramide Signal Amplification (TSA) Indirect ISH
Comparative Genome Hybridization (CGH) using antibody layering for indirect probe detection on fresh and archival tissue.
Degenerate oligonucleotide primed (DOP) PCR, bulk production of genomic painting probes for use in CGH.
Nick translation incorporating substituted nucleotides for DNA labeling: production of genomic probes for CGH.

Karyotyping of human metaphase spreads using inverse DAPI banding.
Spectral Karyotyping (SKY) (human).
Agarose gel electrophoresis with ethidium bromide staining to determine the size of DNA products.
Cloning of PCR products into plasmid vectors.
Transformation of bacteria using plasmids and selection of positive transformants.
Restriction enzyme digestion.
SDS-PAGE.
Southern blot.

PUBLICATIONS (in press or submitted)

Director-Myska AE, White JS and McLean IW (2001) Molecular Cytogenetic Characterization of Ten Uveal Melanoma Cell Lines. Proceedings of the Workshop on Prognostic Factors in Uveal Melanoma, Lieden, The Netherlands (in press).

White JS, Becker RL, McLean IW, Nath J, Director-Myska AE (2002) Molecular Cytogenetic Evaluation of Ten Uveal Melanoma Cell Lines. Cancer Res (submitted).

ABSTRACTS

White JS, McLean IW, Nath J, Becker RL, Director-Myska AE (2001) Molecular prognostic indicators of uveal melanoma: correlation of DNA sequence copy number aberrations with patient follow-up. Environmental and Molecular Mutagenesis 37 (Suppl 32):79.

Director-Myska AE, White JS, Niederkorn JY, McLean IW (2000) Characterization of Structural and Numerical Chromosome Aberrations in Uveal Melanoma Cell Lines using Spectral Karyotyping. Environmental and Molecular Mutagenesis 35 (Suppl 31):20.

White JS, Mclean IW, Nath J, Becker RL, Director-Myska AE (2000) A Characterization of the Chromosomal Aberrations of Uveal Melanoma Using Comparative Genomic Hybridization. Environmental and Molecular Mutagenesis 35 (Suppl 31):66.

INVITED SEMINARS

The Molecular Cytogenetics of Uveal Melanoma. Genetic Toxicology Association Meeting, University of Delaware, Newark, DE, October 2001.